Vers la commande dynamique des manipulateurs-mobiles souples et continuum : approche basée sur les courbes paramétriques

Steeve Kamga Mbakop

Towards Dynamic Shape Control of Mobile Soft Continuum Manipulators: Parametric curve-based approach

PhD THESIS
to obtain the title of

Doctor from University of Lille
Speciality : Robotics

Defended by

Steeve Kamga Mbakop

prepared at
CRIStAL CNRS-UMR 9189
defended on November 22, 2021
at CRIStAL, Lille

Jury

Reviewers :	Pr. Véronique Perdereau	-	University of Paris-Sorbonne, France
	Pr. Ian Walker	-	University of Clemson, USA
Examiners :	Pr. Frederic Boyer	-	IMT Atlantique Bretagne, France
	Pr. Cecilia Laschi	-	National University of Singapore, Singapore
	Pr. Sergey V. Drakunov	-	Embry-Riddle Aernautical University, USA
	Pr. Abdelaziz Benallegue	-	AIST, Japan
Supervisor :	Pr. Rochdi Merzouki	-	University of Lille, France
Co-Supervisor :	Dr. Gilles Tagne	-	JUNIA ISEN, Lille, France
Guest:	Ing. Marc-Henri Frouin	-	CEO, NIRYO Lille, France

Vers la Commande Dynamique des Manipulateurs-Mobiles Souples et Continuum: Approche basée sur les courbes paramétriques

THÈSE

soumise à l'Université de Lille en vue de l'obtention de

Doctorat

Spécialité : Robotique

par

Steeve Kamga Mbakop

préparée au laboratoire

CRIStAL CNRS-UMR 9189

soutenue le 22 Novembre 2021

à CRIStAL

Jury

Rapporteurs :	Pr. Véronique Perdereau	-	University of Paris-Sorbonne, France
	Pr. Ian Walker	-	University of Clemson, USA
Examinateurs :	Pr. Frederic Boyer	-	IMT Atlantique Bretagne, France
	Pr. Cecilia Laschi	-	National University of Singapore, Singapore
	Pr. Sergey V. Drakunov	-	Embry-Riddle Aernautical University, USA
	Pr. Abdelaziz Benallegue	-	AIST, Japan
Directeur de thèse :	Pr. Rochdi Merzouki	-	University de Lille, France
Encadrant:	Dr. Gilles Tagne	-	JUNIA ISEN, Lille, France
Invité:	Ing. Marc-Henri Frouin	-	CEO, NIRYO Lille, France

Towards Dynamic Shape Control of Mobile Soft Continuum Manipulators: Parametric curve-based approach

Abstract

Nowadays, soft continuum robots are increasingly used in everyday life (logistics, agriculture, medical therapy, baking, human collaboration, etc.) due to the multiple advantages they offer over rigid robots. They are often made up of soft and hyper-elastic materials that give them resilience, flexibility and conformation, making them good candidates to meet some real-life needs (form enclosure grasping, obstacle-free navigation, etc.). However, the control of their shape remains a major challenge for the scientific community due to their very large number of degrees of freedom (DoFs). Unfortunately, it is not physically possible to control all the DoFs to drive their 3D motion. To address that issue, the present research work focuses on a Reduced-Order-Model (ROM) based shape control using Pythagorean Hodograph (PH) parametric curves. The proposed approach allows to describe the high-order kinematics of soft continuum manipulators with a set of finite points called control points. Hence, the control dimension of the latter can be reduced to that of this set of finite control points. Moreover, to address shape adaptability issues during external interactions (gripping task, collision-free trajectory, spatio-temporal disturbances, etc.), the motions of the control points (shape kinematics) have been described with respect to real dynamic physical inputs considering the Euler-Bernoulli (EB) theory consistent with the large deflections. To validate the proposed approaches, several experimental tests have been performed on several classes of Soft Continuum Robots in various scenarios: Fluidic Elastomeric Actuators (FEAs) for the control of gripping tasks and a Robotino-XT for the control of motion planning with obstacles avoidance.

Keywords: Soft continuum manipulators, Pythagorean Hodograph curves, Shape kinematics, Shape dynamics, Control.

Vers la Commande Dynamique des Manipulateurs-Mobiles Souples et Continuum: Approche basée sur les courbes paramétriques

Résumé

De nos jours, les robots déformables et continuum sont de plus en plus utilisés dans la vie quotidienne (logistique, agriculture, thérapie médicale, pâtisserie, collaboration humaine, etc.) en raison des multiples avantages qu'ils offrent par rapport aux robots rigides. Ils sont souvent constitués de matériaux deformables et hyper-élastiques qui leur confèrent résilience, flexibilité et compliance, ce qui en fait de très bons candidats pour répondre à certains besoins pratiques (préhension par conformité, navigation sans obstacles, etc. Cependant, le contrôle de leur forme reste un défi majeur pour la communauté scientifique en raison de leur très grand nombre de degrés de liberté (DDL). Malheureusement, il n'est physiquement pas possible de contrôler tous les degrés de liberté pour piloter leurs mouvements dans l'espace tridimensionnel. Dans l'optique de résoudre ce problème, les présents travaux de recherche traitent du contrôle de forme basée sur un modèle d'ordre réduit utilisant des courbes paramétriques à Hodographe Pythagoricienne. L'approche proposée permet de décrire la cinématique d'ordre élevé des robots deformables et continuum via un ensemble de points finis appelés points de contrôle. Ainsi, la dimension de leur contrôle peut être réduite à celle de cet ensemble fini de points de contrôle. De plus, afin d'aborder les problèmes d'adaptabilité de forme lors d'interactions externes (tâche de préhension, trajectoire sans collision, perturbations spatio-temporelles, etc.), les mouvements des points de contrôle (cinématique de la forme) ont été décrits en fonction des entrées physiques réelles en considérant la théorie d'Euler-Bernoulli (EB) en grandes déformations. Afin de valider les approches proposées, plusieurs essais expérimentaux ont été effectués sur diverses classes de robots déformables et continuum dans des scénarios variés: les Actionneurs Fluidiques en Élastomère (AFEs) pour le contrôle des tâches de préhension et une classe de Manipulateurs Mobiles Souples et Continuum (MMSC) à savoir le Robotino-XT, pour le contrôle de la planification des mouvements avec évitement des obstacles.

Mots clés: Manipulateurs souples et continuum, Courbes à Hodographes Pythagoriciennes, cinematique de la posture, dynamique de la posture, commande.

This thesis is dedicated to my parents, Richard KAMGA and Calvine KAMGA, My Grand Mother Pauline DJADJA, Maman Agnes Za'a, my brothers and sisters for their love, endless support and encouragements.

Acknowledgments

First of all, I would like to express my sincere gratitude to my supervisor, Professor Rochdi Merzouki, for all the sacrifices he has devoted to me and for the blind trust he has given me. His patience, his motivation and his immense knowledge and sense of work well done have been probably the key to the success of this research works. He has been very inspiring to me.

My PhD co-supervisor, Dr. Gilles Tagne has been an indisputably valuable support for this research project. His precious advice, his sense of communication as well as his great maturity have contributed to put me in a better conditions for my research.

My special respects to Marc-Henri Frouin, CEO of Niryo, for the opportunity he offered me to conduct this PhD study. His vision, his greatness, his patience and his leadership are all qualities for which I want to show him all my devotion.

Besides my advisor, I would like to thank the reviewers of my thesis Prof. Véronique Perdereau and Prof. Ian Walker for their insightful comments and the time spent for the manuscript revision.

I would especially like to express my best feelings to Mrs. Anne-Marie Kokossy who literally adopted me as my mother, and never failed to be by my side. Her moral guidance, her peace of mind, and the trust she gave me daily, have helped make me a better man. I will never have enough words to describe the unfailing love I have for her. May she be assured of my most sincere feelings.

I would like to thanks the Niryo team for their availability. I particularly appreciated their commitment to me, the warm welcome they gave me during my adventure. I will never be able to thank them, they were so essential to me.

My sincere thanks to my CRIStAL laboratory colleagues, Xin Rui Yang, Mouad Kahouadji, Othman Lakhal, Abdelkader Belarouci, Vincent Coelen, Achille Melingui for their immeasurable support. They have always been close to me and have regularly brought me clarifications in the framework of my research work. May they receive the expression of my sincere considerations.

What can I say about the JUNIA ISEN colleagues, Emmanuelle Gore, Valérie Vandenhende, Florence Alberti, Kevin Hérissé, Julien Duforest, Antoine Frappé, Benoit Larras, Jean-Marc Capron, Bruno Stefanelli, Axel Flament, Andreas Kaiser, Emmanuel Dubois, Justine Philippe, for whom I will never have enough words to describe the hospitality they have shown me. These experiences cannot be told, they must be lived. They have been and remain a true family to me.

I cannot forget mentioning my closest friends Ali, Alexis and Thomas, who have shown me unconditional love. I would like to share with them my warmest considerations.

My best thanks are also extended to JUNIA and Lille University technical support, Francois Gionco, Michael Meul, Michel Pollart and Olivier Scrive for their continuous assistance.

At last, my greatest thank is for my parents, brothers and sisters, Junior, Liliane,

Landry, Rosine, Elodie, Yannick for their love and encouragements during all this intense time of my studies and during my defense. They never forget to ensure me about their love everyday. Without their support and their care, I would not have been able to perform this big workload and to succeed in my education.

Contents

List of Figures

List of Tables

Chapter 1

Introduction

Contents

1.1 General Introduction

Recent technological advances in the engineering fields of electronics, computer sciences and mechanics have allowed the emergence of soft continuum manipulators. These can be manufactured shortly and at lower costs. However, compared to rigid manipulators robots [Siciliano 2016] [Bruno 2010], the performances of soft continuum manipulators are lesser, in terms of rapidity, accuracy and repeatability. Improvements are still required regarding their control. Henceforth, soft continuum manipulators robots have been increasingly used in various industrial applications such as aerospace, food, med-tech industry, etc.

With the era of industry 4.0, the need of collaborative tasks between human operators and robots are more and more requested. This has led the robotic systems to be more collaborative in a shared workspace with operators. For that objective, the human-machine co-existance or collaboration is ensured by a high level of safety. To come to this end, several benefits have been taken from the advances made in recent years in materials science and mechanical design. Henceforth, soft and continuum manipulators have highlighted the interesting characteristics of soft, hyper-elastic and deformable materials used for their manufacturing [Case 2015][Rus 2015].

Soft robotics systems such as soft grippers, soft continuum manipulators, etc., have the ability to guarantee the mechanical integrity of the objects that they

interact with. They can overcome certain difficulties encountered by rigid materials to adapt to their external environments. Nowadays, some practical industrial' issues have been partially resolved, where in agri-food industry, the usage of soft manipulator grippers for harvesting [Gunderman 2021] [Xiong 2018] and fishing [Galloway 2016], has shown considerable performances.

Actually, many advantages can be found within the usage of soft continuum manipulators and therefore, largely justify the rise of the interest for these robots [Hughes 2016]. Among these advantages, one can cite: low cost material, rapid manufacturing, resilience, conformity with respect to external interactions and lightweight systems with low embedded electronics requirements. However, they are characterized by a distributed deformation along their length, where, theoretically, they are composed of an infinite number of Degrees of Freedom DoFs. This yields them a hyper-redundant configuration space wherein the robot tip can reach a target with an infinite number of kinematic postures [Trivedi 2008b]. A kinematic modeling is therefore required to perform an accurate control. This issue is discussed in the scope of the present research works.

Modeling and shape control of mobile soft continuum manipulators MSCM remains a research subject that still requires multiple investigations. Nevertheless, it seems that model reduction techniques [Singh 2018b] [Della Santina 2020b] show very promising results in facilitating real-time control of soft robots [Thieffry 2018b] [Della Santina 2020c], in forward kinematics. However, shape control requires some form of computation techniques that combine conventional control approaches with motion planning. The latter are still very energy-consuming due to their dependence on the configuration of the space [Patle 2019], which increases rapidly with the number of the DoFs that constitute the robot. In the light of all of the above, a motion planning based control applied to a ROM might contribute in resolving the aforementioned issues for related to their shape control. This constitutes the main interest of the present research work.

1.2 Thesis Industrial Context

The present research project is carried out within the framework of a scientific and industrial cooperation with a young robotics company called Niryo[1]. The latter develops a wide range of lightweight and collaborative manipulators for picking and placing of various of objects. These objects can be soft or rigid and their geometries can vary significantly and therefore, yield considerable analysis in order to design specific grippers for grasping and handling. In parallel, the size and the packaging of the objects are regularly modified to meet new marketing requirements. This implies regularly new analyses and modifications in order to obtain gripping solutions always more fitted to the needs stated by the customers. Thus, to cover the wide range of shapes of products to be grasped, the idea of an adaptive gripping solution based on soft materials was investigated by Niryo company trough this research work. The

[1] https://niryo.com/

shape conformation provided by the hyper-elastic materials would be suitable for compliant and safe grasping [Zhou 2021].

1.3 Thesis Scientific Context

This Ph.D. thesis is prepared in the research team "System of Systems Engineering (SOFTE)", of the laboratory "Centre de Recherche en Informatique, Signal et Automatique de Lille (CRIStAL) (UMR CNRS 9189)". The scientific context concerns the development of an integrated approach for modeling, sizing, control and design of Fluidic Elastomeric Actuators FEAs used for grasping tasks in industry. The aim is to overcome the issues related to shape adaptation of soft robotic grippers while attempting a form-enclosure grasping and performing an adaptive shape control. This research work has been developed under the supervision of Dr. Prof. Rochdi Merzouki, Professor at Polytech Lille at University of Lille and Dr. Gilles Tagne, Assistant Professor at Université Catholique de Lille/ JUNIA / ISEN Lille.

1.4 Thesis Objective

Soft continuum manipulators are more and more used for various applications of research, academia and industry. Despite being under-actuated systems, they need to be optimally controlled to reach certain performances of rigid manipulators such as position and shape accuracies. Many works have been conducted for kinematic shape control of this class of soft robots, exhibiting a high number of DoFs. However, some researches have been devoted on the optimisation of the robot shape in interaction with its surrounding environment, such as obstacles avoidance or for grasping tasks. Thus, the work proposed in the present research explores new approaches for the control of MSCM robots in structured and unstructured environments.

The main objective of this PhD work is the development of an integrated approach of Fig. 1.1 for model-based dynamic shape control of MSCM. For that, this integrated approach considers the following:

- Generating automatically a kinematic ROM of the MSCM. This is based on Pythagorean Hodograph (PH) parametric curves and uses bending energy and length constraints optimization, in order to reconstruct the shape of the MSCM under kinematic constraints.

- Integrating jointly an APF to motion planning of the shape of the MSCM and a Sliding Mode Control (SMC) to control bending energy of the PH curve in the space configuration.

- Estimating the dynamic model of the MSCM, based on Euler Bernoulli theory, in order to carry out a relationship between the position of the control points of the PH kinematic ROM and the finite physical inputs FEAs.

- Designing a MSCM based on the optimisation of the number of the physical inputs FEAs and the number of control points representative to its kinematic ROM.

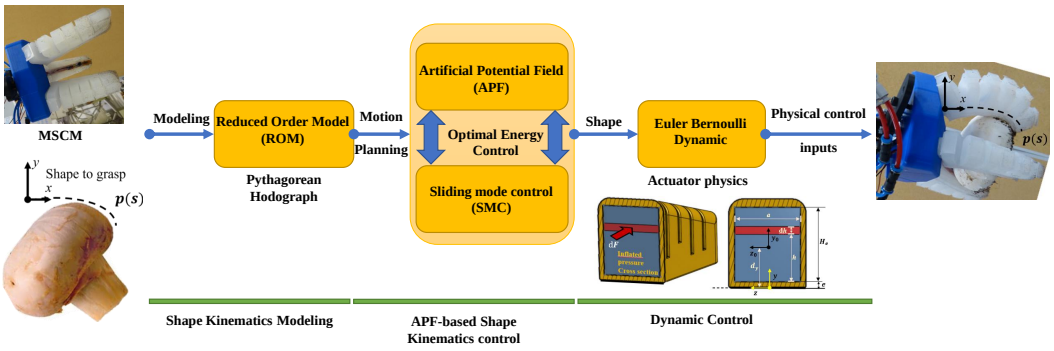

Figure 1.1: Integrated approach for dynamic control of MSCM manipulators

1.5 Research Problem Statement

Let's assume that the infinite DoFs of a MSCM can be described kinematically from a ROM of a quintic PH parametric and time t varying curve $p(s,t) : [0, L] \rightarrow \mathbb{R}^3$, as shown in Fig. 1.2. This quintic PH is controlled from the control polygon $\Lambda_n(p(t))$, crossing the six control points $\{p_k(t)\}$, where $\Lambda_n(p(t)) = \{p_0(t)...p_n(t)\}$. The research problem question is: How the end point $p_5(t)$ can reach the target object with an optimal energy bending of the shape of the curve $p(s,t)$ in presence of obstacles $\mathbb{O}$. To answer to this research question, the motion planning and the minimal potential bending energy $E_p(t)$ of the shape of MSCM, have been obtained by controlling the control points of the polygon of the PH curve. This has been illustrated in Fig. 1.2 by a hand acting on the control points such as the case of puppet toy. Thus, the problem formulation of this research question can be expressed as follows:

$$
\begin{aligned}
&\text{Minimize } E_p(t) = \frac{1}{2}\int_0^L |\omega(s,t)|^2 \, \mathrm{d}h, \\
&\omega = \sqrt{\kappa^2 + \tau^2}, \\
&\text{subject to :} \\
&\kappa = \kappa(p_{in}, F_{ext}) \leq \kappa_{\max}, \\
&\mathrm{d}p_k = -\frac{\nabla\Phi}{\|\nabla\Phi\|}\bigg|_{p_k}, \\
&T_k = T_k(p_{in}, \mathrm{d}p_k, F_{ext}) \\
&0 \leq s \leq L,
\end{aligned}
\tag{1.1}
$$

where s is the curvilinear coordinate along the constant length L of the MSCM, κ and τ describe respectively the curvature and the torsion of the MSCM curve.

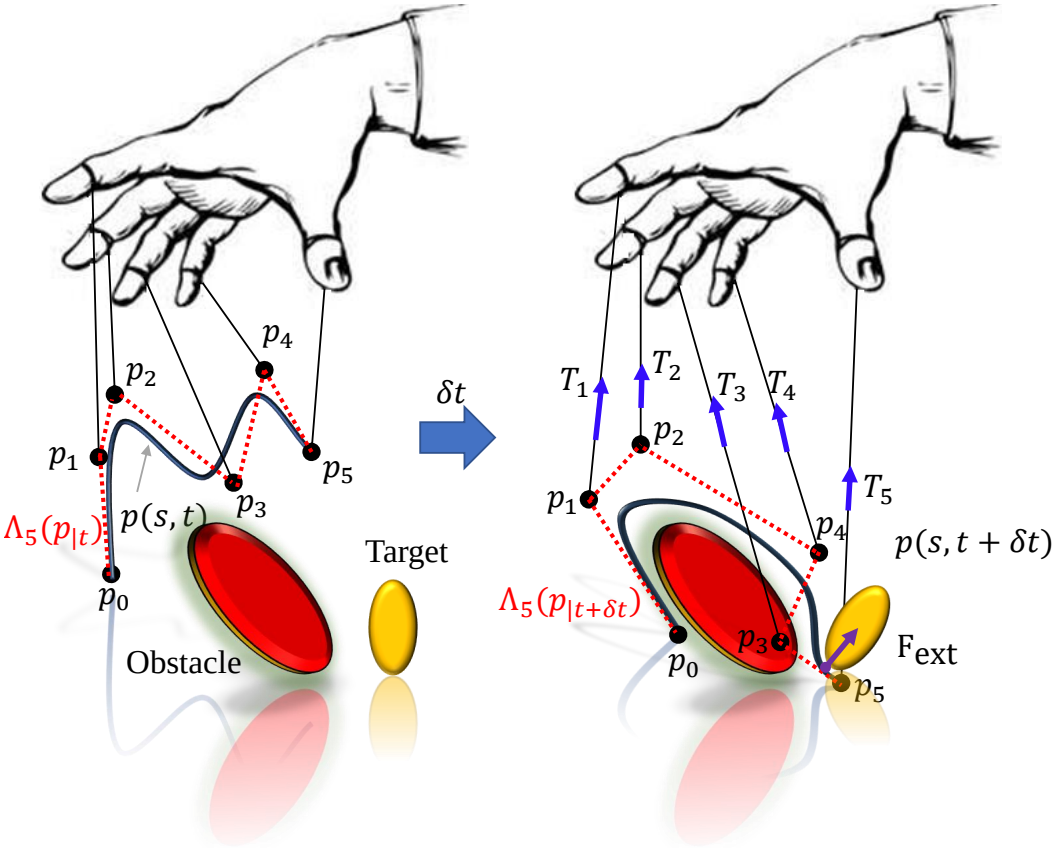

Figure 1.2: Shape control illustration of MSCM manipulators

$\kappa_{\max}$ denotes the maximum curvature allowed by the MSCM under external interactions F_{ext} and p_{in} denotes the physical control inputs (actuating pressure, torque, etc.). The displacement of a control point p_k, card$(p_k) \ll \infty$, is denoted by the quantity dp_k, generated by the set of efforts T_k (mechanical forces, etc.). The motion planning of dp_k is obtained from the APF, with a potential field $\Phi(p_k, p_{k_d}, \mathbb{O})$ where p_{k_d} denotes the target position of the control points p_k.

1.6 Contribution in the framework of the group activities

The research group SOFTE [2] of CRIStAL Lab [3] is working since 2012 on the Design, the modeling and the control of several classes of soft-continuum manipulators robots. The research team SOFTE has devoted a number of their works on the development of qualitative and quantitative kinematics models for real-time applications, especially on a class of continuum manipulator called Compact Bionic Handling Arm CBHA. This continuum robot is made up flexible and compliant by polyamide-based

[2] https://www.cristal.univ-lille.fr/en/teams/softe/?force_lang = true
[3] http://cristal.univ-lille.fr

material. Several modeling techniques have been developed and implemented, where in [Escande 2015], a geometric modeling approach has been proposed under the assumption of Constant Curvature CC. Identification-based technique has also been highlighted through neural network for both modeling and control [Melingui 2015]. Then [Lakhal 2016] has investigated hybrid modeling methods using a serial-parallel kinematic model to calculate the inverse kinematic model of the CBHA robot. In [Bieze 2018b], the team has explored the computational mechanics using the Finite Element Methods (FEM) for control and simulation purposes. Recently, reduced order kinematics using PH parametric curve has been discussed by [Singh 2018b] for the shape reconstruction of soft continuum manipulators. The present research works deal with dynamic modeling and shape control of MSCM, by considering its optimal shape reconstruction under external interactions, such as obstacles avoidance or grasping tasks in industrial environments.

1.7 Main Contributions

In this thesis work, the following contributions are discussed:

- Development of a kinematic ROM of a mobile soft continuum manipulator MSCM robots made up of infinite DoFs, based on the PH parametric curve that uses bending energy optimization and length constraints [Mbakop 2021b],
- Euler-Bernoulli dynamics model-based of MSCM, with respect to their shape kinematics based on quintic parametric curves [Mbakop 2021b] [Mbakop 2021c],
- Design of robust control in the spatial configuration to minimize the bending energy of the soft-continuum manipulators in motion, during the collision-free or grasping contact, based on APF for motion planning and SMC for the control [Mbakop 2021a][Mbakop 2020].
- Experimental validation using 2 classes of MSCM: An integrated multi-fingered soft gripper FEAs robot [Mbakop 2022] and a mobile-bio-inspired trunk of elephant (Robotino-XT).

1.8 Disseminated Results

The results of this research work are disseminated through the following publications:

Journal papers

1. Steeve Mbakop, Gilles Tagne, Marc-Henri Frouin, Achille Melingui and Rochdi Merzouki (2021). Inverse Dynamics Model-Based Shape Control of Soft Continuum Finger Robot Using Parametric Curve. IEEE Robotics and Automation Letters (DOI: 10.1109/LRA.2021.3101874).

2. Steeve Mbakop, Gilles Tagne, Sergey Drakunov and Rochdi Merzouki (2021). Parametric PH Curves-Model Based Kinematic Control of the Shape of Mobile Soft-Manipulators in Unstructured Environment. IEEE Transactions on Industrial Electronics (DOI: 10.1109/TIE.2021.3123635).

3. Steeve Mbakop, Gilles Tagne, Xinrui Yang and Mouad Kahouadji and Michel Pollart and Rochdi Merzouki (2021). Integrated Design of a Bio-Inspired Soft Agri-Food Gripper for Mushroom Harvesting. IEEE/ASME Transactions on Mechatronics (Under review).

International Conferences

1. Steeve Mbakop, Gilles Tagne, Marc-Henri Frouin, Achille Melingui and Rochdi Merzouki (2021). Inverse Dynamics Model-Based Shape Control of Soft Continuum Finger Robot Using Parametric Curve. In Intelligent Robots and Systems (IROS), 2021 IEEE/RSJ International Conference.

2. Inderjeet Singh, Steeve Mbakop, Manarshhjot Singh, Ismael Benskrane, Rochdi Merzouki (2021, August). Curve-Based Approach for Shape Reconstruction and planning of a Mobile-Continuum Manipulator in Structured Environment. In 2021 IEEE 17th International Conference on Automation Science and Engineering (CASE) (pp. 1914-1919). IEEE.

3. Steeve Mbakop, Gilles Tagne, Marc-Henri Frouin and Rochdi Merzouki (2021, April). Interoperable Models for Dynamics and Shape Tracking of Soft Fingers. In 2021 IEEE 4th International Conference on Soft Robotics (RoboSoft) (pp. 199-206). IEEE.

4. Steeve Mbakop, Gilles Tagne, Rochdi Merzouki and Sergey Drakunov (2020, May). Path planning and control of mobile soft manipulators with obstacle avoidance. In 2020 3rd IEEE International Conference on Soft Robotics (RoboSoft) (pp. 64-69). IEEE.

1.9 Manuscript Organization

The manuscript is organized in the following:

- The second chapter introduces a state of art in the literature regarding the ROM-based techniques for soft-continuum manipulators. A scientific positioning in the framework of the present work is outlined at the end of the chapter.

- The third chapter introduces the PH-based shape kinematics control of the MSCM. The Inverse kinematics as well as the forward kinematics model using PH curve are developed by considering the length constraint. Also, the shape kinematic control is studied. Some experiments are presented to prove the validity of the proposed PH-based kinematics control approach.

- The fourth chapter deals with the PH-based dynamic control of MSCM. The fundamentals of the bending kinematics of the MSCM is described. Also, the inverse dynamic modeling is discussed, and lead to the computation of the real physical inputs by exploiting the PH features.
- The fifth chapter presents an integrated design of a soft bionic gripper made up of hyper-elastic soft material. The performance of grasping tasks are obtained using the attractive APF, combined to the SMC and applied to the shape of each soft finger robot. A set of experiments have been discussed and prove the efficiency of the grasping approach.
- Finally the sixth chapter summarizes the PhD work contributions and states on potential directions of the prospective works.

Chapter 2

State of the Art on Reduced Order Model and Shape Control of soft continuum manipulators

Contents

2.1 Introduction

Soft robotics is a field that relies on mimicking the motion of soft bodies to achieve fluid and complex movements. Among these **soft bodies** capable of moving in complex environments are: earthworms, snakes, larval insects, octopuses, and eels present a wide range of different motions bio-inspired strategies developed over the years by scientists. These soft robotic structures have found applications in various fields, such as the medical field, the agri-food industry, etc. However, the continuum aspect of these soft structures makes their shape control non-obvious because of the high order dimension induced by their kinematics. Many techniques have been explored so far to tackle these issues, including the Reduced-Order Modeling strategies, which constitute the main objective of the present state-of-art.

2.2 Soft Continuum Manipulators

2.2.1 Global Overview

As stated earlier, soft continuum manipulators are inspired by several soft bodies existing in nature like the elephant's trunk, the octopus tentacles, the mammal's tongue, etc. All these biological structures are made of soft materials providing them an infinite shape configuration during their interactions with their surrounding environments [Hirose 1993]. The idea with the soft continuum manipulators is to mimic the behavior of such soft biological structures to take benefits from their mechanics such as dexterity, conformation, resilience, smooth motion, etc. Therefore, soft continuum manipulators are made up of soft materials, which have the principal advantage to increase their manoeuvrability [Hughes 2016] [Rus 2015]. In contrast to rigid-bodied robots, the mobility of soft continuum robots is determined by the material's deformation rather than the motion concentrated at the joints [Robinson 1999]. The deformation of a soft continuum manipulator is achieved by its actuation mechanism, which results in a variation of the strain, size, and shape of the actuator material [Polygerinos 2017]. Thus, their number of DoFs are defined

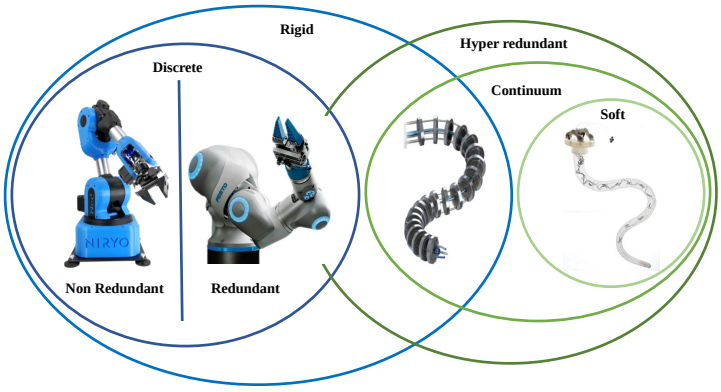

Figure 2.1: Classification of robots based on material and degrees of freedom

by their continuous and infinite deformations leading to hyper-redundancy. Therefore, it is physically impossible to control all these DoFs compared to rigid-bodied robots where each of them is controlled by one actuator. In practice, a small number of actuators can be used so that a soft manipulator can achieve any orientation in its workspace. The combination of this dexterity and their very large number of degrees of freedom result in their navigation in narrow and unstructured areas. The classification of robots based on material and DoFs is presented in Fig. 2.1. The advantages and the drawbacks of the soft robotic systems compared to other robot structures are summarized in Table 2.1 [Trivedi 2008b].

Table 2.1: Soft Robotics features

Features	**Rigid**	**Discret hyper-redundant**	**Hard Continuum**	**Soft**
		Properties		
DoF Actuators	Few, Discrete	Many, Discrete	Continuous	Continuous
Strain	None	None	Small	Large
Materials	Metal, Plastics	Metal, Plastics	Shape memory alloy	Rubber
		Capabilities		
Accuracy	Very high	High	High	Low
Load capacity	High	Lower	Lower	Lowest
Safety	Dangerous	Dangerous	Dangerous	Safe
Dexterity	Low	High	High	High
Working space	Structured	Structured and unstructured		
Object	Fixed size	Variable size		
Conformability	None	Good	Fair	Highest
		Design		
Controllability	Easy	Medium	Difficult	Difficult
Pose Sensing	Easy	Harder	Difficult	Difficult
Inspiration	Mammal limbs	Snakes	Fish	Hydrostats

2.2.2 Classification

There exists several classifications of soft continuum manipulators. Soft manipulators can be classified according to their backbone structures or actuation strategies.

Two main classes of backbone structures can be distinguished: the single backbone structure and the multi-backbone structure. In the case of the single backbone structure, a central elastic structure supports all the material internal constraints caused by the actuation [Kutzer 2011] [Camarillo 2008a]. This latter is often used to allow the insertion of actuation or transmission elements (such as cable, fluid pipe, etc.). Depending on its geometry, the desired motion (torsional, directional bending or axial stretch) can be exhibited. The structure of a multi-backbone continuum robot is made up of multiple elastic elements (rods or tubes) disposed in parallel and constrained with respect to each other [Bryson 2014] [Moses 2013] [Simaan 2009]. This approach has been used for non constant-curvature shapes kinematics and very high number DoFs per section [Till 2015] [Bryson 2014].

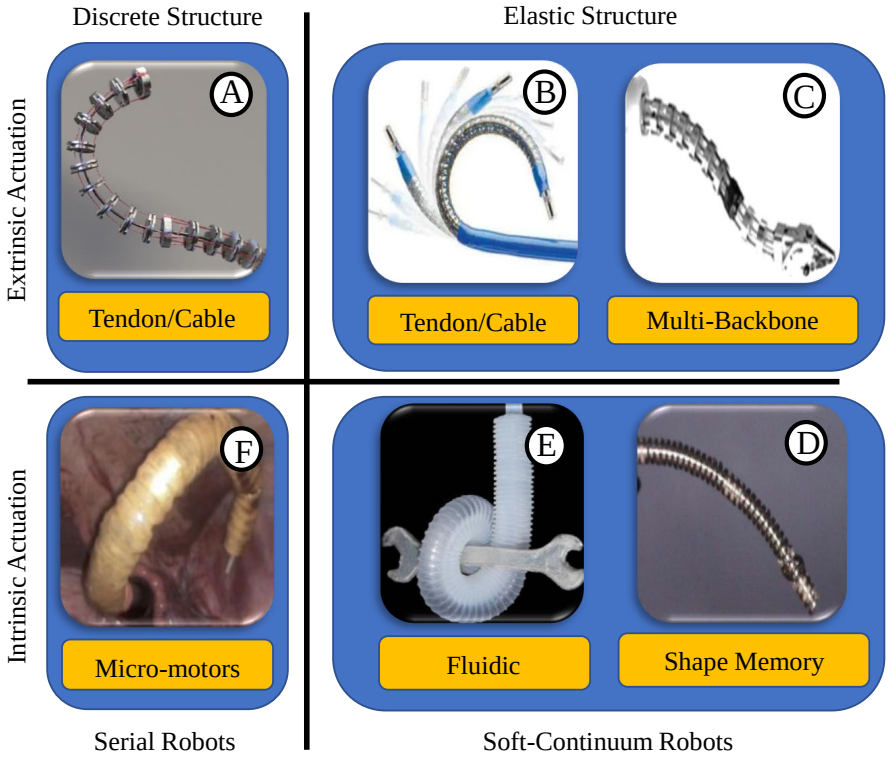

Figure 2.2: Categories of soft continuum robots: A. Tendon driven robot [Amanov 2021], B. Tendon/cable manipulator ©2015 Hansen Medical Inc., C. Multi-Backbone robot ©2015 Advanced Robotics and Mechanism Applications Laboratory, Vanderbilt University [Robotics], D. Shape memory alloy actuators [Cismasiu 2010], E. Fluidic actuators [Martinez 2013]
, F. Micro-motors robot [Kwok 2012].

Regarding the actuation-based classification, three main actuation configurations have been investigated as a standard of classification: intrinsic, extrinsic and hybrid. The intrinsic actuation technique describes a strategy where the actuation system is located on the structure of the soft robotic system and forms a part of it. Several soft continnum manipulators belong to these category [Ikuta 2006] [Bailly 2011] [Ikuta 2011]. The extrinsic actuation strategy makes use of remote actuation. In this case, the motion is transferred into the mechanism (tendon, cable driven, etc) via a mechanical linkage [Dario 2000] [Kutzer 2011] [Camarillo 2008b]. Intrinsic and extrinsic strategy have been sometimes combined and result in a new class of techniques called hybrid approach [Ivanescu 1995] [Immega 1995].

2.2.3 Applications

Number of applications, particularly in the medical and food industries, have taken advantage of the attractive properties of soft robots, including dexterity, flex-

ibility and elasticity.

2.2.3.1 Biomedical applications

In the medical area, new strategies of surgical operations have been mastered, including minimally invasive surgery (MIS), which has become very popular in recent years [Burgner-Kahrs 2015]. Among them, the Neurosurgery has been performed with lower procedural times, higher accuracy, and precision [Neudorfer 2018]. The usage of surgical robot systems such as Rosa (Medtech S.A., Castelnau Le Lez, France), or Renaissance (Mazor Robotics Ltd., Israel) has emerged to assist the surgeon for more specific operations [Mattei 2014].

The Lung surgical interventions have also been improved. The efficiency of the diagnosis as well as the management of the respiratory pathologies have been reported in [Hindman 2019]. In this investigation, the authors outlined the benefits of ultra-thin robotic instruments for the exploration of airways. To achieve real-time control of continuum robot of medical devices, some technologies, such as Magellan and Sensei (Hansen Medical, Mountain View, CA, USA), and CorPath GRX (Corindus, Inc. Waltham, MA, USA) have helped to cover a wide range of surgical operations [Clements 2019] [Gong 2016].

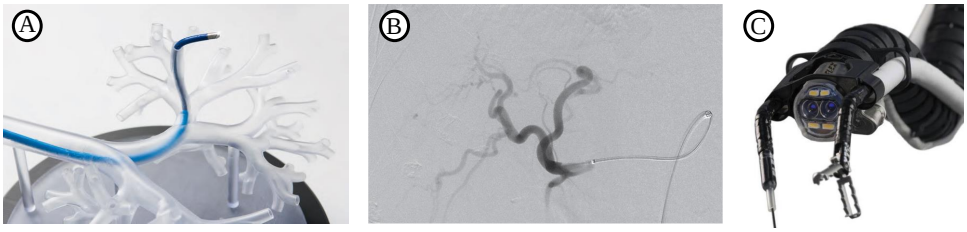

Figure 2.3: Soft continuum robots for surgery operations: A. Lung intervention illustration [Hindman 2019], B. Endovascular robotic catheter navigating in the hepatic artery [Clements 2019], C. Robot flexible distal end including 2 working channels with a needle knife and grasper [de Moura 2019]

The issues of the path planning due to the obstruction caused by some anatomical organs while moving to the surgical target have been largely tackled; thanks to the dexterity, the flexibility, and the manoeuvrability of those continuum robot surgical tools [Petruska 2016]. Parallel to the above, the soft robotics technologies have also been applied in the urologic surgery as they can be miniaturized to the required scale. A tele-operated multi-backbone continuum robot has been designed in [Petruska 2015], for Transurethral Resection of Bladder Tumors (TURBT) procedures. A handheld robot is suggested in [Hendrick 2015] for the Transurethral Prostate Surgery to overcome the difficulties encountered for the treatment of benign prostatic hyperplasia by means of Holmium Laser Nucleation of the Prostate (HoLEP).

Better alternatives regarding the Gastroenteritis treatment have been pointed out in [de Moura 2019] regarding the comfort and the pain reduction. Soft con-

tinuum manipulators applications have also been highlighted in [Ahmed 2016] [Rosemurgy 2019], for the gastro-intestinal surgery. Parallel to this, soft continuum manipulators have been involved in Cardiac Surgery to performed MIS approaches [Gosline 2012].

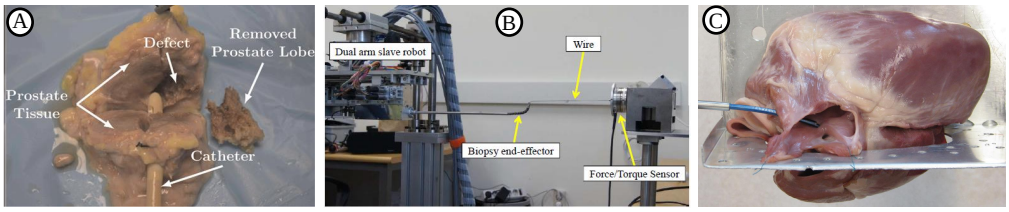

Figure 2.4: Soft continuum robots for surgery operations: A. Prostate surgery [Hendrick 2015], B. Maxillary Sinus Surgery device [Yoon 2013], C. Percutaneous intracardiac beating-heart surgery tools [Gosline 2012]

In addition to surgical robots, wearable robots are also popular applications in the field of soft robotics. New approaches using soft robotic technology have emerged with assistive and rehabilitative device designs that use soft flexible materials to support finger movement [Polygerinos 2015]. When people have lost skills regarding the use of their biological limbs, some robotic devices can safely interface with soft tissue and provide them assistance during rehabilitation. They are commonly used as a tool to assist people with disabilities [Maeder-York 2014] [Park 2014].

2.2.3.2 Agricultural applications

Soft robots have found several applications in the field of agriculture, especially for the harvesting process. Recent studies have demonstrated the effectiveness of the gripping systems and strategies based on hyper-elastic materials [Sinatra 2019].

The work of [Reed 2001] describes an approach of automated mushroom harvesting using a suction mechanism. The designed system is able to determine their pose and size, select a picking order, pick the mushrooms and trim them. The approach has been assessed using a wide range of cultivated Agaricus bisporus mushrooms. A success rate of 80% regarding mushroom pick attempts has been reported by the authors.

Tendon-driven actuation techniques have been analysed in [Gunderman 2021]. In this latter, a tendon-driven soft robotic gripper equipped with force sensors has been designed and results in maintaining a harvesting reliability of 95%. A similar approach has also been addressed in [Xiong 2018] for strawberries harvesting. The authors succeeded in minimizing the picking execution by designing a six-finger cable-driven continuum gripper with perception capabilities. Fluidic Elastomeric Actuators (FEAs) have also been investigated in [Galley 2019]. A flexible robotic gripper incorporating a pneumatically driven hyper-elastic actuator has been proposed. Polydimethylsiloxane (PDMS) material was used for this purpose. A record of 100% has been claimed with 0% of mushroom damage for each of the harvest attempt. Another soft gripper consisting of FEAs for mushroom harvesting has been

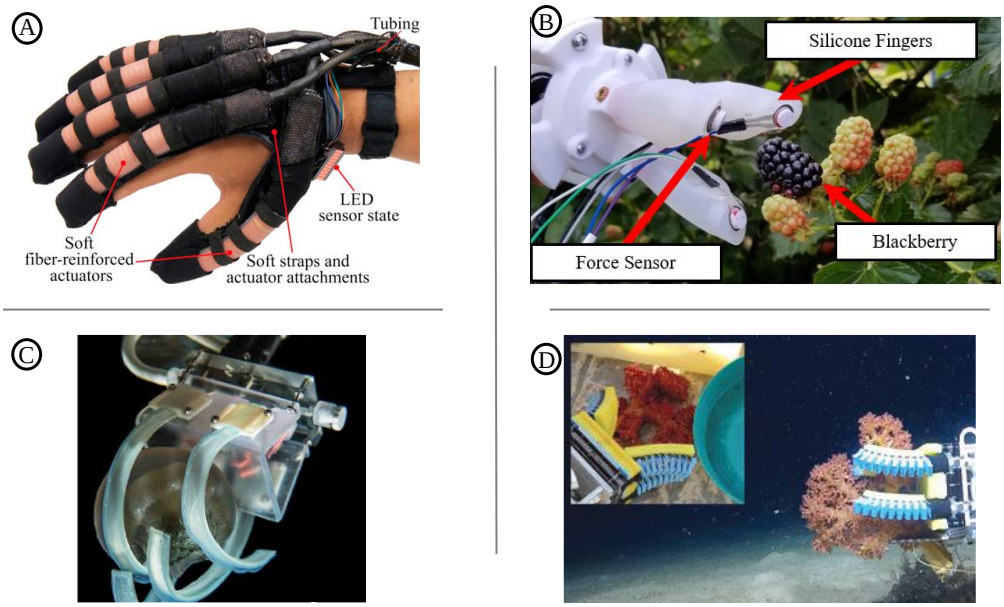

Figure 2.5: Soft continuum robots in agro-pastoral context: A. Rehabilitation glooves [Polygerinos 2015], B. Soft gripper for strawberries harvesting [Gunderman 2021], C and D. Soft fiber-reinforced actuators grasping Biological Sampling on Deep Reefs [Sinatra 2019] [Galloway 2016]

studied in [Rong 2021]. The authors proposed a three-finger gripper design, which yielded a success rate of 86.8%. [Brown 2021] has also analysed the use of FEAs for the harvesting process. A success rate of 42% has been observed by the authors when using their soft gripper with complex motion.

Other soft robotic systems have proved to be successful in grasping and manipulating delicate and underseas species. In [Galloway 2016], soft robotic grippers deployed at a depth ranging from 100 to 170 m have been discussed. The designed soft grippers could grab specimens without any removal. [Sinatra 2019] also took benefit from soft material robots to propose a grasping technique for delicate specimens of gelatinous marine life. The soft gripper is made up of 6 fibers reinforced soft actuators. The gripper is lightweight (123 g) and can be actuated using very low hydraulic pressure (1 to 6 psi, or 6.9 to 41.4 kPa, with respect to ambient).

2.3 Shape control of soft continuum manipulators

Unlike standard rigid link manipulators, whose mechanical properties have been fully discussed and mastered [Bruno 2010], the modeling of soft continuum manipulators is still an open subject in terms of modeling and control. There are three types of modeling approaches often utilized for soft continuum robots: classical methods, modeling reduction techniques, and motion planning strategies.

2.3.1 Classical techniques

The classical methods applied to the modeling and control of continuum soft robots can be classified into two main categories: **quantitative models**, highlighting a mathematical approach based on the physics of the robot, and **qualitative approaches**, which make use of experimental data in order to get the closest solutions to the given kinematic problem.

Qualitative approaches have been explored in order to tackle the modeling challenges caused by the model-based techniques. Model-free techniques [Kuntz 2020] [Zheng 2020] [Melingui 2015] simplify the complexity of the modeling, by passing through various learning algorithms. To come to more accurate modeling, some researchers have resorted to data-driven methods [Elgeneidy 2018], which require intensive modeling calibration. Data-driven techniques have found several applications, namely, for specific grasping [Zhong 2019]. As one can remark, most of the cases only focus on the tip motions of the soft continuum manipulators. Such local control methods do not allow full use of the soft robots richness in kinematic DoFs for applications that require a global control of their overall shapes such as form-enclosure grasping or obstacle avoidance strategy. In addition, the fact that these approaches can be specific to learning conditions might not be suitable for real-world applications.

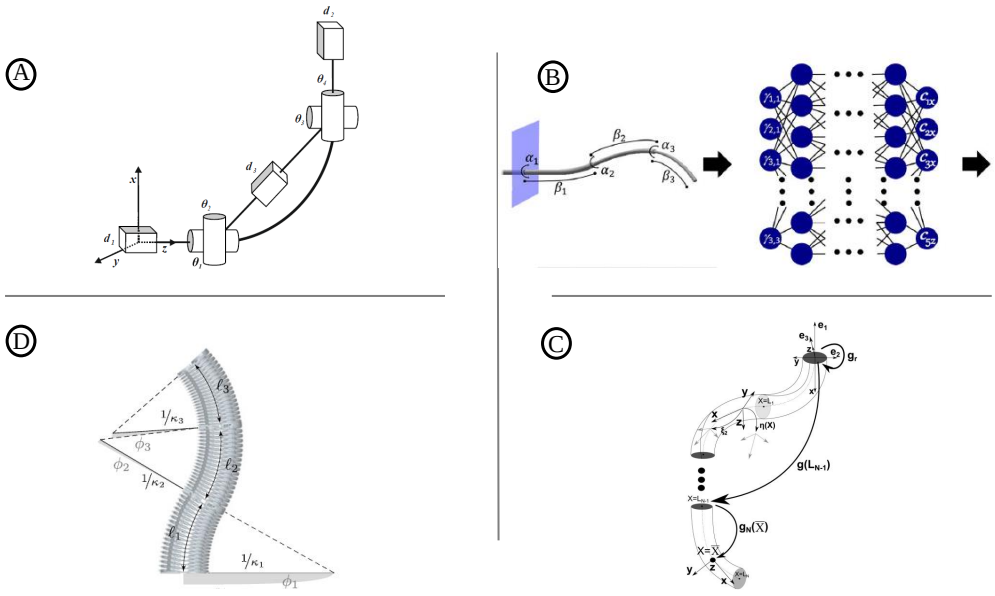

Figure 2.6: Soft continuum robots modeling approaches: A. Rigid link techniques [Hannan 2003], B. Deep neural network modeling [Kuntz 2020], C. Cosserat rod modeling techniques [Rucker 2010], D. PCC modeling method [Falkenhahn 2016]

.

Quantitative models are physical model-based approaches that use intensive mathematical formulations in order to get the convenient robot behavior. The Piecewise Constant Curvature (PCC) modeling approach is the most pop-

ular adopted in the soft robotics community [Webster III 2010]. It defines the soft robot as a finite collection of circular arcs, which can be described by only three parameters (radius of curvature, angle of the arc, and bending plane). This constitutes a significant simplification when compared to Cosserat Rod [Renda 2018a] and leads to possible analytical solutions for kinematics [Escande 2015] and dynamics [Falkenhahn 2015].

Virtual rigid links assumptions are often used [Della Santina 2019] [Katzschmann 2019], and help to address the modeling and control issues, using well-established approaches for rigid-bodied robots. Even if the PCC modeling techniques may constitute a valuable trade-off between the difficulties induced by the Cosserat rod approach and the assumptions of rigid link models [Runge 2017], most works have focused on the single Constante Curvature (CC) [Grazioso 2019] without exploiting the larger generalization provided by combining constant curvature segments [Falkenhahn 2016]. In spite of the advantages of PCC approaches, their lack of compliance, which results in significant deviations from the real robot behaviour is one of their main drawbacks. Also, the CC assumption might not always be valid, especially when the robot is subject to out-of-plane external loads, such as gravity. To overcome these modeling limitations, **elastic techniques** [Lyons 2009] [Webster, III 2009] [Renda 2012] [Trivedi 2007] [Bieze 2018b] have been largely investigated, and thus, remain the most reliable techniques for shape computation because of the material behavior taken into account while modeling the kinematics. Nowadays, these modeling approaches are mostly based on Cosserat approach or FEM.

The **Cosserat approach** [Renda 2018a] is an infinite DoFs model, where the soft robot is represented by continuously stacking an infinite number of infinitesimal microsolids. More recently, the Cosserat approach has been explicitly applied to soft robotics [Boyer 2015] [Rucker 2011]. Static and dynamic considerations have also been explored [Renda 2012] [Renda 2014], and have been extended to a wide range of soft robotics applications [Renda 2018b], [Renda 2015]. Despite their accuracy, the models based on the Rod theory are governed by nonlinear Partial Differential Equations (PDEs). These PDEs may be very time consuming for fast online simulations and real time control. Therefore, these approaches can pose several difficulties in designing and implementing in real-time, a suitable feedback control strategy. These drawbacks have motivated the scientific community to explore simpler but accurate alternative, such as FEM that can capture the kinematics and the dynamics of soft continuum manipulators with large deformations.

FEM is the most popular numerical tool used to model the kinematics and dynamics of a soft robot [Bieze 2018a]. Forward and inverse kinematics problems have been solved in [Zhang 2016], and have allowed a real-time modeling and control of the soft manipulators' deformation [Duriez 2013]. However, soft continuum manipulator models generated by FEM are very high dimensional. Analyzing such systems and designing controllers using such full-order models of infinite dimensions is not obvious. These have motivated some approaches based on model reduction, which map the entire dynamics of the soft robots to a simple and Reduced-Order-Model

(ROM).

2.3.2 ROM-based techniques

The ROM methods are modeling approaches based on the state space reduction of continuous and bounded systems of high dimensions. They proceed by discretization, and thus the difficulties in solving differential equations are simplified; thanks to a low dimensional space where, the constraints are easily considered.

ROM often proceed with weak formulations to address the complexity posed by very high dimensional spaces. The modal approach [Chirikjian 1994] remains the most popular, used in the soft robotics field. To design a controller, the integrability properties and the reduction of the state space of a solution are required. For that, several modal-based approaches such as the eigenvalues-based technique for linearized systems, spectral series [Chirikjian 1992] or power expansion series approximations [Sadati 2017] or space parametrization [Singh 2018b] for nonlinear systems, help to characterize the modes. The modal approaches can be split into 3 categories : Assumed Modes (AM) techniques, the Parametrization of the Curvature (PC), and the Parametrization of the Shape (PS). All these methods have allowed to reduce the dimension of the problem to a space of lower dimension. Table 2.2 presents a quantitative and qualitative analysis of the model reduction techniques often used in the literature.

ROM-based AM techniques allow to drastically reduce the costs and the computation time, although the accuracy of the model is reduced. They proceed by reducing the state space of a very high-dimensional system by identifying the main subsets or assumed modes. Thus, the reduction problem is solved by interpolating assumed modes in a pre-calculated base. The assumed modes are not the solution of the problem, but allow to interpolate it as well as possible or to approximate it. This simplifies the solution of the infinite spatial dimensional system into a fitting problem with a few weighting coefficients as system states, which reduces the theoretical complexity. The authors in [Sayahkarajy 2018] utilized a linear modal reduction technique to solve the dynamic modeling problems related to large deformations. It is based on the derived modes approach, and uses the Craig-Bampton technique to realize the coupling between the different reduced subsets. A third-order polynomial interpolation approach, whose coefficients have been pre-calculated, has been used for shape kinematic modeling. The author's approach allows a significant reduction in computation time. In the work of [Wu 2016], an iso-geometric collocation method is described. The authors make use of a parametrization of the structure by means of Non-Uniformal Rational B-Splines (NURBS) curves to accurately describe the mean line of the shape of the studied soft continuum manipulator. The Cosserat Rod approach is used for dynamic modeling. The data obtained from this latter are then used to describe the kinematics of the robot via the parameterization performed by the NURBS, while the geometric collocation allows specifying the geometric modes, namely, the control points of the curve according to the observed dynamics. A polynomial spectral collocation method has also been extensively dis-

cussed in [Weeger 2017]. Based on this approach, the spatial configuration of a soft manipulator has been reduced using the discrete Kirchhoff model applied to two different classes of control points of the polynomial curve (representative of the kinematics to be described). The results of this approach, unlike the previous one, allow describing a 3D kinematics of a soft robot subjected to external interactions. The results of their work showed that the accuracy of their technique is very sensitive to the number of nodes used for the polynomial interpolation. Later, non-linear normal modes, representing a non-linear system with linear eigenspaces, have been investigated by [Della Santina 2018] to address the elastic joint stabilization of robots. In this study, the author succeeded in characterizing a subspace of a reduced dimensionality on which the system would naturally evolve.

ROM-based PS approaches for soft continuum manipulators are widely discussed in the literature. The Lagrangian formulation for Shape Functions (SF) has been investigated in [Godage 2011], where the researchers used the Taylor series with a 6^{th} order approximation. This method simplified the shape kinematics complexity caused by the dynamics, and the infinite dimension of the shape kinematics modeling was reduced to a problem of 56 unknowns. The analyses made in [Sadati 2017] introduced a ROM technique for continuum robots dynamics control based on the Principle of Virtual Works (PVW). An approximate series-solution has been used for the kinematics while reconstructing the robot shape by fitting the Lagrange polynomial function at control points. These control points have been defined as the system modeling states. They have been used to describe the continuum manipulator shape kinematics. [Boyer 2020] has based some investigations on the Cosserat-Rod modeling technique to minimize the set of Ordinary Differential Equations (ODEs). The authors succeeded in improving the computation time of the robot dynamics modeling. They used a new reduced inverse Newton-Euler algorithm. Parallel to this, another dynamics modeling based on Cosserat-Rod has been suggested with the use of Magnus series solutions for dimension reduction purposes [Orekhov 2020]. Polynomial fitting techniques have also been used in that case for the shape kinematics reconstruction. In recent years, parametric curves-based techniques have been intensively explored for ROM in the static case. The investigation of [Singh 2018b] has solved the kinematics of continuum robots using a PH curve to reconstruct the overall robot shape. As well as in [Wiese 2019], a reduced number of the curve control points is highlighted for the kinematics modeling. These have allowed an accurate shape kinematic computation in a static context. Their technique differs from the others because of the boundary conditions, namely, the endpoint poses (position and orientation), taken into account within the formulation. The potential energy minimization criterion is considered in the formulation to specify the optimal position of these control points. Another key feature of this modeling is the shape-preserving properties: the reconstructed shape always follows the control polygon. The PH quintic polynomial curve appears to be the smallest degree PH curve allowing the reconstruction of very complex shapes. In addition, among polynomial curves, they appear to be unique in having arc lengths that are exactly determined by simple algebraic expressions in their coefficients. These might offer

the possibility of modeling soft continuum actuators while considering their spatial arc length. Therefore, the workspace computation might be greatly simplified.

ROM-based PC methods have also been explored. Many works demonstrated that these methods have one less state compared to Cartesian space parametrization used for the PS approach. However, deriving the Cartesian parameters is still required for calculating the local effect of external loading and the system inertial dynamics. In a recent work, [Della Santina 2019], a model-based shape control using a finite order polynomial curvature method is suggested for soft continuum robots kinematics modeling. Instead of operating a spatial discretization as discussed in the above techniques, the authors described the robot with a curvature function in the standard polynomial base of the Hilbert space. In this way, the continuum shapes are specified as a mathematical series with the CC approximation as the first term, and linear curvature approximations for the other terms. These allow addressing the issues related to the infinite-dimensional formulation of the problem. Also, they have enabled the authors to lower the modeling order by order truncation according to the desired accuracy. In recent research, [Della Santina 2020c] proposed a dynamical feedback controller to stabilize a desired trajectory in the curvature space. A dimension reduction has been analyzed using an augmented formulation linking a soft robot to a classic rigid serial manipulator under the PCC hypothesis. An augmented state space of six dimensions has been designed. The required shape features of the soft continuum manipulator have been mapped. The equivalent vector has been then used for the controller design. Later in [Della Santina 2020b], a topology reduction for robot kinematics with singularities-free has been developed to control soft robot shape dynamics. A new bending parametrization for PCC approximation is outlined by the authors to overcome some unsuitable behaviors issued from the common PCC approaches often used. Based on some comparison studies, the latter has been claimed as an improvement for PCC modeling techniques to address singularity issues. An extension to external interactions with high accelerations has been studied in [Della Santina 2020a]. The issues related to infinite DoFs using a finite dimension reduction approach have also been addressed.

2.3.3 MOR-based techniques

Model reduction aims at simplifying the complexity of physical systems in terms of dimension and computational cost [Benner 2005], [Panzer 2010]. Modeling-Order-Reduction (MOR) techniques are used to reduce the state space dimension of an already developed soft robot FEM model. MOR, unlike ROM, is not a modeling technique. It refers to a computational approach. In [Thieffry 2018b], [Goury 2018], a MOR technique was proposed to represent the full-order dynamics model by a subset of the large Finite Element mesh elements using Proper Orthogonal Decomposition (POD), a snapshot POD. The POD was on a linearized FEM model around an equilibrium point. This has enabled the formulation of a stable observer and controller for the reduced linearized system. The work of [Thieffry 2018a] highlights a state feedback controller in the states of the reduced subspace. This approach

is also discussed in the research works of [Ficuciello 2018] [Koehler 2019], and has proved to be very computationally efficient.

2.3.4 Motion planning approaches

Several studies [Lamiraux 2001a] have been devoted to the modeling and control of the shape of MSCM using the classical path planning techniques often used for mobile robots. Most of them use sampling-based approaches. These methods require prior information about the entire workspace, i.e., a mathematical representation to describe the workspace. They typically sample the environment as a set of nodes, cells, or other shapes. Then the environment is mapped, or a random search is performed to obtain a feasible path. Sampling-based approaches can be subdivided into two categories: active and passive methods. Active methods, such as Rapid Random Tree (RRT) or APF, can obtain the best possible path to the goal by their processing procedure. Passive algorithms, such as PRM, only generate a road network from start to finish, thus, a combination of search algorithms to find the best feasible path in the network map where many feasible paths exist.

The RRT approach, proposed first by [LaValle 1998], aims at solving path planning problems under holonomic and non-holonomic constraints. The RRT method has the advantage of handling hyper-redundancy problems [Chitta 2012], even though it does not take into account information from local environments, thereby causing inappropriate sampling, which can lead to low time efficiency. RRT algorithm has been performed in [Roussel 2014b] and [Roussel 2014a] for deformable robotic structures in complex environments. The algorithm has been applied to a catheter for liver chemoembolization. While using the RRT method, similar results have also been reported in [Kuntz 2017] for surgical operations. The proposed sampling-based motion planner has been able to avoid collisions with anatomical obstacles inside the body. Although the RRT approach is a good planning technique, the quality of the results is not guaranteed. To address this issue mainly related to the asymptotic convergence of the RRT method, the authors of [Karaman 2010] introduced a Rapid Random Graph (RRG). Several experimental results of RRG show its effectiveness compared to other RRT-based path planning techniques. [Torres 2015] has made use of this approach to achieve automatic collision avoidance by precomputing a roadmap of collision-free robot configurations based on a description of the anatomical obstacles. The motion planning approach has been used for the teleoperation of concentric tube robots with automatic obstacles avoidance along with the entire structure. Although RRT can find a path to the goal, there remains a problem because RRT relies on the Monte Carlo random sampling, which biases the explored region as it increases with time. Thus, the method will take a long time to find a way out when the environments are cluttered.

Unlike RRT, the Probabilistic Road Map (PRM) considers different choices for the set of states to which connections are checked. PRM [Kavraki 1996] is the first popular multiple query method for constructing a road map using a sampling approach. In [Lamiraux 2001b], a path planning has been analysed using Proba-

Table 2.2: Reduced-Order-Models and Model-Order-Reduction for soft continuum robots in the litterature

Categories	**MOR** (Compression)		**ROM**			
Solution	FEM		Series Solution (Modal)			
SF	POD modes		Mode Shapes			
SF Selection	PCA Analysis		Assumed modes (shape functions)			
Method	POD			Power series	Configuration fitting	
SF Index	Principle Component Index		Wave number	Power	Control point index	
Types	Nonlinear System	Linearized System	Harmonic	Continuous polynomials	Lagrange polynomials	Hermite, Bezier, PH, BSplines, NURBS
States	Element's deformation & velocities	Element's deformation & velocities	Modal participation coefficients	Continuous polynomials	Control points' Cartesian states	Fitting method control parameters (Cartesian points and local slopes)
Control	Jacobian inverse	Jacobian inverse	Feedback linearization	Feedback linearization, Inverse Jacobian/map	not applicable	Inverse kinematics
Advantages	The most accurate ROM, faster than FEM, Can be real-time	Faster than FEM, Can be real-time	Convergence guarantee, Real-time , Computationally efficient	Convergence guarantee, Real-time, Dynamic Implementation	Easy states' tracking, Real-time	Easy states' tracking, Real-time, handles discontinuity
Drawbacks	Needs a prior FEM model, Computationally expensive, Complex states without physical meanings	Needs a prior FEM model, Linearization inaccuracy, Complex states without physical meanings	Nontrivial shape functions, Less accurate than MOR, Integration issues for VC kinematics	IC solution sensitive to Runge's phenomenon, First order is parabolic not CC, No discontinuity	Converges only with special point placement, Extra state needed for curvilinear frame twist	Extra state needed for curvilinear frame twist, Complex modes, Non linear optimization
References Illustration	[Goury 2018]	[Thieffry 2018b] [Thieffry 2018a]	[Chirikjian 1994]	[Sadati 2019] [Della Santina 2020c] [Godage 2016] [Della Santina 2020b] [Grazioso 2019]	[Sadati 2017]	[Singh 2018b] [Della Santina 2020a]

SF: Shape Function, POD: Proper Orthogonal Decomposition, PCA: Principal Components Analysis

Table 2.3: **Analysis of sampling based algorithms**

Methods	Drawbacks	Advantages
RRT	Single path, Non Optimal, Static threat only	Low time complexity, fast searching ability
RPM	Expensive collision check, Static threat only, Nonoptimal	Appropriate for complex environments and replanning situations
APF	Local minima	Fast convergence

bilistic Road Map (PRM) after sampling the configuration space of the robot. The computation of stable configurations of the soft robot has been done, subject to manipulation constraints using a global energy minimization. A modeling based on minimal-energy curves has also been highlighted by [Moll 2006]. This modeling is coupled with PRM to address space configuration issues. Rather than sampling the configuration space of the soft continuum manipulator, [Gayle 2005] used the PRM for sampling the workspace. The path is generated for each point of the soft robot in the road map, in order to drive the soft structure as long as the physical constraints are satisfied. A recent investigation [Kuntz 2019] has based on PRM to propose surgical robots. The approach is coupled with a local optimization to drive a concentric tube robot in order to avoid obstacles.

The APF approach for mobile robot navigation has been first introduced in [Khatib 1986]. The robot follows the negative gradient to avoid the obstacle and reach the desired target point. Since then, several works in the scientific community have adopted it to describe the kinematics of soft robots for shape control purposes when avoiding obstacles. In [Ataka 2017], the author computed APF-based motion planning strategy for MSCM in dynamic environments. The results showed that their investigations can be a promising alternative for a dynamic industrial environment. Another work presented in [Hilario 2011] has applied the same method to modify the shape of Bezier curves, representing the path of a mobile robot. However, such a planning motion method often suffers from local minima issues where the robots are prone to be trapped. They are often subject to oscillations and Goals Non Reachable with Obstacle Nearby (GNRON) problem. Many contributions have been proposed to overcome the local minima issues using navigation functions or APF with constraints. Amongst many others, [Connolly 1990] has discussed on a APF-based Harmonic function [Kim 1992] using Laplace equation to constrain the generation of a potential function. In [Montiel 2015], alternatives to solve local minimum issues in the dynamic environment have been suggested by considering the dynamics robots navigation [Borenstein 1989]. [Rimon 1992] proposed a Morse function with a single minimum at the desired destination strategy to form a strong and stable robot navigation method to jump out of the local minima. That was the

first formally proposed navigation method. Then, the GNRON problem has been tackled in [Ge 2000] with the introduction of a new repulsive artificial potential field. This latter has allowed the development of a superior potential function and a superior repulsive potential function [Shi 2009]. An improved version of the APF has been considered by [Sfeir 2011]. The authors' approach minimizes the oscillation and conflicts when the target is close to the obstacle. A summary of the performances of the sampling based approaches often used for soft manipulators motion planning is summarized in Table 2.3.

2.4 Thesis Positioning with Respect to the Literature

Given the preceding, the modeling of the shape of MSCM using parametric polynomial curves proves to be a promising alternative because of the balance between the accuracy and the computational time, which allows for the control compared to MOR-based techniques. Although these latter are more accurate and realistic, some key issues remain regarding the need for a prior FEM model, which is costly computation-wise. As a result, expensive and specialized hardware might be required for real-time applications. Despite the advantages of spectral and power series modeling approaches in terms of real-time implementation, they are limited compared to parametric polynomial curves, which can master discontinuity issues, particularly those involving complex shape functions and Runge's phenomenon sensitivity.

Regarding the parametric polynomial curves, Lagrange polynomials curves appear not to allow any control strategy and only converge for special points placement. Bernstein basis functions are used in the case of Bezier and PH curves, and B-Spline basis functions are used for Bézier Splines (B-Spline) and NURBS curves. The solutions of Bernstein basis functions are analytical, and the solutions to the B-Spline basis functions are iterative. It implies that Bernstein's basis functions are computationally effective compared to B-Spline and NURBS curves. In addition, the calculation of the length of the curve does not have the closed-form solution in the case of Hermite, Bezier, B-Spline , and NURBS. Therefore, numerical methods are needed to approximate the solutions of their length, while in the case of PH-curves, the length calculation has a closed-form solution. Intensive investigations on parametric curves modeling technique are discussed in [Singh 2018a] [Singh 2017] [Singh 2018c].

In the light of the above reviews, the present investigation has been oriented to ROM-based PH for dynamic shape control. A principal aspect regarding the PH curve modeling is the consistency concerning bending energy minimization criteria of a physical system.

The real-time dynamic control of the shape of soft manipulators combines the traditional techniques and the motion planning approaches because of the consideration of environmental constraints. APF-based motion planning coupled with a Sliding Mode Control, is applied to the PH-curve modeling to drive the robot shape

while navigating in unstructured environments for various tasks. The APF-based algorithm has the advantage of allowing fast convergence, suitable for real-time control. The APF-based strategy is only applied on the control points of the PH curves (rather than all the points of the curves), while the suggested Sliding Mode control law allows the curve to meet optimal bending energy requirements during its motion. Thanks to Euler-Bernoulli's modeling techniques, the physical control inputs are mapped to the motion of the control points driving the curve posture. This operation allows mapping the physical control inputs to the shape of the soft continuum manipulator, suitable for adaptive shape control.

2.5 Conclusion

The current literature studies illustrate the interest of the scientific community regarding the shape control of MSCM. However, very few works are devoted to this subject. For real-time control applications, several simplified modeling approaches exist. Amongst these latter, PCC techniques remain the widely used although ROM-based techniques and MOR approaches are emerging as the most promising alternatives. However, several limitations related to these classical approaches are claimed, in particular about the non-consideration of the local environmental constraints for the shape kinematics control of MSCM. Many of them appear to deal with the pose control of the soft robot tip only. This may be very compromising for navigation operations in confined spaces. To tackle these limitations, control methods based on trajectory planning techniques have been analyzed. They are an effective solution to the difficulties raised in the context of MSCM motion control. The advantage of these methods compared to conventional control methods is that the environmental constraints are considered. The combination of the classical techniques and the trajectory planning is indispensable for MSCM shape control. However, the shape control remains unclear if there is no explicit relation between the physical control inputs and the shape of the soft continuum manipulator. These major issues constitute one of the main interests of the present research works.

Chapter 3

Shape Kinematic Control Soft-Continuum Manipulators: PH-APF approach

Contents

3.1 Introduction

This research work aims to provide a framework that would allow to compute the shape kinematic control of MSCM. To come to this end, the present chapter discusses the inverse kinematics as well as the forward kinematics modeling of MSCM by means of quintic Pythagorean Hodograph (PH) curves. These quintic PH curves have proved to be enough to describe very complex shape kinematics [Farouki]. The

PH curves are formulated with a predefined length and hence, allow to efficiently take into consideration the workspace of the soft continuum manipulators. The bending energy optimization taken into consideration allows the system to achieve its optimal shape kinematics during the motion. The configuration states of the system are described by the position of the control points. All these have allowed to describe the shape high order kinematics with five control points only. Therefore, the Inverse Kinematics Modeling (IKM) is to compute the MSCM shape by specifying its control points poses, from the knowledge of its end points pose. While, the Forward Kinematics Modeling (FKM) is to specify the posture from the independent motions of the control points. APF-based motion control is applied on the control points to drive the shape of the soft continuum manipulators accordingly. The Sliding Mode strategy is coupled to Artificial Potential Field (APF) strategy to guarantee that the configuration states of the system are consistent with optimal bending energy requirements.

3.2 PH-based Inverse Kinematics Modeling (PH-IKM)

The kinematics of the MSCM can be described by a set of infinite DoFs, which make complex its shape control. In this section, the soft continuum manipulator is modeled by parametric PH curves. This allows reconstructing the soft continuum manipulator shape, by considering the overall total bending energy of the curve. Two types of shape reconstruction by PH can be applied to the soft continuum manipulator: a static shape reconstruction [Singh 2018b], defined at one time instant; a continuous shape reconstruction, when the curve is varying with the time. The following development focuses on continuous shape reconstruction for the control [Mbakop 2020] [Mbakop 2021a]. For that, in addition to the optimization of bending energy of the curve, other geometric constraints need to be imposed such as the curve length. Thus, the control points of the curve of the soft continuum manipulator are placed optimally according to its unstructured environment. To obtain the PH parametric curve-based model of the soft continuum manipulator for continuous shape reconstruction, the following steps are considered.

3.2.1 Quaternion form of PH curve of the soft continuum manipulator using complex polynomials functions

The aim is to establish an explicit form of the PH of the instantaneous posture of the MSCM with a predefined length in the space. This form will be used to establish the interpolation conditions considering length constraints of the MSCM.

The quaternion form is chosen to simplify the writing in 3D. However, the length constraint is not trivial in its quaternion form but in complex one. Thus, a relation linking the complex formulation and the quaternion one of the hodograph is given.

Let us consider (p_s, d_s) , (p_f, d_f), respectively the pose of the starting point of the MSCM curve (i.e. mobile base) and the pose of the final point of the MSCM curve (i.e. tip of the continuum manipulator). p_s, p_f describe the Cartesian positions and

d_s, d_f their respective directions, given in **polar** form (3.17). Thus, the posture of the MSCM can be written as follows, after considering the normalized curvilinear coordinate ξ $(0 \leq \xi \leq 1)$, along the MSCM of length L :

$$p(\xi) = (x(\xi), y(\xi), z(\xi)); \qquad 0 \leq \xi \leq 1 \tag{3.1}$$

then, the following expressions are obtained:

$$\begin{aligned} p_s &= p(0) = (x(0), y(0), z(0)), \qquad \xi = 0 \\ p_f &= p(1) = (x(1), y(1), z(1)), \qquad \xi = 1. \end{aligned} \tag{3.2}$$

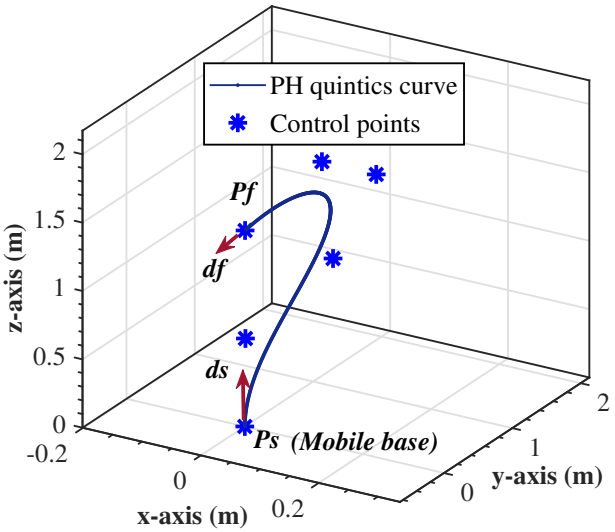

Figure 3.1: 3D Posture of soft continuum manipulator using PH curve

The MSCM boundaries conditions namely, the poses of p_s , p_f, and the MSCM length are consistent with a PH quintic formulation, necessary for the shape reconstruction. PH can be expressed in quaternion polynomial form [Choi 2002], or in complex polynomial form [Farouki 1990]. First, the PH curve $p(\xi)$ and its hodograph $p'(\xi) = (x'(\xi), y'(\xi), z'(\xi))$, namely the first derivative can be expressed in function of quaternion polynomial $\mathcal{A}(\xi)$ and its conjugate $A^*(\xi)$, as follows:

$$\begin{aligned} \mathcal{A}(\xi) &= u(\xi) + v(\xi)\mathbf{i} + r(\xi)\mathbf{j} + q(\xi)\mathbf{k} \\ \mathcal{A}^*(\xi) &= u(\xi) - v(\xi)\mathbf{i} - r(\xi)\mathbf{j} - q(\xi)\mathbf{k} \end{aligned} \tag{3.3}$$

where $\mathbf{i}, \mathbf{j}, \mathbf{k}$ represent the 3 quaternions basis elements of the set of quaternions $\mathbb{H}$. u, v, r and q define polynomial functions. In that case:

$$p'(\xi) = \mathcal{A}(\xi)\mathbf{i}\mathcal{A}^*(\xi) \tag{3.4}$$

with,

$$\begin{aligned} x'(\xi) &= u^2(\xi) + v^2(\xi) - r^2(\xi) - q^2(\xi) \\ y'(\xi) &= 2u(\xi)q(\xi) + 2v(\xi)r(\xi) \\ z'(\xi) &= 2v(\xi)q(\xi) - 2u(\xi)r(\xi) \end{aligned} \tag{3.5}$$

Second, the PH curve $p(\xi)$ and its hodograph $p'(\xi)$ can be expressed in function of complex polynomials $\alpha(\xi)$ and $\beta(\xi)$ as follows:

$$\alpha(\xi) = u(\xi) + iv(\xi), \qquad \beta(\xi) = q(\xi) + ir(\xi). \tag{3.6}$$

Thus,

$$\begin{aligned} x'(\xi) &= |\alpha(\xi)|^2 - |\beta(\xi)|^2, \\ y'(\xi) &= 2\mathrm{Re}(\alpha(\xi)\overline{\beta}(\xi)), \\ z'(\xi) &= 2\mathrm{Im}(\alpha(\xi)\overline{\beta}(\xi)), \end{aligned} \tag{3.7}$$

with $\overline{\beta}$ the conjugate of β.

To obtain the same $p'(\xi)$ expressed in Eq. 3.5 and Eq. 3.7, the quaternion polynomial $\mathcal{A}(\xi)$ should be expressed in function of complex polynomials $\alpha(\xi)$ and $\beta(\xi)$, as follows :

$$\mathcal{A}(\xi) = \alpha(\xi) + \ \mathbf{k}\beta(\xi) \tag{3.8}$$

where the imaginary unit i is considered equivalent to the quaternion basis element $\mathbf{i}$.

3.2.2 End points interpolation using length constraints

Now, the quaternion form of the PH has been reduced through a complex formulation, the equations governing the interpolation at the end points of the curve as well as the one considering the length constraint can be obtained. The main objective is to establish a system Eq. 3.15 to uniquely determine the coefficients α_m and β_m of the polynomial functions α and β, written with regard to Bernstein form as described by Eq. 3.14.

The parametric velocity polynomial $\Gamma(\xi)$ is then expressed as follows:

$$\Gamma(\xi) = |p^{'}(\xi)| = |\mathcal{A}(\xi)|^2 = |\alpha(\xi)|^2 + |\beta(\xi)|^2 \tag{3.9}$$

Integrating $p'(\xi) = (x'(\xi), y'(\xi), z'(\xi))$ of Eq. 3.7 leads to end points displacement ($\Delta\mathbf{p} = p_f - p_s$) satisfaction, described by equations Eq. 3.10 and Eq. 3.11 as follows:

$$\int_0^1 |\alpha(\xi)|^2 - |\beta(\xi)|^2 \, \mathrm{d}\xi = \Delta x. \tag{3.10}$$

$$\int_0^1 2\alpha(\xi)\overline{\beta}(\xi) \, \mathrm{d}\xi = \Delta y + i\Delta z. \tag{3.11}$$

while the MSCM length constraint is calculated after integrating the equation Eq. 3.9 as follows:

$$\int_0^1 |\alpha(\xi)|^2 + |\beta(\xi)|^2 \, \mathrm{d}\xi = L. \tag{3.12}$$

After combining Eq. 3.10 with Eq. 3.12, the following relations are obtained:

$$\begin{aligned}\int_0^1 |\alpha(\xi)|^2 \,\mathrm{d}\xi &= \frac{1}{2}(L+\Delta x),\\ \int_0^1 |\beta(\xi)|^2 \,\mathrm{d}\xi &= \frac{1}{2}(L-\Delta x).\end{aligned} \tag{3.13}$$

Note that, PH quintic curve can be generated by complex polynomials using **Bernstein** form:

$$\begin{aligned}\alpha(\xi) &= \alpha_0(1-\xi)^2 + 2\alpha_1(1-\xi)\xi + \alpha_2\xi^2\\ \beta(\xi) &= \beta_0(1-\xi)^2 + 2\beta_1(1-\xi)\xi + \beta_2\xi^2\end{aligned} \tag{3.14}$$

The canonical form ($\mathbf{\Delta p} = (1,0,0)$) should be adopted without out loss of generality. By replacing Eq. 3.14 into Eq. 3.11 and Eq. 3.13, the following is obtained:

$$\begin{cases} [4\alpha_1 + 3(\alpha_0+\alpha_2)][4\overline{\beta}_1 + 3(\overline{\beta}_0+\overline{\beta}_2)] \\ \quad = 5[\alpha_0\overline{\beta}_2 + \alpha_2\overline{\beta}_0 - 3(\alpha_0\overline{\beta}_0 + \alpha_2\overline{\beta}_2)], \\ |4\alpha_1 + 3(\alpha_0+\alpha_2)|^2 \\ \quad = 5[12(L+1) - 2(|\alpha_0|^2 - |\alpha_2|^2) - |\alpha_0 - \alpha_2|^2], \\ |4\beta_1 + 3(\beta_0+\beta_2)|^2 \\ \quad = 5[12(L-1) - 2(|\beta_0|^2 - |\beta_2|^2) - |\beta_0 - \beta_2|^2]. \end{cases} \tag{3.15}$$

It can be observed that the system of equations Eq. 3.15 consists in determining the couples of (α_q, β_q), where $q = 0, 1, 2$.

The quintic PH curve has been considered for the shape modeling of the soft continuum manipulator, because the latter can have a maximum of 2 inflection points. Quintic PH curve is a polynomial curve of degree 5, which allows reconstruction of curvilinear geometries with 6 control points (2 end points and 4 intermediate points). The canonical form ($\mathbf{\Delta p} = (1,0,0)$) should be adopted without loss of generality. By substituting Eq. 3.14 into Eq. 3.11 and Eq. 3.13, the system obtained is consistent with Eq. 3.16.

3.2.3 Calculation of Bernstein coefficients

To guarantee optimal solutions in the case of a predefined length, the symmetry conditions of the end directions (tangents) interpolations should be applied. Thus, the solutions do not depend on the norm of the direction vectors but only on the directions themselves. For this purpose, the end direction vectors are all formulated as μ-proportional to the associated unit vectors, expressed in polar form Eq. 3.17 and Eq. 3.18. Thus, to have the first equation of Eq. 3.15 compatible with the remaining, the following relation is obtained:

$$\begin{aligned}&|\alpha_0\overline{\beta}_2 + \alpha_2\overline{\beta}_0 - 3(\alpha_0\overline{\beta}_0 + \alpha_2\overline{\beta}_2)|^2\\ =&[12(L+1) - 2(|\alpha_0|^2 - |\alpha_2|^2) - |\alpha_0 - \alpha_2|^2]\\ \cdot&[12(L-1) - 2(|\beta_0|^2 - |\beta_2|^2) - |\beta_0 - \beta_2|^2]\end{aligned} \tag{3.16}$$

By specifying the unit end tangents in terms of polar and azimuthal angles, relative to x-axis as follows:

$$\begin{aligned} d_s &= (\cos\theta_s, \sin\theta_s\cos\phi_s, \sin\theta_s\sin\phi_s), \\ d_f &= (\cos\theta_f, \sin\theta_f\cos\phi_f, \sin\theta_f\sin\phi_f), \end{aligned} \tag{3.17}$$

the interpolation at end tangents yields to:

$$\begin{aligned} \alpha_0 &= \mu c_s \exp(i\phi_s)\exp(i\psi_0), \qquad \beta_0 = \mu s_s \exp(i\psi_0), \\ \alpha_2 &= \mu c_f \exp(i\phi_f)\exp(i\psi_2), \qquad \beta_2 = \mu s_f \exp(i\psi_2), \end{aligned} \tag{3.18}$$

where ψ_0 and ψ_2 are free angular parameters [Farouki 2002] and c_s and s_s are defined as:

$$\begin{aligned} (c_s, s_s) &= (\cos\frac{1}{2}\theta_s, \sin\frac{1}{2}\theta_s), \\ (c_f, s_f) &= (\cos\frac{1}{2}\theta_f, \sin\frac{1}{2}\theta_f). \end{aligned} \tag{3.19}$$

The use of Eq. 3.18 in Eq. 3.16 leads to the following reduced bi-quadratic equation [Farouki 2019]:

$$p(\mu^2) = c_2\mu^4 + c_1\mu^2 + c_0, \tag{3.20}$$

where

$$\begin{cases} c_2 = 2(c_s^2 s_f^2 + s_s^2 c_f^2) - 4c_s s_s c_f s_f \cos\Delta\phi, \\ c_1 = 6[(L-1)c_s c_f \cos(\Delta\phi + \Delta\psi) \\ \quad + (L+1)s_s s_f \cos\Delta\psi - 3L] + 9(c_s^2 - s_s^2 + c_f^2 - s_f^2), \\ c_0 = 36(L^2 - 1). \end{cases} \tag{3.21}$$

3.2.4 Optimal position of the control points

As one can remark, the coefficients of α_q and β_q, where $q = 0, 1, 2$, reflect the length features of the MSCM. However, the minimization of the potential energy needs to be determined for optimal shape reconstruction. In view of Eq. 3.18, the minimal values of $\mu \geq 0$ minimize the quaternion polynomials in Eq. 3.22 and Eq. 3.24. This implies a minimization of the potential energy from Eq. 3.27 and Eq. 3.28.

After having formulated that $\mathcal{A}(\xi) = \alpha(\xi) + \mathbf{k}\beta(\xi)$ in Eq. 3.8, the complex polynomial Eq. 3.6 can be expressed by the following quaternion polynomial :

$$\mathcal{A}(\xi) = \mathcal{A}_0(1-\xi)^2 + 2\mathcal{A}_1(1-\xi)\xi + \mathcal{A}_2\xi^2.$$

Then, the interpolation of the tangents of end points yields to the coefficients $\mathcal{A}_0 = \alpha_0 + \mathbf{k}\beta_0$ and $\mathcal{A}_2 = \alpha_2 + \mathbf{k}\beta_2$. Both are obtained from Eq. 3.18 with regard to Eq. 3.8 as follows:

$$\begin{aligned} \mathcal{A}_0 &= \mu[c_s \exp(\phi_s\mathbf{i}) + s_s\mathbf{k}]\exp(\psi_0\mathbf{i}), \\ \mathcal{A}_2 &= \mu[c_f \exp(\phi_f\mathbf{i}) + s_f\mathbf{k}]\exp(\psi_2\mathbf{i}), \end{aligned} \tag{3.22}$$

where the imaginary unit i is identified with the quaternion element $\mathbf{i}$.

The satisfaction of the arc length constraints is achieved by choosing the positive smaller root μ^2 of Eq. 3.20. The end point displacement $\Delta\mathbf{p}$ allows us to define $\mathbf{d}$ as:

$$\mathbf{d} = 120\Delta\mathbf{p} - 15\mu^2(d_s + d_f) + 5(\mathcal{A}_0\mathbf{i}\mathcal{A}_2^* + \mathcal{A}_2\mathbf{i}\mathcal{A}_0^*). \tag{3.23}$$

The coefficient $\mathcal{A}_1$ is thus carried out through the end point displacement interpolation by the following expression:

$$\mathcal{A}_1 = -\frac{3}{4}(\mathcal{A}_0 + \mathcal{A}_2) + \frac{\sqrt{|\mathbf{d}|}}{4}\frac{|\mathbf{d}|\mathbf{i} + \mathbf{d}}{|(|\mathbf{d}|\mathbf{i} + \mathbf{d})|}\exp(\psi_1\mathbf{i}), \tag{3.24}$$

where ψ_1 is a free angular parameter. The knowledge of $\mathcal{A}_0, \mathcal{A}_1$ and $\mathcal{A}_2$ enables to completely define the control points p_k in the $p(\xi)$ Bézier form :

$$p(\xi) = \sum_{k=0}^{5} p_k \binom{5}{k} (1-\xi)^{5-k}\xi^k, \tag{3.25}$$

Thus, expression Eq. 3.25 describes the **PH-based Forward Kinematics Modeling (FKM)**. After formulating each PH quintic control points, the following expression is obtained :

$$\begin{aligned}
&p_1 = p_0 + \frac{1}{5}\mathcal{A}_0\mathbf{i}\mathcal{A}_0^*, \quad p_2 = p_1 + \frac{1}{10}(\mathcal{A}_0\mathbf{i}\mathcal{A}_1^* + \mathcal{A}_1\mathbf{i}\mathcal{A}_0^*),\\
&p_3 = p_2 + \frac{1}{30}(\mathcal{A}_0\mathbf{i}\mathcal{A}_2^* + 4\mathcal{A}_1\mathbf{i}\mathcal{A}_1^* + \mathcal{A}_2\mathbf{i}\mathcal{A}_0^*),\\
&p_4 = p_3 + \frac{1}{10}(\mathcal{A}_1\mathbf{i}\mathcal{A}_2^* + \mathcal{A}_2\mathbf{i}\mathcal{A}_1^*), \quad p_5 = p_4 + \frac{1}{5}(\mathcal{A}_2\mathbf{i}\mathcal{A}_2^*),
\end{aligned} \tag{3.26}$$

with: $p_f = p_5$ and $p_s = p_0$. If p_f is well identified, then expression Eq. 3.26 will describe the **PH-based Inverse Kinematics Modeling (IKM)** of the MSCM.

The successive derivatives of $p(\xi)$ can be expressed as follows:

$$\begin{aligned}
&p'(\xi) = \mathcal{A}(\xi)\mathbf{i}\mathcal{A}^*(\xi),\\
&p''(\xi) = \mathcal{A}'(\xi)\mathbf{i}\mathcal{A}^*(\xi) + \mathcal{A}(\xi)\mathbf{i}\mathcal{A}'^*(\xi),\\
&p'''(\xi) = \mathcal{A}''(\xi)\mathbf{i}\mathcal{A}^*(\xi) + 2\mathcal{A}'(\xi)\mathbf{i}\mathcal{A}'^*(\xi) + \mathcal{A}(\xi)\mathbf{i}\mathcal{A}''^*(\xi).
\end{aligned} \tag{3.27}$$

The potential energy should therefore be evaluated. For a curve-based kinematic model, it can be written in the canonical form as follows: :

$$E_p = \frac{1}{2}\int_0^L |\omega(h)|^2 \,\mathrm{d}h. \tag{3.28}$$

If the normalized parameter is chosen, one can remark that:

$$\mathrm{d}h = \frac{\mathrm{d}h}{\mathrm{d}\xi}\mathrm{d}\xi \text{ and } \frac{\mathrm{d}h}{\mathrm{d}\xi} = \Gamma(\xi).$$

$$\kappa(\xi) = \frac{|p'(\xi) \times p(\xi)''|}{|p'(\xi)|^3},$$
$$\tau(\xi) = \frac{(p'(\xi) \times p''(\xi)).p'''(\xi)}{|p'(\xi) \times p''(\xi)|^2}. \tag{3.29}$$

It is demonstrated from Eq. 3.25 and Eq. 3.26 that the MSCM shape can be reconstructed, thanks to control points knowledge through the end points pose. Amongst them, 2 are independent (p_2 and p_3) and are responsible of the shape changes.

One can note that the μ value ensures that the potential energy is minimised, see Eq. 3.22, Eq. 3.24, Eq. 3.27 and Eq. 3.28.

However, the free parameters ψ_0 and ψ_2 can influence the shape of the curve representing the MSCM posture since they vary from 0 to π. The reason for this observation is their effects on the value of the potential energy (see Eq. 3.22 and Eq. 3.24). By imposing $\psi_1 = 0$, it is possible to determine the appropriate combination (ψ_0, ψ_2) inducing a minimum value of the potential energy.

3.3 PH-based Forward Kinematic Modeling (PH-FKM)

The adaptive shape issue implies the deformation of the PH-curve (representative of the soft continuum manipulator shape) from an initial one to the required one as described in Fig. 3.2. This results in moving the control points p_k independently using the **PH-based Forward Kinematics Modeling (FKM)** namely Eq. 3.25.

However, the Bézier control points defined in Eq. 3.25 can not have independent motions while keeping PH advantageous features (prescribed length, interpolation, etc.). In [Farouki 2015], this issue is largely analyzed. To solve that problem, a rectifying control polygon based on the Gauss-Lobatto quadrature is investigated. This technique enables to deform a PH curve from its control points while keeping all the interesting properties of PH curves, contrary to the drawbacks caused by the direct motions of the Bézier control points. Furthermore, one interesting feature of using Gauss-Lobatto control points is the endpoints interpolation properties and the length preserving properties during the shape modeling.

3.3.1 Gauss-Lobatto quadrature

In Eq. 3.25, the Bézier control points p_k are supposed to have independent motions from each other. Unfortunately, this appears to be not possible while keeping PH features [Farouki 2015]. In the following, a method using a rectified control polygon by using Gauss-Lobatto control polygon is discussed through Gauss-Lobatto quadrature [Abramowitz 1964] [Quarteroni 2010].

In the case of a MSCM of length L, a quadrature rule can estimate the integral of a function (describing the MSCM shape) $p(s) : [0, L] \rightarrow \mathbb{R}^3$ as a weighted sum $\sum_{k=1}^{m} \bar{\omega}_k p(s_m)$ of m function values, sampled at nodes $s_m \in [0, L]$ along the manipulator length. When the nodes and the weights are chosen conveniently, the estimate is exact for a maximum degree dependent of m, of the polynomial curve.

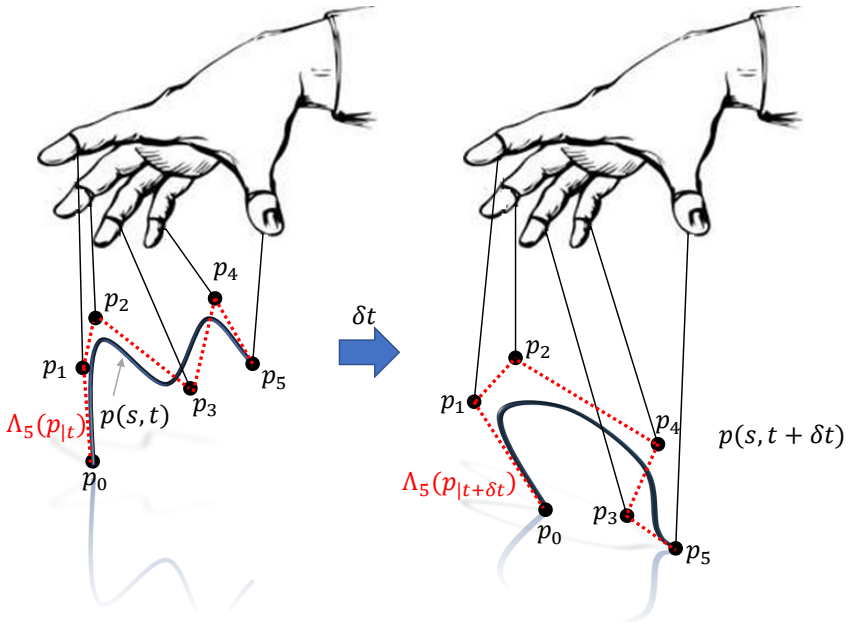

Figure 3.2: Deformation of a PH curve using control points

The exactitude of a quadrature rule for sufficiently high m, for MSCM, may be exploited to identify the PH curves representative of their shapes [Kythe 2005].

The Gauss-Lobatto polygon uses the Gauss-Lobatto quadrature. For the integrable function $p(\xi)$ on $[-1, 1]$, the Gauss-Lobatto quadrature utilizes both end parameters (-1 and 1) as preselected nodes. With m nodes, it takes the form of:

$$\bar{I}_m = \bar{\omega}_{m,0} p(-1) + \bar{\omega}_{m,m-1} p(1) + \sum_{k=1}^{m-2} \bar{\omega}_{m,k} p(\bar{\tau}_{m,k}) \tag{3.30}$$

When the domain of the integration is $[0, 1]$, consistent with the normalized parametrization of MSCM to be described, the Gauss-Lobatto quadrature is scaled as follows:

$$\bar{I}_m(p; [0,1]) = \frac{1}{m(m-1)}(p(0) + p(1)) + \sum_{k=1}^{m-2} \bar{\omega}_{m,k} p(\frac{1+\bar{\tau}_{m,k}}{2}) \tag{3.31}$$

This quadrature is used to define the Gauss-Lobatto polygon of a regular curve $p(\xi)$ (defining the shape of the MSCM) in the Euclidean space $\mathbb{R}^3$.

The rest of the nodes $\bar{\tau}_{m,k}$ for $k = 1 \cdots m-2$ and the weights are chosen so that this quadrature evaluates the exact integral of the polynomial of the degree as high as possible. According to [Abramowitz 1964] [Quarteroni 2010], the values of the nodes and the weights for small number of nodes are listed in Tab. 3.1.

Recall that, quintic PH curves are generally recognized to have sufficient shape flexibility for any complex MSCM shape kinematics reconstruction. Henceforth, the investigation is made on the consistency of a 5^{th} order PH polynomial curve.

Table 3.1: Nodes and weights of Gauss-Lobatto quadrature up to order 5

No. of Nodes m	**Nodes** $\bar{\tau}_{m,k}$	**Weights** $\bar{\omega}_{m,k}$
2	± 1	1
3	± 1,0	$\frac{1}{3}$, $\frac{4}{3}$
4	± 1,$\pm\sqrt{\frac{1}{5}}$	$\frac{1}{6}$, $\frac{5}{6}$
5	± 1,$\pm\sqrt{\frac{3}{7}}$,0	$\sqrt{\frac{1}{5}}\frac{1}{10}$, $\frac{49}{90}$, $\frac{32}{45}$

3.3.2 Gauss Lobatto control polygon

Definition 3.3.1. Let define $p(\xi) : [0,1] \to \mathbb{R}^3$, a regular parametric curve describing the shape of a soft continuum manipulator. The Gauss-Lobatto control polygon $\Xi_m(p) = \{r_k\}$ of $p(\xi)$, with m edges is defined by:

$$\begin{aligned} r_0 &= p(0), \\ r_{k+1} &= r_k + \frac{\bar{\omega}_{m,k}}{2} p'\left(\frac{1+\bar{\tau}_{m,k}}{2}\right) \quad \text{for } k = 0, \cdots, m-1 \end{aligned} \tag{3.32}$$

One can note that the number of edges of a Gauss-Lobatto polygon is specified by the number of nodes of the Gauss-Lobatto quadrature. So any Gauss-Lobatto polygon should have at least 2 edges since the Gauss-Lobatto quadrature has two pre-selected nodes. Therefore, from Definition 3.3.1, it is obvious that the MSCM shape and its Gauss-Lobatto control polygon share the same tangents at the endpoints (starting and final points). In the remaining, Gauss-Lobatto control points are denoted r_k.

Proposition 3.3.1. *Let define $p(\xi) : [0,1] \to \mathbb{R}^3$, a regular parametric curve describing the shape of a soft continuum manipulator. Any both terminal edges of the Gauss-Lobatto polygon $\Xi_m(p)$ read the tangents of p as:*

$$\begin{aligned} p'(0) &= \frac{2}{\bar{\omega}_{m,0}} \Delta r_0 = \frac{2}{\bar{\omega}_{m,0}} (r_1 - r_0), \\ p'(1) &= \frac{2}{\bar{\omega}_{m,m-1}} \Delta r_{m-1} = \frac{2}{\bar{\omega}_{m,m-1}} (r_m - r_{m-1}), \end{aligned} \tag{3.33}$$

In the present context that the Gauss-Lobatto control polygon is specified with end tangents interpolation properties, it is of crucial importance to ascertain whether this latter meets endpoint interpolation properties regarding the polynomial curve $p(\xi)$ representing the MSCM shape.

Proposition 3.3.2. *Let define $m, l \in \mathbb{N}$. $p(\xi) : [0,1] \to \mathbb{R}^3$, a regular polynomial curve of degree l, representing the soft continuum manipulator shape. If $m \geq \frac{l}{2} + 1$, then its Gauss-Lobatto polygon has endpoint interpolation property: $r_m = p(1)$*

According to Definition 3.3.1, it is obvious that $p(\xi)$ and $\Xi_m(p)$ share the same starting point. Also, it is obvious that

$$r_m = r_0 + \sum_{k=0}^{m-1} \bar{\omega}_{m,k} p'(\frac{1+\bar{\tau}_{m,k}}{2}) \tag{3.34}$$

Since p' is of degree $l-1$, for any $l-1 \leq 2m-3$, the Gauss-Lobatto quadrature computes the exact integral. Hence:

$$r_m = r_0 + \int_0^1 p(\xi)\mathrm{d}\xi = p(1) \tag{3.35}$$

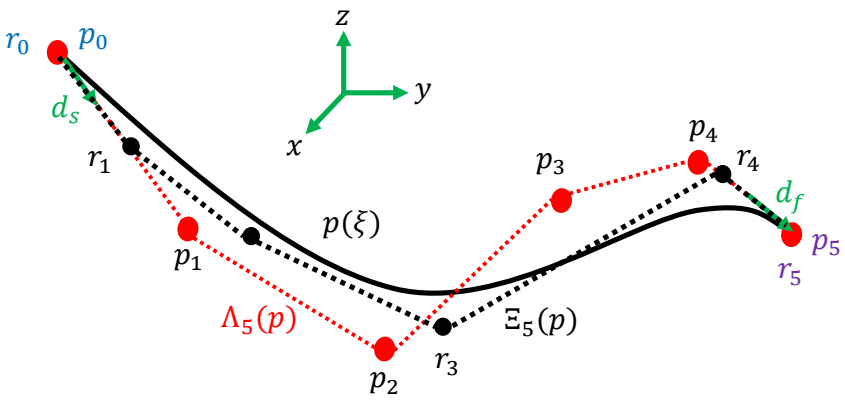

Figure 3.3: Gauss-Lobatto control points illustration

It has been established that the Gauss-Lobatto control polygon of the PH parametric curve representing the MSCM posture has both endpoints and end tangents interpolation properties.

3.3.3 Properties

The rectifying properties of a given control polygon regarding a PH curve $p(\xi)$ have been discussed in [Kim 2017] by three properties :

- The endpoint interpolation,
- The rectifying property, i.e., the polygon has the same length as the PH curve $p(\xi)$,
- The polygon has the same degree of freedom as the PH curve $p(\xi)$.

With the preceding rectifying properties, the Gauss-Lobatto control polygon is analyzed accordingly.

Let us remind that if the complex or the quaternion polynomial is of degree n, then the corresponding PH curve is of degree $2n+1$.

The endpoint interpolation and the rectifying property of the Gauss-Lobatto polygon have already been investigated in proposition 3.3.1 and 3.3.2. Now DoFs of the Gauss-Lobatto polygon have to be discussed.

Proposition 3.3.3. *Let $m, n \in \mathbb{N}$ and $p(\xi) : [0,1] \to \mathbb{R}^3$, a regular parametric curve of degree $2n+1$. Also, let be $\Xi_m(p)$, a Gauss-Lobatto control polygon of $p(\xi)$. Suppose that $p(\xi)$ is the representative shape of a soft continuum manipulator. The necessary and sufficient condition for the existence of $\Xi_m(p)$ as a rectifying control polygon is consistent with $m \geq n+2$.*

The proposition 3.3.3 is easily derived from the observation on the endpoints and end the tangents interpolations. Analyzing spatial PH curves, it is known from rectifying properties that the Gauss-Lobatto control polygon must have the same degree as the PH curve to be controlled. This implies that $3m = 4n + 3$. This observation keeps valid if $n = 3h$, for any $h \in \mathbb{N}$. Thus, all pairs of numbers $(m, n) = (4h+1, 3h)$ satisfy $m \geq n+2$. Henceforth, the following must be considered for the modeling of spatial motions of MSCM with PH curves:

Proposition 3.3.4. *Let define $p(\xi) : [0,1] \to \mathbb{R}^3$, a regular parametric curve describing the shape of a soft continuum manipulator and let be $m, n \in \mathbb{N}$, 2 integers. Assume $p(\xi)$, a spatial PH curve of degree $2n+1$. Take $\Xi(p)$, a Gauss-Lobatto polygon of $p(\xi)$ with m edges. $\Xi(p)$ is the rectifying control polygon of $p(\xi)$ if $n = 3h$ and $m = 4h+1$ for $h \in \mathbb{N}$.*

3.3.4 Toward Bézier control points correspondance

Now, it is desired to control the MSCM shape described by a PH curve $p(\xi)$ by moving its control points. However, according to proposition 3.3.4, the first nontrivial case arises for septic PH curves. The idea is to increase the degree of the quintic PH curve by degree elevation (see Eq. A.12). After that, the Gauss-Lobatto polygon has to be specified from Eq. 3.3.1. After that, the Bézier control points are carried out by computing the quaternion pre-image $\mathcal{A}_{m=0\cdots3}$, issued from Gauss-Lobatto rectifying polygon motion.

So, for a given rectifying control polygon $\Xi(p)$, the quaternion pre-image $\mathcal{A}_{m=0\cdots3}$, leading the Bézier control points p_k kinematics, need to be specified. From Eq. 3.3.1, the following holds:

$$\Delta r_k = r_{k+1} - r_k = \frac{\bar{\omega}_{m,k}}{2} p'\left(\frac{1+\bar{\tau}_{m,k}}{2}\right) \tag{3.36}$$

Hence,

$$\Delta r_k = \frac{\omega_k}{2} \mathcal{A}\left(\frac{1+\bar{\tau}_{m,k}}{2}\right) \mathbf{i} \mathcal{A}\left(\frac{1+\bar{\tau}_{m,k}}{2}\right)^* \tag{3.37}$$

which is equivalent to

$$\mathcal{A}\left(\frac{1+\bar{\tau}_{m,k}}{2}\right)^{2\bigstar} = \frac{2}{\omega_k} \Delta p_k. \tag{3.38}$$

Eq. 3.38 can be solved by determining $\mathcal{A}$ (see Eq. A.7 and Eq. A.3.1 of the Appendix) by :

$$\mathcal{A}\left(\frac{1+\bar{\tau}_{m,k}}{2}\right) = \sqrt[\star]{\frac{2}{\bar{\omega}_{m,k}}\Delta r_k}\,\mathcal{Q}(\phi_k) \tag{3.39}$$

Recalling that quaternion polynomial $\mathcal{A}(\xi)$ has a free parameter θ (see [Farouki 2002]), the real system is:

$$\mathcal{A}\left(\frac{1+\bar{\tau}_{m,k}}{2}\right)\mathcal{Q}(\theta) = \sqrt[\star]{\frac{2}{\bar{\omega}_{m,k}}\Delta r_k}\,\mathcal{Q}(\phi_k) \tag{3.40}$$

Without loss of generalities, one can take $\theta = \phi_0$ and redefine $\phi_k = \phi_k - \theta$ for $k = 1 \cdots 4$. Henceforth, an over-determined linear system is obtained and reads:

$$\bar{M}\begin{bmatrix}\mathcal{A}_0\\ \mathcal{A}_1\\ \mathcal{A}_2\\ \mathcal{A}_3\end{bmatrix} = \begin{bmatrix}\sqrt[\star]{\frac{2}{\bar{\omega}_{5,0}}\Delta r_0}\\ \sqrt[\star]{\frac{2}{\bar{\omega}_{5,1}}\Delta r_1}\,\mathcal{Q}(\phi_1)\\ \sqrt[\star]{\frac{2}{\bar{\omega}_{5,2}}\Delta r_2}\,\mathcal{Q}(\phi_2)\\ \sqrt[\star]{\frac{2}{\bar{\omega}_{5,3}}\Delta r_3}\,\mathcal{Q}(\phi_3)\\ \sqrt[\star]{\frac{2}{\bar{\omega}_{5,4}}\Delta r_4}\,\mathcal{Q}(\phi_4)\end{bmatrix} \tag{3.41}$$

with 4 free parameters $\phi_1, \cdots, \phi_4 \in [-\pi, \pi]$. $\bar{M}$ defines the Bernstein-Vandermonde matrix [Marco 2007]:

$$\bar{M} = \begin{bmatrix} B_0^3(\frac{1+\tau_{5,0}}{2}) & B_1^3(\frac{1+\tau_{5,0}}{2}) & B_2^3(\frac{1+\tau_{5,0}}{2}) & B_3^3(\frac{1+\tau_{5,0}}{2})\\ B_0^3(\frac{1+\tau_{5,1}}{2}) & B_1^3(\frac{1+\tau_{5,1}}{2}) & B_2^3(\frac{1+\tau_{5,1}}{2}) & B_3^3(\frac{1+\tau_{5,1}}{2})\\ B_0^3(\frac{1+\tau_{5,2}}{2}) & B_1^3(\frac{1+\tau_{5,2}}{2}) & B_2^3(\frac{1+\tau_{5,2}}{2}) & B_3^3(\frac{1+\tau_{5,2}}{2})\\ B_0^3(\frac{1+\tau_{5,3}}{2}) & B_1^3(\frac{1+\tau_{5,3}}{2}) & B_2^3(\frac{1+\tau_{5,3}}{2}) & B_3^3(\frac{1+\tau_{5,3}}{2})\\ B_0^3(\frac{1+\tau_{5,4}}{2}) & B_1^3(\frac{1+\tau_{5,4}}{2}) & B_2^3(\frac{1+\tau_{5,4}}{2}) & B_3^3(\frac{1+\tau_{5,4}}{2}) \end{bmatrix} \tag{3.42}$$

The linear system (Eq. 3.41) can be expressed as $\bar{M}x = q$. This allows the least square solution to be found ($\hat{x} = (\bar{M}^T\bar{M})^{-1}\bar{M}^T q$) using the standard theory of linear algebra. Note that $\bar{M}^T\bar{M}$ is invertible since $\bar{M}$ has a full rank.

The new Bézier control points p_k used to describe the deformed shape are computed as described in [Kim 2019a] by considering a degree reduction (see Eq. A.12) as follows (Eq. 3.43):

$$\begin{aligned} p_1 &= p_0 + \frac{1}{5}\mathcal{A}_0\mathbf{i}\mathcal{A}_0^*, \quad p_2 = p_1 + \frac{1}{10}(\mathcal{A}_0\mathbf{i}\mathcal{A}_1^* + \mathcal{A}_1\mathbf{i}\mathcal{A}_0^*),\\ p_3 &= p_2 + \frac{1}{30}(\mathcal{A}_0\mathbf{i}\mathcal{A}_2^* + 4\mathcal{A}_1\mathbf{i}\mathcal{A}_1^* + \mathcal{A}_2\mathbf{i}\mathcal{A}_0^*),\\ p_4 &= p_3 + \frac{1}{10}(\mathcal{A}_1\mathbf{i}\mathcal{A}_2^* + \mathcal{A}_2\mathbf{i}\mathcal{A}_1^*), \quad p_5 = p_4 + \frac{1}{5}(\mathcal{A}_2\mathbf{i}\mathcal{A}_2^*), \end{aligned} \tag{3.43}$$

As one can see in the above development, multiple instances of a quintic PH curve should be obtained. However this is a typical situation for a PH curve construction problems. For a real physical system, it is suggested to deal with the one that

exhibits the smallest bending potential energy (Eq. 3.28). The PH-FKM is thus described by:

$$p(\xi) = \sum_{k=0}^{5} p_k \binom{5}{k} (1-\xi)^{5-k} \xi^k. \tag{3.44}$$

3.4 APF-based Shape Kinematic Control Theory

3.4.1 Control Law

The following control strategy is applied on the control points to drive the MSCM to target with obstacles avoidance. A single soft robotic arm is represented by a PH quintic curve with length L and is expressed in the form of the arc-length parametrization $p(\xi) : [0, 1] \to \mathbb{R}^3$. Such approximation is valid since the geometrical dimensions of a particular design can be taken into account by the corresponding potential field considered below. The initial point $p_s = p_0 = p(0)$ is a position of the mobile part of the MSCM. It is assumed that the position p_0 as well as the curvature of the soft manipulator can be controlled. Also, it is assumed for the shape control, that the MSCM has a pure bending (the torsion $\tau(\xi) = 0$).

Let $T(\xi) = p'(\xi)$ be the unit tangent vector to the curve, then the curvature is

$$\omega(\xi) = \kappa(\xi) = \|T'(\xi)\| = \|p''(\xi)\| = \frac{1}{R(\xi)}, \tag{3.45}$$

where $R(\xi)$ is the radius of the osculating circle to the curve $p(\xi)$. It is assumed that the curvature is bounded by a function $\kappa_{\max}(\xi)$, as follows:

$$\kappa(\xi) \leq \kappa_{\max}(\xi). \tag{3.46}$$

This assumption describes the design constraints of the soft manipulator part of the MSCM, having possibly variable thickness or stiffness (e.g. thicker at the base than at the end) or constraints on the distributed control actions along the curve. Note that, a real physical system allows a maximal curvature which can be interpreted as the upper bound $\kappa_{\max}$, consistent with its design.

Let $\Phi(p_k, p_d; \mathbb{O}) \geq 0$ be a potential function depending on the position of $p_k \in \mathbb{R}^3$, the control points of the curve $p(h, t)$ and such that, $p_d \in \mathbb{R}^3$ is the desired position (attractor) and $\mathbb{O} \subset \mathbb{R}^3$ is a set of obstacles to be avoided. In the case of the MSCM, the potential field acts on the control points p_k of the PH curve $p(\xi, t)$, instead of acting on all the curve points. It is assumed that the potential is made up in two parts: one at the desired point which is $\Phi(p_k, p_d; \mathbb{O}) = 0$, where $p_f = p_d$, and another at $p_f \neq p_d$, where $\Phi(p_k, p_d; \mathbb{O}) > 0$ so that the positions of obstacles represents the poles of the potential:

$$\lim_{p \to \mathbb{O}} \Phi(p_k, p_d; \mathbb{O}) = +\infty. \tag{3.47}$$

or at least $\Phi(p_k, p_d; \mathbb{O})$ for $p \in \mathbb{O}$ is big enough to guarantee that the arm never touches the obstacles in real-life situations.

Let us note that we allow the target position and the obstacles to move i.e. being functions of time $p_d(t)$, $\mathbb{O}(t)$. Also the obstacles set may include the own manipulator points to avoid self-intersections of the curve $p(s) \in \mathbb{O}(t)$ for all $s \in [0, L]$.

First, consider that the displacement of the PH curve $p(\xi, t)$ is described by the kinematic relations:

$$\frac{\partial p(\xi, t)}{\partial t} = v(\xi, t), \tag{3.48}$$

where $v(\xi, t) \in \mathbb{R}^3$ is a velocity function of ξ at time t, and

$$\frac{\partial p(\xi, t)}{\partial \xi} = T(\xi, t), \tag{3.49}$$

where $T(\xi, t)$ is an instant tangent unit vector to the curve representing manipulator. It is clear that the best way moving to the target with desired speed $v_d > 0$ that can be done to avoid obstacles is to have the robot position $p_0(t)$ moving along the minimum potential:

$$\dot{p}_0(t) = -v_d \frac{\nabla_p \Phi(p_0(t), p_d; \mathbb{O})}{\|\nabla_p \Phi(p_0(t), p_d; \mathbb{O})\|}. \tag{3.50}$$

The manipulator curve is moved along the minimum potential line according to the displacement T of control points from the point p_0 to p_5 as follows:

$$T(t) = -\frac{\nabla_p \Phi(p_k(t), p_d; \mathbb{O})}{\|\nabla_p \Phi(p_k(t), p_d; \mathbb{O})\|}. \tag{3.51}$$

Thus Eq. 3.50 and Eq. 3.51, are the equations for the planning motion of the manipulator.

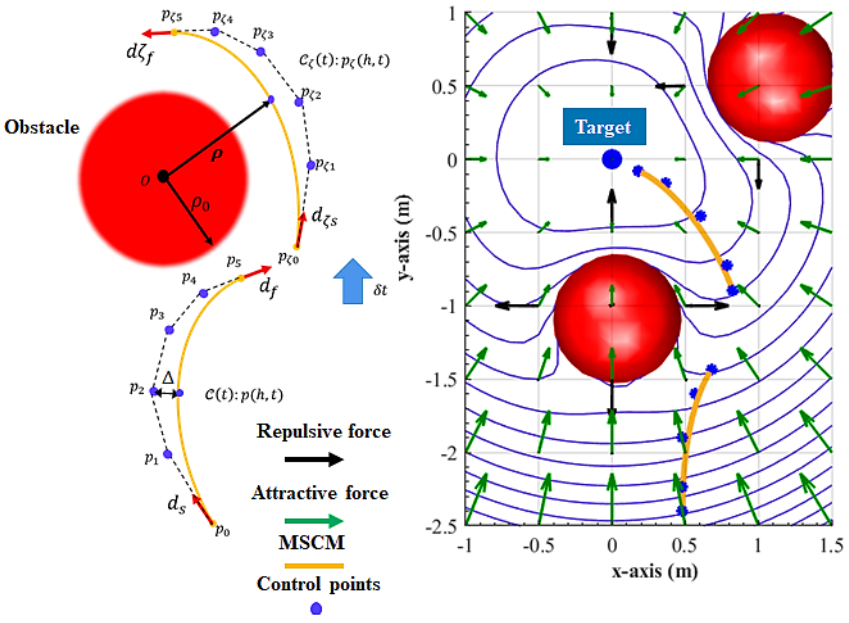

Figure 3.4: Avoidance illustration for a MSCM subject to APF

There may be two types of difficulties to implement this plan: 1. the minimum potential line may have curvature exceeding maximum allowed curvature of the manipulator, and 2. the end of the manipulator may have already located in the vicinity of the target object that has to be handled.

In addition, feedback control is needed to make the planned motion stable. To solve the first difficulty, an algorithm utilizing sliding-mode along the length of the arm, is suggested. This allows to keep the minimum potential energy of the PH curve $p(\xi, t)$ representing the MSCM during its motion with respect to the real-time implementation using the independent normalized variable ξ. So, the independent variable in this algorithm equations is ξ not the time t.

Thus, we consider the following system of equations to describe the MSCM from its control points, calculated in space configuration:

$$\begin{cases} \dfrac{\partial p_k}{\partial \xi} = T, \\ \dfrac{\partial T}{\partial \xi} = \omega, \end{cases} \tag{3.52}$$

where the vector $\omega \in \mathbb{R}^3$ is viewed as a control input which describes the total bending of the curve. Thus, the sliding manifold can be expressed as follows:

$$\sigma = \|\nabla_p \Phi\| \, T + \nabla_p \Phi = 0. \tag{3.53}$$

This equation represents a manifold in the system state space represented by Eq. 3.52. To make it sliding manifold, we can use the following bounded control of the total bending of the curve PH:

$$\omega = -\kappa_{\max} \frac{\sigma}{\|\sigma\|} = -\kappa_{\max} \frac{\|\nabla_p \Phi\| \, T + \nabla_p \Phi}{\|\|\nabla_p \Phi\| \, T + \nabla_p \Phi\|}. \tag{3.54}$$

If the initial orientation of the MSCM is tangent to the gradient $\nabla_p \Phi(p_0, p_d; \mathbb{O})$, then it means that the state system (3.52) is already on the manifold $\sigma = 0$ then the sliding may continue along the variable ξ and therefore along the potential minimum decent line.

To describe completely the system behavior, ω is replaced by its equivalent value ω_{eq} which norm is less than the maximum allowed curvature $\|\omega_{eq}\| < \kappa_{\max}$. In the absence of sliding $\omega \neq 0$, the vector ω is defined by Eq. 3.54. Its magnitude is exactly $\kappa_{max}(s)$, so the curvature is maximum then this piece of the MSCM lies along the circle of minimum allowable radius.

3.4.2 Convergence and stability analysis

To analyze the sliding mode existence condition, let us differentiate σ as follows:

$$\frac{\partial \sigma}{\partial \xi} = \|\nabla_p \Phi\| \frac{\partial T}{\partial \xi} + \Psi = \|\nabla_p \Phi\| \, \omega + \Psi,$$

where Ψ includes all other terms from differentiating σ with respect to ξ:

$$\Psi = \frac{\partial \|\nabla_p \Phi\|}{\partial \xi} T + \frac{\partial \nabla_p \Phi}{\partial \xi},$$

using (3.54)

$$\frac{\partial \sigma}{\partial \xi} = - \|\nabla_p \Phi\| \kappa_{\max} \frac{\sigma}{\|\sigma\|} + \Psi. \tag{3.55}$$

If we consider a Lyapunov function $V = \sigma^T \sigma = \|\sigma\|^2$, then

$$\frac{\partial V}{\partial \xi} = -2[\|\nabla_p \Phi\| \kappa_{\max} \sqrt{V} + \sigma^T \Psi].$$

knowing that:

$$|\sigma^T \Psi| \leq \|\sigma\| \|\Psi\| \Leftrightarrow -\|\sigma\| \|\Psi\| \leq \sigma^T \Psi \leq \|\sigma\| \|\Psi\|.$$

Using the lower bound, we obtain:

$$\frac{\partial V}{\partial \xi} \leq -2[\|\nabla_p \Phi\| \kappa_{\max} - \|\Psi\|] \sqrt{V} < 0,$$

if

$$\|\nabla_p \Phi\| \kappa_{\max} > \|\Psi\|. \tag{3.56}$$

This guarantees the sliding mode existence [Drakunov 1992].

3.5 Experimental validations

3.5.1 Materials and Methods

1. **Materials**

Experiments are carried on Festo Robotino-XT robot (Fig. 3.5), a type of MSCM which is made up of two parts: a mobile part named Robotino (omni-drive mobile base robot) and the soft continuum manipulator part named Compact Bionic Handling Assistant (CBHA). The backbone's length is almost constant. The Optitrack system is used for tracking the displacement of the two parts of the MSCM. For this purpose, the Robotino-XT is equipped with markers on the CBHA, allowing the online reconstruction of its posture, while tracking the collision-free path of the whole MSCM.

The validation shape control scheme is described in Fig. 3.10. The implementation of the collision free path is divided into two processes : the simulation process is to compute the MSCM required posture $p(\xi, t)$ and the online process is to validate the shape control of the MSCM, after the backbones posture reconstruction from the Optitrack $P_r(\xi, t)$.

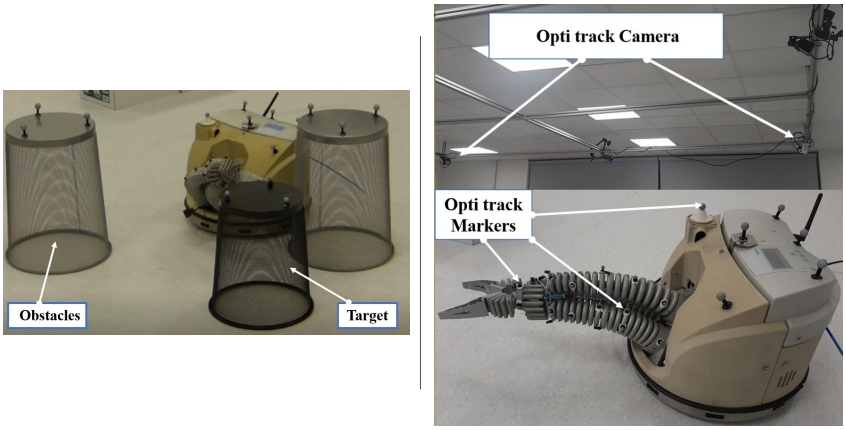

Figure 3.5: Robotino-XT in real environment

2. **Methods**

- **Kinematic control of MSCM mobile base**

A non-holonomic motion of the MSCM mobile base is considered (Fig. 3.6).

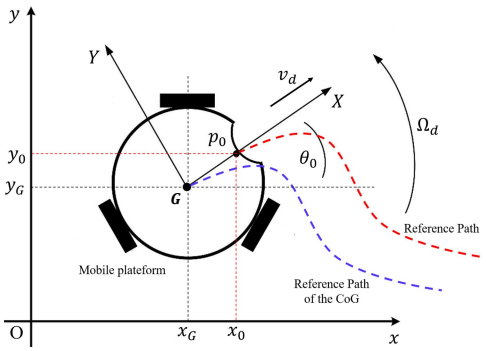

Figure 3.6: Mobile base kinematics

The kinematics of the mobile base of the MSCM (Robotino) is described by the couple (v_d,Ω_d) where v_d are the longitudinal velocity and Ω_d the yaw angular velocity at the starting point control $p_0(t) = (x_0(t), y_0(t))$ of the PH curve representative of the soft manipulator (CBHA). Thus, the desired longitudinal velocity at point p_0 is calculated as follows:

$$v_d = \sqrt{\dot{x}_0^2(t) + \dot{y}_0^2(t)} \tag{3.57}$$

The tangent angle for the planar path of the mobile base is defined as follows:

$$\theta_0 = \arctan 2(\dot{y}_0(t), \dot{x}_0(t)) \tag{3.58}$$

The angular velocity of the MSCM mobile base is obtained by calculating the time derivative of (3.58) as :

$$\Omega_d(t) = \frac{\dot{x}_0(t)\ddot{y}_0(t) - \dot{y}_0(t)\ddot{x}_0(t)}{\dot{x}_0^2(t) + \dot{y}_0^2(t)} = v_d(t)\kappa_0(t) \tag{3.59}$$

where $\kappa_0(t)$ (equation (3.29)) is the curvature of the path of the MSCM mobile base at p_0 ($v_0(t) \neq 0$).

- **Offline Simulation Process**

The considered APF formulation is given as follows:

$$\begin{cases} \Phi_{rep}(p_k; \mathbb{O}) = \frac{1}{2} k_{rep} \left(\frac{1}{\rho(p_k, O)} - \frac{1}{\rho_0(O)} \right)^2 & O \in \mathbb{O}, \\ \Phi_{att}(p_k, p_d) = \frac{1}{2} k_{att} \big(\rho_g(p_k, p_d) \big)^2, \\ \Phi(p_k, p_d; \mathbb{O}) = \Phi_{rep}(p_k; \mathbb{O}) + \Phi_{att}(p_k, p_d), \end{cases} \tag{3.60}$$

where, ρ, ρ_g and ρ_0 are respectively, distance from point p_k to obstacle O, distance from point p_k to target p_d and the operating range radius of the obstacle O. k_{rep}, k_{att} define scale positive coefficients. $\Phi_{rep}(p_k; \mathbb{O})$ and $\Phi_{att}(p_k, p_d)$ are respectively repulsive potential field due to obstacle O and attractive potential because of the attractor target p_d. The considered parameters for this simulation are given in TABLE 3.2.

Table 3.2: Offline process parameters

Parameters	**values**
(k_{att}, k_{rep})	$(2, 2)$
ρ_0	$50\ mm$
$\kappa_{\max}$	$2.0\ m^{-1}$
L	$330\ mm$

Fig. 3.7 shows a 3D shape control of the MSCM, characterized by $p(\xi, t)$, in presence of three obstacles between the MSCM and the target. It shows the behavior of the MSCM which is bending along its length to avoid the obstacle. It is noted that the shape control allows $p(\xi, t)$ to avoid obstacles with a minimum bending configuration.

The sliding mode maintains the optimal bending (optimal placement of the control points) in the presence of the obstacles. However, a MSCM practical shape is affected by the safety distance. A maximum distance can be observed $\Delta_{\max}$ (Fig. 3.4) between the curve and the control polygon. With that, the following holds to guarantee the non-collision with obstacles:

$$\rho_0 \leq \frac{1}{\kappa_{\max}} - \Delta_{\max} \tag{3.61}$$

In Fig. 3.8, it can be observed that the sliding surface vector is vanishing along the MSCM length through the control points. It ensures that the simulated MSCM posture remains in its minimal energy configuration.

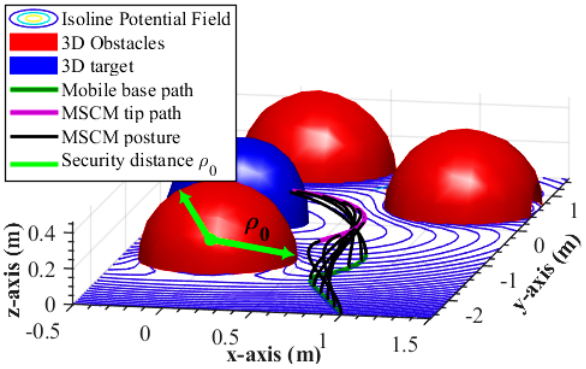

Figure 3.7: 3D potential field with dynamic shape reconstruction

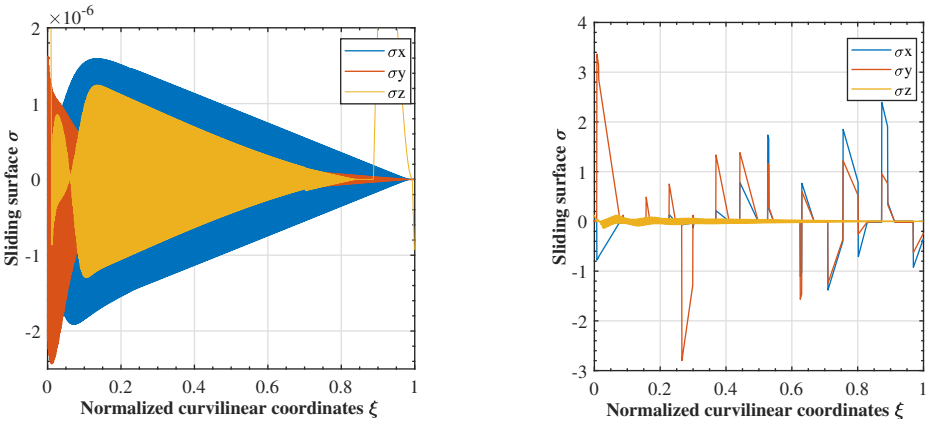

(a) Simulation (b) Real world experiments

Figure 3.8: Real world experiments

3.5.2 Results and discussions

For the experiments, an obstacle is placed between the 3D target point and the robot. TABLE 3.3 describes the Robotino-XT experimental parameters. Like in the

Table 3.3: Real Parameters of RobotinoXT for Shape Reconstruction

CBHA Manipulator	**Robotino** Mobile base
Length L: 330 mm **Pressure range**: $0 - 2.5$ bar **Total weight**: 1020 g	**Velocity** v_d: 100 $mm.s^{-1}$ **Height**: 320 mm **Total weight**: 11 kg

simulation, the curve $p(\xi, t)$ is reconstructed according to the directions $\nabla\Phi$ based on the minimum potential of the curve. This allows to place, in the optimal positions,

the control points p_k which drive the MSCM posture as observed in Fig. 3.7. The experimental reconstruction of the MSCM shape from the Robotino-XT backbone, is obtained after making the relation between the PH curve $p(\xi, t)$ [Singh 2018b] and the pressure distribution [Lakhal 2015], described by $[P_i]$ (Fig. 3.10) for each tube of the CBHA. Simultaneously, the planar components of $\nabla\Phi(0, t)$ at p_s (robot base) allow computing a collision free path at ground with non-holonomic kinematic motion (Fig. 3.10), where v_d descibes the longitudinal velocity of the centre of mass of the robot base and $\Omega_d(t)=v_d(t)\kappa_0(t)$ describes its yaw velocity.

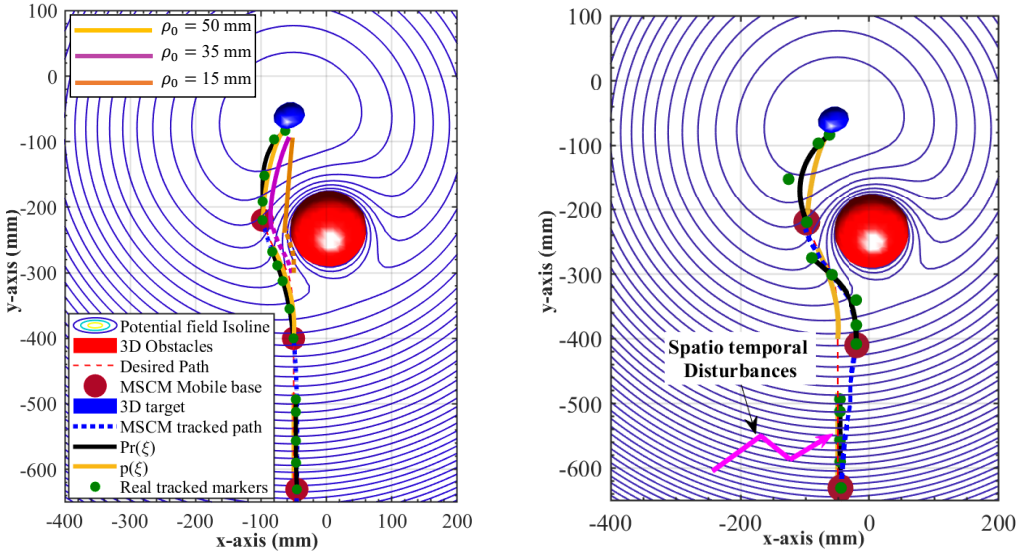

(a) Without disturbances

(b) With disturbances

Figure 3.9: Planar view of the collision-free path tracking of the MSCM

Fig. 3.9 shows the results of the experimental obstacle-free path in xy-planar view. The obstacle avoidance concerns the whole MSCM. Around 10 seconds was necessary to achieve the navigation. When the mobile part comes close to the obstacle, it deviates its trajectory to avoid the collision. At the soft continuum manipulator side, it can be observed in Fig. 3.9, how the bending is exhibited along the soft structure to reach the 3D target while avoiding the obstacle. It is noticed with the change of ρ_0, that the MSCM stays away from the obstacle.

The proposed motion control method is a unified approach that allows achieving obstacles avoidance at the robot base and its soft continuum manipulator, both simultaneously. To check the tracking of the shape, a superposition of both shapes: $p(\xi, t)$ issued from the shape control during the simulation and $P_r(\xi, t)$, the PH quintic curve obtained from the OptiTrack, obtained during the online process, is given in Fig. 3.13. This figure describes a sample of posture of the Robotino-XT taken from 359 postures along the robot trajectory to reach the target while avoiding the obstacles during the experiments.

According to Fig. 3.13a, the control point position along x-axis seems constant

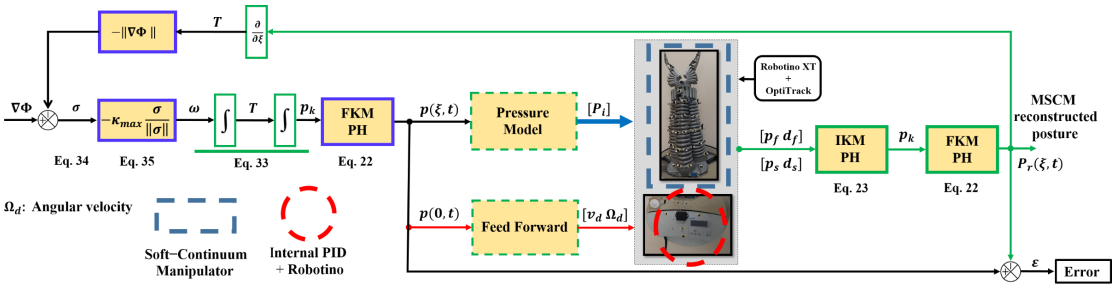

Figure 3.10: Shape kinematic control scheme of the Robotino-XT

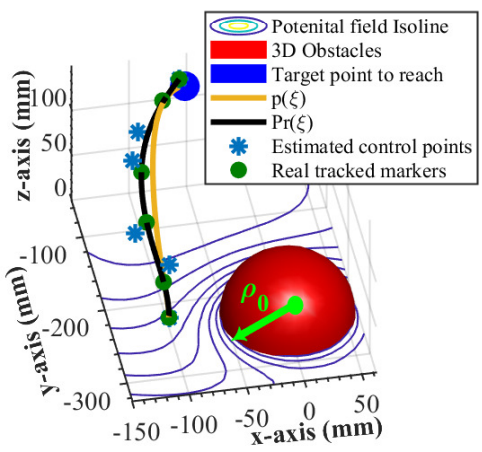

(a) Reconstructed posture

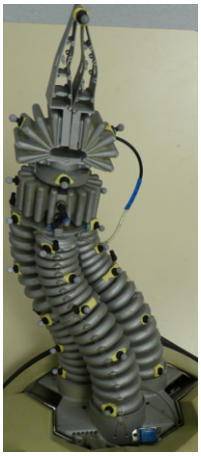

(b) Real world posture

Figure 3.11: 3D posture comparison during the obstacle avoidance

until around 6 sec. This is because within this period, the MSCM is moving more or less in a straight way without any big changes in its dynamics (without obstacles), as also described by the bending energy variation (Fig. 3.13b).

From around 6 seconds, a deviation is observed when approaching the obstacle. This occurs at the curved path. A control occurs both at CBHA and Robotino sides. The Fig. 3.12 illustrates the absolute mean Cartesian error, observed along the MSCM shape during its obstacle-free motion. Note that the collision free path was repeated during eight times with close outcomes. Based on that observations, it is noted that the MSCM positions is kept constant in y and z directions.

As the implemented control is focused on the kinematics, the tracking observed errors in the x direction can be due to the dynamics of the MSCM (Fig. 3.12a). In addition, the soft structure dilation due to the properties of the material constituting the CBHA might have contributed to these errors, using a nonlinear pressure-based control to compensate spatio-temporally disturbances. The maximum error observed along the robot length (Fig. 3.12b) is $\varepsilon = 19.6$ mm (6% wrt to the manipulator length) while the mean error of tip tracking is $\varepsilon = 13.86$ mm (4.2% wrt to

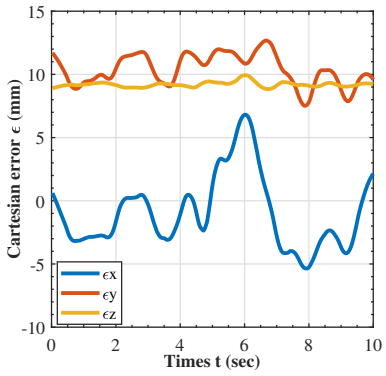

(a) Error vs time

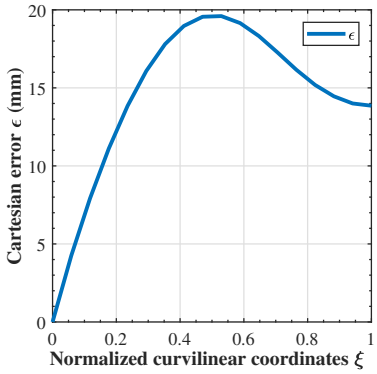

(b) Mean error of the collision-free path tracking

Figure 3.12: Mean error of the collision-free path tracking

the manipulator length).

It is observed from Fig. 3.13b, a change in the shape, where the curvature varies as well as the bending energy. This explains the observation of Fig. 3.13a, which describes the variation of the control points p_k, after obstacles detection.

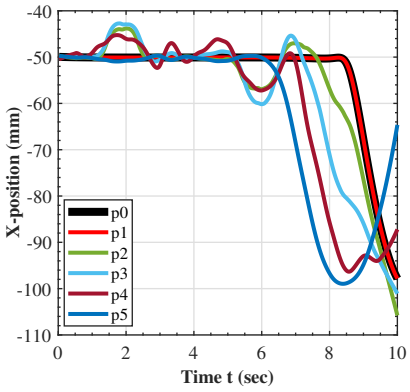

(a) Control points position in x-axis

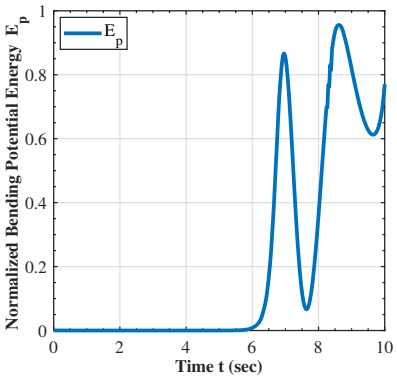

(b) Normalized bending energy during the obstacle avoidance

Figure 3.13: 3D posture comparison during the obstacle avoidance

Other approaches [Singh 2018b] [Sadati 2019] have been investigated to evaluate the relevance of the results obtained. Table 3.4 summarizes the results of the qualitative and the quantitative analyses obtained after the experiments. The PH curve modeling proposed by [Singh 2018b] gives an average error of 28.43 mm, higher than that of the present contribution of about 16.35 mm. The length constraints omission in [Singh 2018b] and the search for the optimal solution to obtain a shape reconstruction consistent with the prescribed length might explain these errors regarding the accuracy and the higher computation time. Also, the energy-based optimization relies only on fixed values of two free parameters ϕ_0, ϕ_2, which is less flexible

Table 3.4: Comparison of curve-based techniques for MSCM shape kinematics control

Modeling approach	**PH curves [Singh 2018b]**	**Spline curves [Sadati 2019]**	**PH curves (proposal)**
Optimization	Minimum potential energy	No	Minimum potential energy
Length constraints	No	No	Yes
Time cost (sec)	0.0853	0.50142	0.031433
MERS (mm)	28.43	14.61	16.35

MERS: Mean Error of Robot Shape

than the proposed approach, where a third free parameter ϕ_1 allows a larger range for the optimal solution. All these latter have probably contributed to the error compared to the suggested method. In addition, the results showed that an average error of 14.61 mm is exhibited using the technique suggested by [Sadati 2019]. This error is smaller than the proposed reconstruction method. Indeed, this approach is a point-by-point local shape reconstruction technique. It requires too many control points, all belonging to the curve to be reconstructed. Therefore, it does not require any optimization technique based on curve energy or curve length. This would explain its better accuracy compared to the present investigation, which is a global reconstruction technique. However, its high computation time might be due potentially to a large number of control points necessary to achieve a shape reconstruction compatible with the length of the manipulator, which could be not suitable for real-time control. The advantage of considering the length constraints is found in the present study. It allows the uniqueness of the solution to the issues stated above while reducing the modeling and control dimension. This latter might be suitable for real-time control purposes.

However, it is worth noting that considering length constraints supposes a perfect knowledge of the behavior of the robot material, in particular about its extension (Hooke's law, etc.). It can be sometimes hard to assess, especially in the case of hyper-elastic materials, see Fig. 3.14. In addition, some Artificial Potential Field-based obstacle avoidance formulations can suffer from a lack of convergence guarantee for the obstacles' special arrangements, such as a concave arrangement. So, careful attention needs to be taken to the APF formulation for motion planning. Curve energy-based optimization cannot solve that issue. Also, the curve fitting process might have potentially contributed to some control errors. Indeed, the accuracy of curve-based modeling is related to the spatial configuration's step

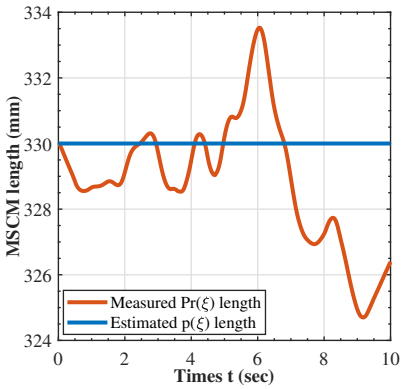

Figure 3.14: Estimated and measured MSCM length

3.6 Conclusion

In this chapter, a kinematic model-based control of the MSCM shape is proposed in space configuration. It consists of applying an APF on the finite control points of the PH parametric curve of the MSCM for obstacle avoidance and sliding mode control for shape optimization. Thus, a PH quintic curve is formulated with length constraints to consider the prescribed length and the variable curvature for 3D reconstruction of the MSCM. The PH curves are subject to APF and allow to drive the posture of the MSCM in presence of obstacles. The applied Sliding Mode control is used to keep the MSCM posture in its minimal bending energy during the collision-free path. The algorithm of shape control was tested on a class of MSCM called Robotino-XT. The results obtained show us the effectiveness of the proposed approach as well as its limitations. For shape adaptability issues, the relationship between the control points and the physical control inputs needs to be established explicitly. This constitutes the main interest of the next investigation.

Chapter 4

Dynamic Control of Soft-Continuum Manipulators: PH-Euler Bernoulli approach

Contents

4.1 Introduction

In the previous chapter, the shape kinematics using the quintic PH curves with length constraints have been analysed. This has been used in the context of an APF coupled with SMC for the CBHA motion planning with obstacles avoidance. However, the control inputs were computed through learning-based methods [Lakhal 2015]. In the following, dynamics model-based shape control of soft continuum robots in the presence and absence of external efforts is discussed. For that, the modeling based on PH curves with prescribed lengths is combined with Euler-Bernoulli modeling to reconstruct the robot shapes and then calculate the actuator

inputs considering the external interactions. Thus, a relationship between the actuator inputs and the PH control points is obtained. With this, the actuator inputs can be computed accordingly, and therefore, a real-time shape control of the soft robots for various tasks becomes possible. The results of the proposed approach are validated both numerically and experimentally using two classes of soft continuum robots: FEAs describing a 2D soft finger robot, with a single and multiple phalanges, and a 3D continuum manipulator (CBHA).

4.2 Actuation dynamics model

This section aims to model the FEAs dynamics in 3D, based on EB theory, where a relationship between the curvature of the soft actuator can be established with the actuator inputs. The idea is to adaptively control the shape of the FEAs in presence of external efforts. The curvature can be constant or variable. In the case of soft fingers, it implies the consideration of one or multiple actuators described by phalanges, where each phalange is modeled by a constant curvature. Finally, the PH curves are used for shape kinematics reconstruction of the FEAs, according to the curvature, which also depends on the actuator inputs.

4.2.1 Actuation Modeling

The Euler-Bernoulli theory enables describing the influence of the external efforts on a beam of soft actuators. In the case of FEAs, the dynamics of the bending can be observed by varying the actuator inputs (air pressure) trapped inside the chamber.

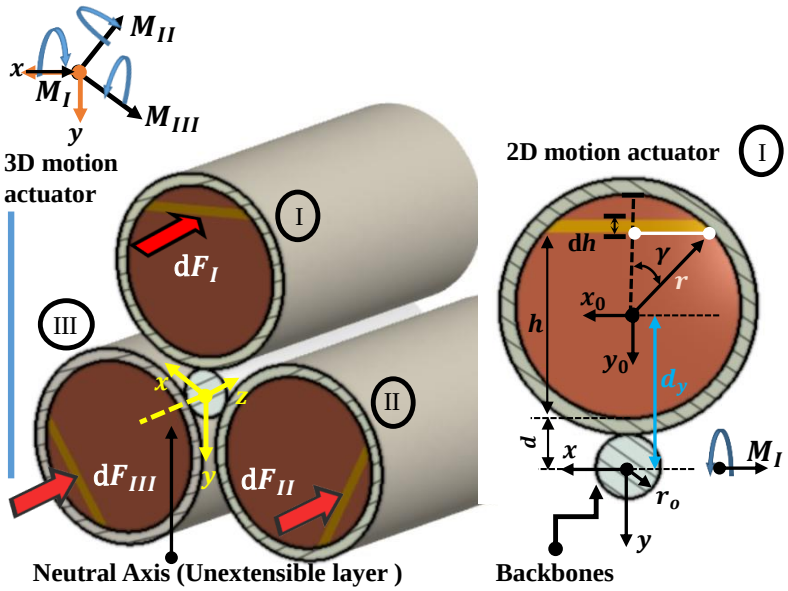

Figure 4.1: FEA concept and sizing

Considering the given FEAs concept of Fig. 4.1, the normal force generated by the actuator input, namely air pressure, along the horizontal line of the actuator, being at a distance h from the bottom layer, is given as follows:

$$\mathrm{d}F_I = (2rp_{in}\sin\gamma)\mathrm{d}h, \tag{4.1}$$

where p_{in}, r, and γ denote respectively the actuator input of air pressure, the radius of the cross section for the soft actuator, and the angle of an infinitesimal distance located on the cross section. $\mathrm{d}F$ is the infinitesimal normal force acting on the cross section due to the air pressure along the infinitesimal distance $\mathrm{d}h$.

Assuming one controlled actuator input p_{in} for a given actuator, following (4.1), the bending moment M_e (Fig. 4.2) can be expressed as a function of p_{in} and a geometric parameter Ψ:

$$M_e = \int (h+d)\mathrm{d}F = \Psi p_{in}. \tag{4.2}$$

However, the deviated bending issued from the combined action of end moments (Fig. 4.1) should be considered for the 3D motion :

$$M_e = [M_{ex} \quad M_{ey} \quad M_{ez}]^T. \tag{4.3}$$

From Fig. 4.1, the following is obtained:

$$M_e = [M_{I_x} - M_{II_x} - M_{III_x} \quad M_{II_y} - M_{III_y} \quad M_{II_z} - M_{III_z}]^T. \tag{4.4}$$

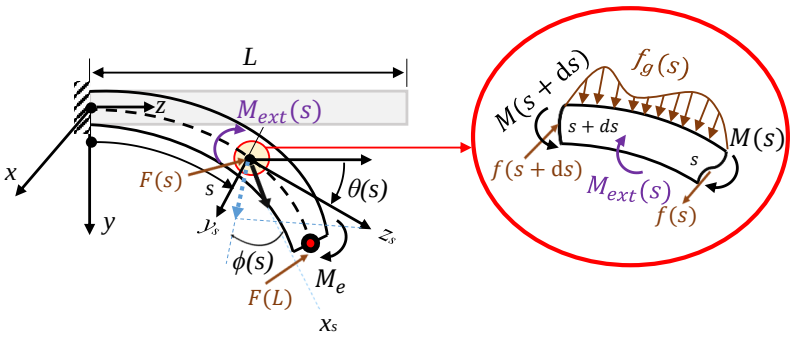

Figure 4.2: 3D bending of FEA

4.2.2 Flexural stiffness modeling

The ability of FEAs to exhibit a given bending behavior depends on some of their intrinsic properties that take into account both micro and macro structures, called the flexural stiffness (EI). The microstructure is represented with E, the elastic Young Modulus for material properties. The macro-structure is described by $I(s)$, representing the local static moment of inertia. For the particular case of a

circular cross-section actuator ($I_{y_0}(s) = I_{x_0}(s)$), the local static moment of inertia can be calculated using the Huygens-Steiner theorem as follows:

$$I_x(s) = I_{x_0}(s) + A_s(s){d_y}^2, \tag{4.5}$$

where $I_{x_0}(s)$ represents local quadratic moment of inertia relative to x_0 in the y_0z_0-frame. During the actuation, the flexural stiffness might increase because of the additional stiffness induced by the compressed fluid pressure. In order to consider this aspect, the following modeling has been considered [Wielgosz 2005] :

$$(EI)_{eq_x} = (E + p_{in})I_x(s). \tag{4.6}$$

4.2.3 Euler-Bernoulli theory

In the following development, it is assumed that the soft finger length remains constant. For modeling purposes, a soft finger can be viewed as a thin cantilever **3D** beam. The FEAs is supposed to be subject to an end moment as stated in [Mihael Brojan 2007]. Let us consider a thin cantilever beam of length L subjected to a moment M_e, which is applied at the free end of the beam, as shown in Fig. 4.2.

We denote s $(0 \leq s \leq L)$ as the curvilinear coordinate along the axial line, measured from the clamped end and $p(s)$ its Cartesian position. Also, let us define $\theta(s)$ and $\phi(s)$, respectively, the polar and the azimuthal positive angles (relative to x-axis) of the tangent $p'(s)$ to the neutral axis at point s (Fig. 4.2). In addition, let M, f denote the bending moment and the internal forces at the location s, respectively. The external forces and moments are denoted by F and M_{ext}, respectively. The effects of gravitational actions on the structure are described with f_g, while g denotes the gravity.

The dynamics of the structure yields [Trivedi 2008a] :

$$\mathrm{d}F(s) + f(s) = \rho\ddot{p}(s), \tag{4.7}$$

$$\mathrm{d}M(s) + p'(s) \times F(s) + M_{ext}(s) = J\ddot{\Theta}(s). \tag{4.8}$$

where $\Theta(s) = [\theta(s) \quad \phi(s) \quad 0]^T$ denotes the rotation angle given in polar form $J = diag(J_{x_s}, J_{y_s}, J_{z_s})$ the quadratic moment of inertia, and ρ is the linear mass distribution. The bending moment that acts at each point of the beam can also be described thanks to EB approach:

$$\kappa(s) = [\frac{M_{x_s}(s)}{(EI)_{eq_{x_s}}} \quad \frac{M_{y_s}(s)}{(EI)_{eq_{y_s}}}]^T, \quad \tau(s) = \frac{M_{z_s}(s)}{(EI)_{eq_{z_s}}}. \tag{4.9}$$

$\kappa(s)$ and $\tau(s)$ denote the local curvature and the local torsion of the FEAs, respectively. However, the twisting motion will be neglected (τ=0) in the remaining of

the proposal. The boundary conditions read:

$$\begin{cases} p(s)|_{s=0} = 0, \\ [\theta(s) \quad \phi(s)]_{s=0} = 0, \\ F(s)|_{s=L} = F_e, \\ [\theta'(s) \quad \phi'(s)]_{s=L} = [\dfrac{M_{e_x}}{(EI)_{eq_{x_s}}} \quad \dfrac{M_{e_y}}{(EI)_{eq_{y_s}}}]. \end{cases} \tag{4.10}$$

The soft finger is subjected to a combined bending. The stretch and compression can be neglected. With that, the hodograph $p'(s) = (x'(s), y'(s), z'(s))$ of $p(s)$ (the FEAs shape) meets with the following:

$$p'(s) = (\cos\phi(s)\sin\theta(s), \sin\phi(s)\sin\theta(s), \cos\theta(s)). \tag{4.11}$$

According to Eq. 4.7 and Eq. 4.10, the static equilibrium ($\mathrm{d}F(s) + f(s) = 0$) of the structure yields:

$$F(s) = F_e - \rho g(s - L)\mathbf{y}. \tag{4.12}$$

Considering that the distributed moment $M_{ext}(s) = 0$, and substituting Eq. 4.11 and Eq. 4.12 into Eq. 4.8, the following is obtained:

$$\begin{cases} \theta''(s) = \dfrac{F_{e_z}\sin\phi(s)\sin\theta(s) - (F_{e_y} - \rho g(s-L))\cos\theta(s)}{(EI)_{eq_{x_s}}}, \\ \phi''(s) = \dfrac{F_{e_x}\cos\theta(s) - F_{e_z}\cos\phi(s)\sin\theta(s)}{(EI)_{eq_{y_s}}}, \end{cases} \tag{4.13}$$

with

$$(F_{e_y} - \rho g(s-L))\cos\phi(s)\sin\theta(s) = \sin\phi(s)\sin\theta(s)F_{e_x}. \tag{4.14}$$

By considering FEAs with multiple control inputs, the procedure can be generalized by introducing the convenient boundary conditions at the portion linkages. In this research works, only two portions FEAs have been considered (see Fig. 4.3), and the following holds:

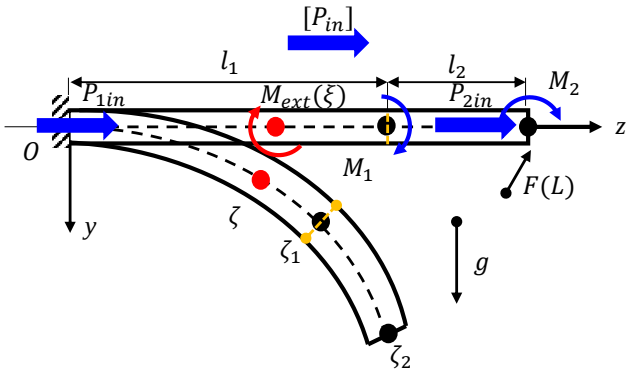

Figure 4.3: Two serial FEA geometry

1. **First phalange** $(0 \leq s \leq \zeta_1)$

$$p_1(s) = \int_0^s p'(\xi)\,\mathrm{d}\xi,$$

2. **Second phalange** $(\zeta_1 \leq s \leq \zeta_2)$

$$p_2(s) = \int_0^s p'(\xi)\,\mathrm{d}\xi + p_1(\zeta_1), \tag{4.15}$$

where the subscripts 1 and 2 stand for the first and second portion of the soft actuator, respectively.

4.3 PH-EB based model for shape control

4.3.1 Forward Dynamics Modeling based on PH curves

The advantageous features of parametric PH curves are combined with the EB model to control the FEA shape under external loads. This is to ease the modeling of the FEAs shape. For this purpose, the Bézier control points of the PH curve, representative of the FEAs shape, can be expressed as functions of the actuation inputs $[p_{in}]$ and the external loads. Assume that p_c and p_f describe respectively the clamped and the tip positions of the FEAs with d_c and d_f, their respective directions under actuation input (eg. pressure effort).

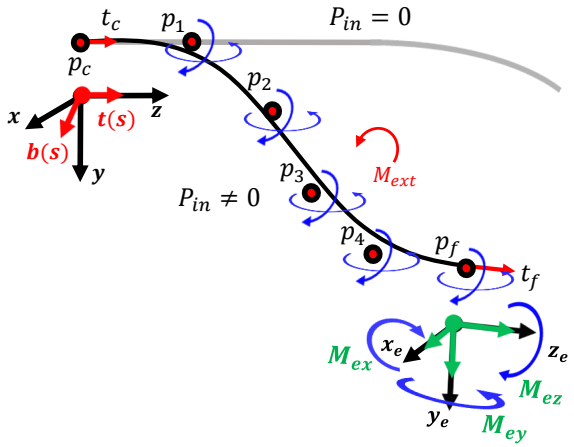

Figure 4.4: PH virtual control points

From Eq. 4.13 and Eq. 4.15, the pose of the robot tip can be computed regarding Eq. 4.10. Therefore, the following holds:

$$\begin{aligned} p_c &= (0,0,0), \qquad & t_c &= (0,0,1) \\ p_f &= p_f(p_{in}), \qquad & t_f &= d_f(p_{in}). \end{aligned} \tag{4.16}$$

According to Eq. 4.16, Eq. 3.17- Eq. 3.24, the quaternions pre-image $\mathcal{C}_m$, where $m = 0, 1, 2$, can be computed relative to the dynamics control inputs $[p_{in}]$. That is:

$$\mathcal{C}_m = \mathcal{A}_m(p_{in}), \quad m = 1, 2, 3. \tag{4.17}$$

The minimization of the potential bending energy of the FEAs through PH formulation leads to five virtual control points that fully describe the related shape dynamics subject to an actuation input vector $[p_{in}]$:

$$\begin{gathered} p_1 = p_0 + \frac{1}{5}\mathcal{C}_0\mathbf{i}\mathcal{C}_0^*, \quad p_2(p_{in}) = p_1 + \frac{1}{10}(\mathcal{C}_0\mathbf{i}\mathcal{C}_1^* + \mathcal{C}_1\mathbf{i}\mathcal{C}_0^*), \\ p_3(p_{in}) = p_2(p_{in}) + \frac{1}{30}(\mathcal{C}_0\mathbf{i}\mathcal{C}_2^* + 4\mathcal{C}_1\mathbf{i}\mathcal{C}_1^* + \mathcal{C}_2\mathbf{i}\mathcal{C}_0^*), \\ p_4(p_{in}) = p_3(p_{in}) + \frac{1}{10}(\mathcal{C}_1\mathbf{i}\mathcal{C}_2^* + \mathcal{C}_2\mathbf{i}\mathcal{C}_1^*), \quad p_5(p_{in}) = p_4(p_{in}) + \frac{1}{5}(\mathcal{C}_2\mathbf{i}\mathcal{C}_2^*), \end{gathered} \tag{4.18}$$

with $p_f = p_5$ and $p_c = p_0$. The above control points p_k $(k = 1, \cdots, 5)$, are all termed relative to the actuation inputs $[p_{in}]$ (see Eq. 4.10 and section 3.2.3). The shape of the soft structure is recovered with:

$$p(\xi, p_{in}) = \sum_{k=0}^{5} p_k(p_{in}) \binom{5}{k} (1-\xi)^{5-k}\xi^k. \tag{4.19}$$

4.3.2 Inverse Dynamics Modeling based on PH curves

To set the real actuating pressure that drives the shape of the soft actuator, one needs to determine first the equivalent curvature κ_{eq} of the actuated finger portion. Second, the corresponding control input p_{in} thanks to EB dynamics modeling (See Eq. 4.9).

Fig. 4.3 illustrates the kinematics of a 3 tubes-soft finger once actuated. The curvature $\kappa_{\alpha eq}$ in Eq. 4.9 should be taken as the mean curvature exhibited by the considered portion of the structure. Note that the subscripts $\alpha = 1, 2$ account for the first and the second phalanges of the soft finger, respectively.

In order to meet this requirement, the mean curvature $\kappa_{\alpha eq}$ of the desired shape, described using the PH curve, can be evaluated as described by Eq. 4.23 using the ***Darboux*** vector (Eq. 4.22).

The desired shape can be identified by knowing the control points r_k [Farouki 1994].

$$p_d(\xi) = \sum_{k=0}^{5} p_{k_d} \binom{5}{k} (1-\xi)^{5-k}\xi^k. \tag{4.20}$$

The computation of the required control input $[p_{in}]$ can be done by calculating the desired local curvature $\kappa_r(\xi)$ along the soft actuator. Since $r(\xi)$ denotes the desired

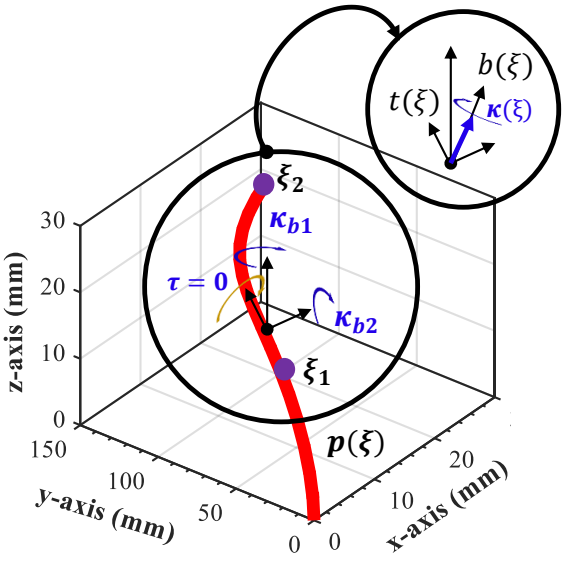

Figure 4.5: Local curvature illustration

posture, it can be written in the matrix form as [Singh 2018b]:

$$r_d(\xi) = \begin{bmatrix} 1 \\ \xi \\ \xi^2 \\ \xi^3 \\ \xi^4 \\ \xi^5 \end{bmatrix}^T \begin{bmatrix} 1 & 0 & 0 & 0 & 0 & 0 \\ -5 & 5 & 0 & 0 & 0 & 0 \\ 10 & -20 & 10 & 0 & 0 & 0 \\ -10 & 30 & -30 & 10 & 0 & 0 \\ 5 & -20 & 30 & -20 & 5 & 0 \\ -1 & 5 & -10 & 10 & -5 & 1 \end{bmatrix} \begin{bmatrix} p_{d0} \\ p_{d1} \\ p_{d2} \\ p_{d3} \\ p_{d4} \\ p_{d5} \end{bmatrix} \tag{4.21}$$

Then, the variable curvature (Eq. 3.29) of Fig. 4.5, can be calculated as follows :

$$\omega(\xi) = \kappa(\xi)\mathbf{b}(\xi) + \tau(\xi)\mathbf{t}(\xi), \quad \tau(\xi) = 0. \tag{4.22}$$

Thus, the equivalent curvature κ_{eq} is derived according to Eq. 4.23. After that, the equivalent curvature for each section of the soft finger is carried out with:

$$\begin{aligned} [\kappa_{1eq}] &= \frac{1}{l_1}\int_0^{\xi_1} \omega(\zeta)\mathrm{d}\zeta, \\ [\kappa_{2eq}] &= \frac{1}{l_2}\int_{\xi_1}^{\xi_2} \omega(\zeta)\mathrm{d}\zeta, \end{aligned} \tag{4.23}$$

where ξ_1 and $\xi_2(\xi_2 = 1)$ denote respectively the normalized curvilinear coordinates on the length of the soft finger. In accordance with Eq. 4.9 and Eq. 4.2, in the case of a 2-phalanges fingers (two actuated portions), it is possible to invert the dynamics using the EB beam modeling as [Mbakop 2021b]:

$$\begin{aligned} [M_2] - (\sum P_{2in}) I_2(s)\kappa_{2eq} &= E_2 I_2(s)\kappa_{2eq}, \\ [M_1] + [M_2] - (\sum P_{1in}) I_1(s)\kappa_{1eq} &= E_1 I_1(s)\kappa_{1eq}, \end{aligned} \tag{4.24}$$

where $I_\alpha(s) = diag(I_{\alpha_x}(s), I_{\alpha_y}(s), I_{\alpha_z}(s))$, $E_\alpha(\text{dim} = 1)$ are related to the portion $\alpha = 1, 2$ of the soft actuator. Eq. 4.24 describes a system of six equations with six unknowns, and thus allows us to define the actuation inputs of the robot corresponding to a prescribed shape.

4.4 Materials and Methods

This section describes the materials and validation method for the developed model used in dynamic shape control.

4.4.1 Materials

A single and a multiple actuators have been designed and manufactured. They are made up of Agilus 30 soft material. Tensile tests using Instron (Mechanical testing machine) have been carried out to get the material properties. The results of these tests were fitted using Ansys 2019. The Yeoh hyperelastic model for incompressible materials has been used. See Fig. 4.6, Tab. 4.1 for description and parameters.

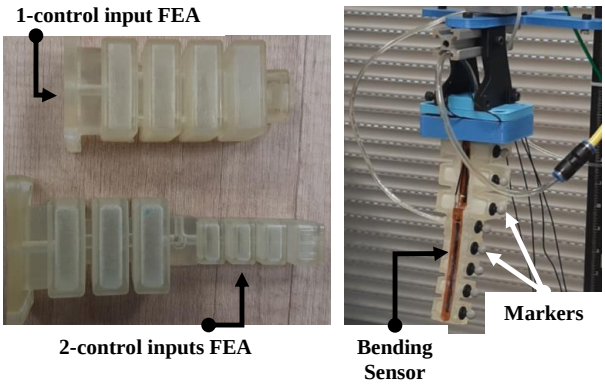

Figure 4.6: Experiments materials on 2D soft fingers

Table 4.1: 2D FEA parameters

FEA's materials constants	**FEA geometrical features**
C_1=0.062 Mpa	L_0: 87 mm **(single input)**
ν=0.45	L_1: 57 mm (1^{st} **phalange)**
E=0.4 Mpa	L_2: 63 mm (2^{nd} **phalange)**

In addition, 3D shape control experiments on CBHA (see Fig. 4.7 and Tab. 4.2) have been performed.

The actuators were equipped with markers. During the experiments, these have enabled the Optitrack acquisition system to capture shapes and displacements of

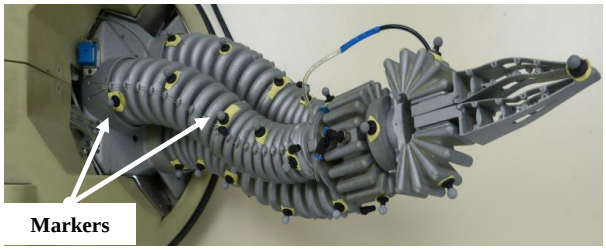

Figure 4.7: CBHA continuum robot with its 6 actuator inputs

Table 4.2: CBHA model parameters

CBHA materials constant	**CBHA geometrical features**
ρ=1015 kg.m^{-3}	**Backbone Length** L: 330 mm
ν=0.45	L_1: 185 mm (**1st section**)
E=1.1 Gpa	L_2: 145 mm (**2nd section**)

the actuators. The accuracy of the Optitrack system is approximately 0.34 mm. The bending sensors (Flexpoint Sensor System) were also embedded at the bottom of the in-extensible layer to assess the actuator shape in real-time. The real object shape to be tracked is measured using a 3D-camera. The present approach has been investigated in the case of a static object. Therefore, only one image capture by the camera largely holds by following the protocols presented in section 4.4.2. For more insight, the parameters used for the experiments are given in the table 4.3. The Festo Proportional air regulators (FESTO VPPM-6L-L-1-G18-0L6H-V1P) have been employed for the air pressure control, while the Simulink Dspace has been used for the real-time acquisition and control system.

Table 4.3: **Experiment test bench parameters**

Hardware	**Performances**
Optitrack System	**Mean 3D error**: 0.348 mm **Frequency**: 120 FPS **Marker size (diameter)**: 6.4 mm
Dspace controler	**Frequency**: 20 kHz
Air regulator	**Response time**: 0.5 ms **Accuracy**: 2 %
Bending sensors	**Repeatability error**: 0.3°

FPS: Frame Per Second

4.4.2 Methods

This subsection deals with the inverse computation of the dynamics of the flexible finger. The objective is to define the actuation inputs such that they can control the overall shape in a non-contact case. The essential steps for the proposed approach are discussed as follows:

Extraction of the target object contour: The object contour is extracted for shape reconstruction of the soft finger, by computing the data images got from the 3D camera. The data are split into 2 parts for parallel grasping positioning, according to the geometry of the object.

Object shape extraction: A reference shape is identified using a PH control polygon (See Fig. 4.4) since the poses of the endpoints of the grasping process are known. This modeling enables adjustment of the control points poses for shape adaptability or accuracy issues.

Curvature computation : After having identified the shape to be tracked, the equivalent curvature as discussed by Eq. 4.23 is computed. This latter one is varying depending on the control polygon configuration.

Control inputs setting : The calculation of the dynamic inputs is defined by Eq. 4.24 for the studied classes of soft fingers. The input air pressure is converted to an analog signal and is provided to the Festo air regulator using the Simulink Dspace controller.

As described in the methodology, the validation scheme is given in Fig. 4.8. After extracting the object shape to be gripped, the reference shape of the soft gripper is obtained by PH modeling. Then, the geometrical features allowing to have the complex shape are estimated. The inverse model is used to determine the different control inputs to obtain the complex reference shape. Finally, these control inputs are applied to the real system. A comparison of the real data with those from the model simulation allows estimating the model deviations.

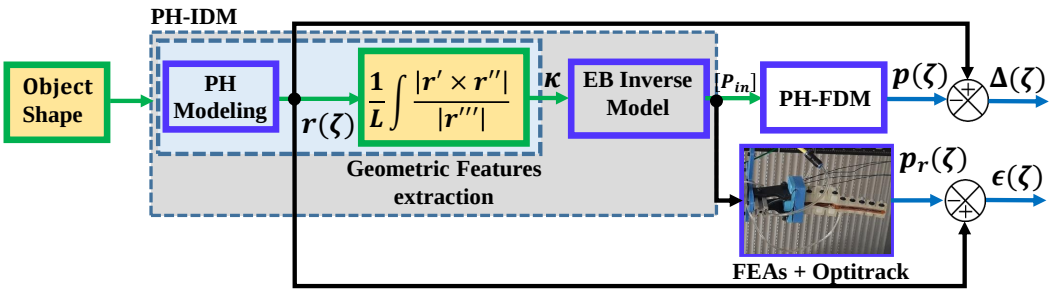

Figure 4.8: PH and inverse EB Model validation scheme

4.5 Results and discussions

The validation process consists of two main steps: In the first step, a simulation analysis (Section 4.5.1) is performed where the outputs of the proposed PH-EB are compared to the shape of the object to be tracked. In the second step, an online analysis (Sections 4.5.2 and 4.5.3) yields the real-world experiments.

4.5.1 Numerical results of shape reconstruction

In the following, the shape reconstructions for two types of objects are presented; one with a constant curvature describing a ball (Fig. 4.9) and another with a variable curvature (Fig. 4.10) describing a mango.

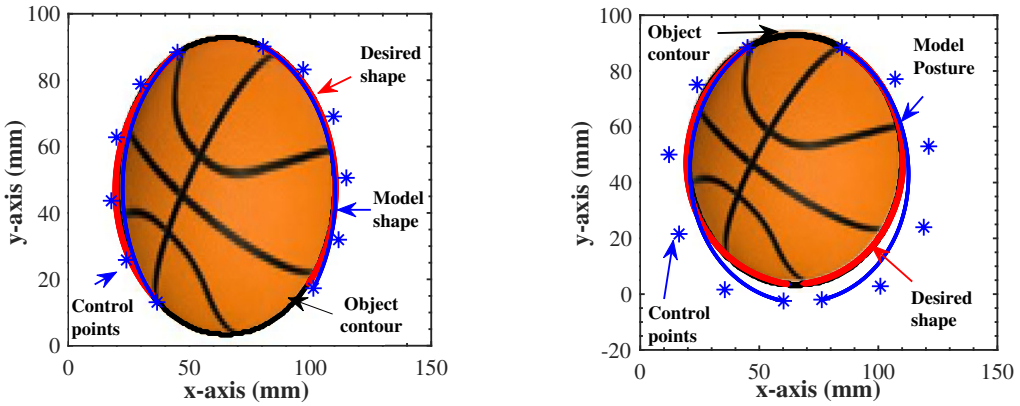

(a) Single input actuator

(b) Multiple inputs actuator

Figure 4.9: Shape reconstruction of a basket-ball

In these figures, it is shown two soft fingers encapsulating the objects from each side for shape reconstruction and grasping tasks. The red contour legend represents the desired shape of the object extracted from the object contour. The blue curve with its control points describes the reconstructed shape, from the PH modeling allowing estimating by EB inverse dynamics, the corresponding desired actuation inputs. The grasping process is made on the xy-plane.

On Fig. 4.9a, the data using one control input actuator are plotted. Fig. 4.9b shows an accurate reconstructed shape (Blue legend) with two phalanges soft actuator. On Fig. 4.9a, the reconstruction of the object exhibits errors bigger than those observed in Fig. 4.9b. The errors observed in Fig. 4.9a can be explained by the complex shape geometry of the considered object. Indeed, a variable curvature is induced along the length of the desired shape. This is following the Eq. 4.11, where the actuation pressure input is computed using a constant curvature.

However, when experimenting with a constant curvature shape reconstruction described by a ball, the reconstructed shape of the ball (90 mm of diameter) using two phalanges appears less accurate compared to the case of one phalange, where a single actuator is considered. This observation can be explained by the difference

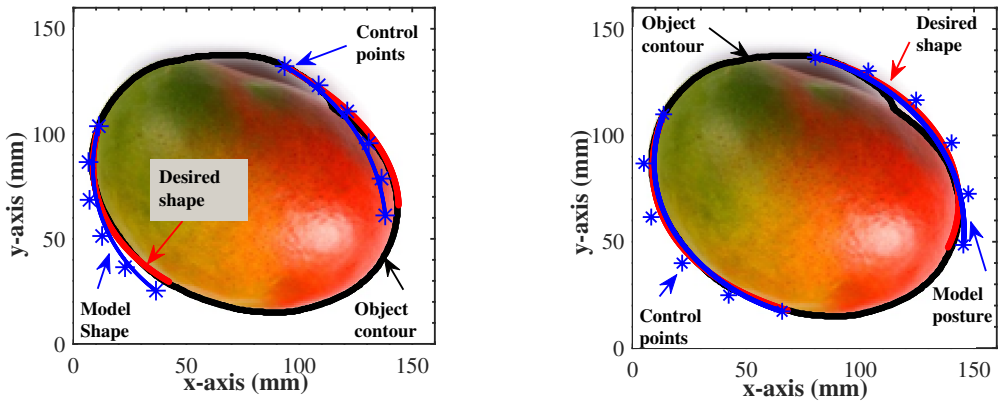

(a) Single input actuator (b) Multiple inputs actuator

Figure 4.10: Shape reconstruction of a Mango

in the arc length between the desired shape and the reconstructed one. These results show that for optimal shape reconstruction, it is necessary to find an optimal distribution of actuation inputs along the length of the soft fingers.

4.5.2 Validation on 2D soft fingers

Experimental tests of the PH-EB model-based control have been carried out on the soft fingers described previously. They have been compared to the ANSYS numerical modeling and real truncated shapes (the right side) for the two studied contours of objects (Ball, Mango). Fig. 4.11a describes a shape tracking experiments with a single phalange. Only one set of data (the ones at the right side of experiments) was chosen to investigate the shape tracking.

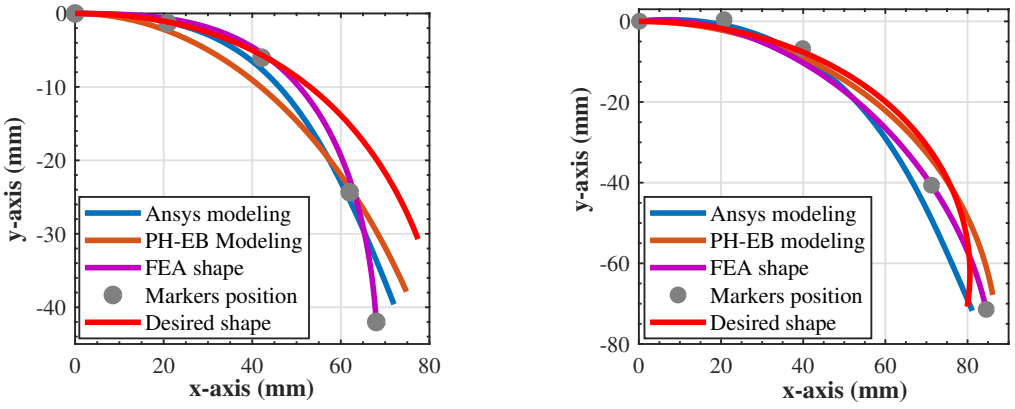

(a) Shape with a single input (b) Shape with multiple inputs

Figure 4.11: Shape reconstruction with soft fingers

The Ansys Data analysis and the position of the Optitrack markers have also

been described. The Cartesian errors are analyzed along the soft actuator length to assess the pertinence of the results. A maximum error of Δ_{max}=15 mm along the FEAs is observed (at the tip) comparing to the desired shape. This error is greater than the one given by the model relative to the experiments, where the maximum reached is around 8 mm (9.2 % of the robot length). This value of Δ_{max} confirms the difficulties to meet the shape adaptation requirements using a single actuation input (single phalange), as explained in 4.5.1. However, the value of $\varepsilon_{max} \approx 8$ mm (9.2 % of the robot length) explains the error given by the PH-EB modeling relative to the experiments, where the maximum reached is around 8 mm.

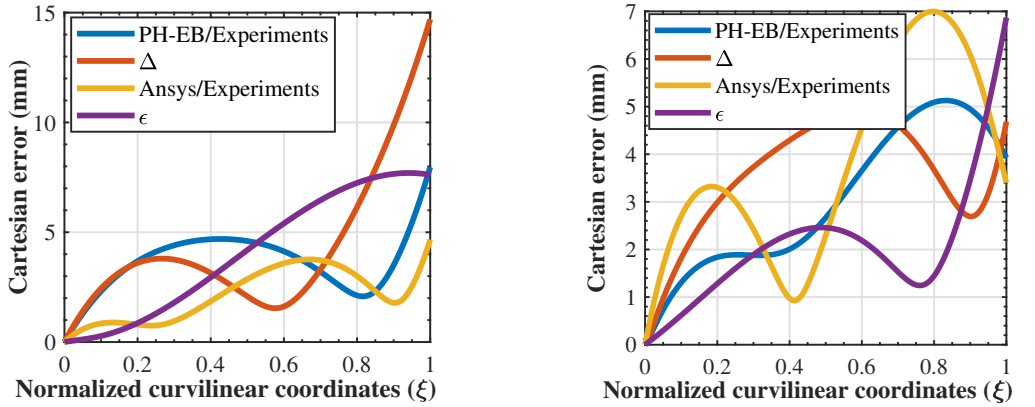

(a) Errors of shape reconstruction of the basket ball

(b) Errors of shape reconstruction of the mango

Figure 4.12: Shape reconstruction with soft fingers

From Fig. 4.12b, one can note that the error between the desired shape and the one reconstructed from PH-EB model has a maximum of $\Delta_{max} \approx 5$ mm (4.2 % of the robot length). Also, the error observed between the PH-EB model and the experiments have a maximum value close to 5 mm. These values are smaller compared to the analysis of 4.12a. It confirms the influence of using multiple actuation inputs for accurate shape reconstruction. In addition ε exhibits a biggest value at the tip, $\varepsilon_{max} \approx 7$ mm (5.83 % of the robot length).

In addition, the results show that the Ansys modeling and the proposed approach have similar behavior even though Ansys modeling results appear more accurate. However, some gaps exist between the real shape and the simulated shape. Some dynamics aspect omission, using PH-EB model, such as shear forces, normal stresses induced by the inflated pressure, and material properties uncertainties related to the fitting process might probably lead to the errors observed. Overall, the results are consistent. Also, it is worth noting that the accuracy of the shape measured by the vision system depends on its accuracy. This latter can significantly affect the experimental results.

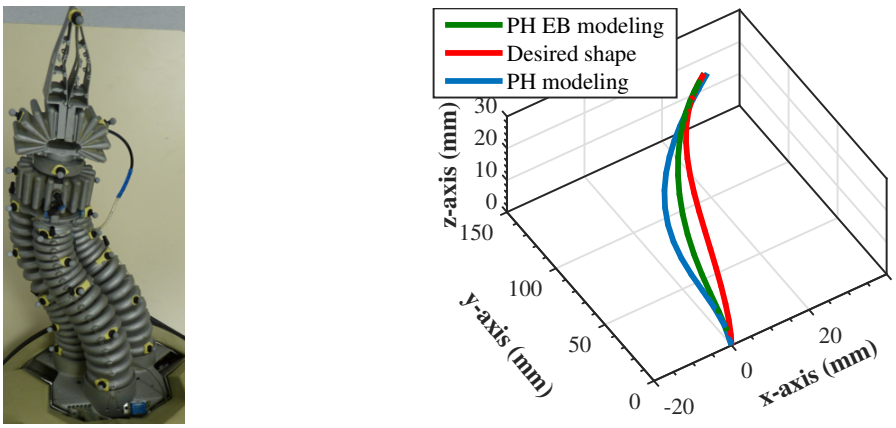

(a) Real soft continuum robot

(b) Kinematics reconstruction

Figure 4.13: 3D CBHA Shape in free case

4.5.3 Validation on 3D CBHA continuum manipulator

For the 3D CBHA shape of Fig. 4.13a, a reference shape is tracked (red curve) in a free case. The PH modeling (blue color) described in [Singh 2018b] makes a shape kinematics reconstruction without considering the length of robot constraint. By observing the experiment results, a mean position error between the 400 points of the real robot shape and those given by the PH modeling is equal to 4.4 mm (1.5 % of the robot length). Using the PH-EB modeling (green color), which respects the length constraint of the robot, the obtained mean error is about 2.3 mm (0.7 % of the robot length).

Table 4.4: **Comparison results in case of external load**

Methods	SME	MTE	Time cost
PH EB modeling	7.1 mm (2.4 %)	3.8 mm (1.26 %)	0.0004 s
PH modeling	12.3 mm (4.1 %)	11.2 mm (3.7 %)	0.00031 s

SME: Shape Mean Error, MTE: Mean Tip Error

Furthermore, external efforts on the robot (Fig. 4.14) have been investigated in load cases by adding a mass of 200g at the tip of the robot. For the same desired endpoint (tip point) as in the free case, a shape deformation occurs along the soft continuum manipulator. This deformation is kinematically reproduced by the PH modeling with fewer accuracy performances according to the desired endpoint. However, the PH-EB modeling allows calculating the optimal actuator inputs (pressures) for accurate shape reconstruction and the desired endpoint tracking. Comparative performances between the PH modeling reconstruction [Singh 2018b] and the PH-EB modeling with adaptive reconstruction from actuator inputs are given in Table

4.4. Fig. 4.14 presents the 3D shape kinematics while considering external load.

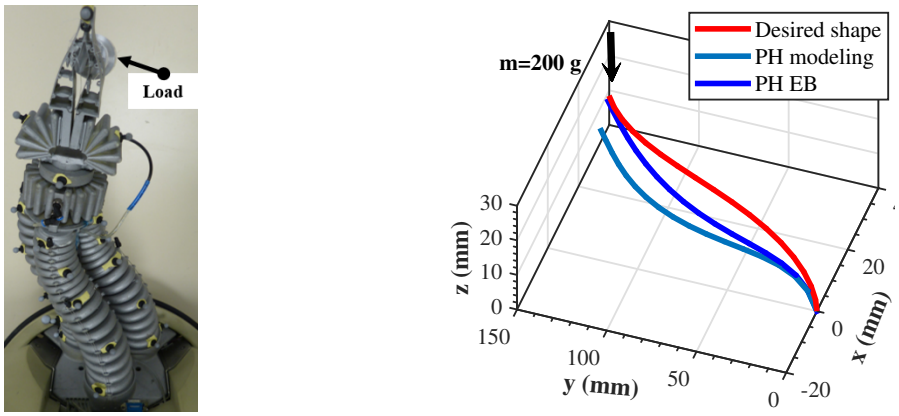

(a) Real soft continuum robot

(b) Kinematics reconstruction

Figure 4.14: CBHA Shape kinematics in case of external load

The results of the experiments have been analyzed and showed for PH modeling reconstruction, indicating a mean error position for the shape of 12.3 mm (4.1 % of the robot length) and of 11.2 mm (3.7 % of the robot length) for the tip point tracking. After applying the PH-EB modeling, the mean error of the shape is about 7.1 mm (2.4 % of the robot length) and the tip tracking error 3.8 mm (1.26 % of the robot length).

4.6 Conclusion

The inverse dynamic modeling for 2D and 3D shape reconstruction of soft continuum robots based on the PH-EB approach has been investigated. The proposed modeling combines features of EB beam mechanics and those of PH parametric curves with the macro and micro properties of the soft structure. EB beam mechanics can be coupled with PH quintic. This allowed identifying the relationship between the desired actuator inputs and the position of the finite virtual control points. These latter have been been studied in more detail for shape reconstruction in the contact-free cases and external load cases. The results obtained show the consistency and the relevance of the proposed approach to reconstruct complex-shaped objects in 2D and 3D with different types of soft continuum robots. Moreover, the developed approach allows implementing a form of enclosure grasping. In the next chapter, this control approach is used for the integrated design of a bio-inspired soft gripper for mushrooms harvesting.

Chapter 5

Application to Integrated design of a Soft Gripper

Contents

5.1 Introduction

The current soft gripping systems developed in the previous chapters, although soft, can be limited because, in most of the cases, they do not have feedback information for the grasping control. However, the advantages of hand-picking lie simultaneously in the shaped feedback for compliance and the force feedback control for target quality preserving. This chapter gathers together and applies of the techniques analyzed in the previous chapters for the application of automated mushroom harvesting. An integrated design of a soft agri-food gripper for mushroom harvesting is described. The soft gripper is made up of three soft fingers

based on the kinetic configuration of the human hand fingers during the harvesting process. An APF approach discussed in chapter 3 is considered, to tackle the shape kinematics control issues during the grasping. An adaptation to an attractive potential field is used for the grasping task. This APF strategy is applied to the control points of the PH-based , allowing the control of the soft fingers to realize a form enclosure grasping. Also, a model-based inverse dynamics that uses EB beam modeling in presence of external efforts [Mbakop 2021c], coupled to parametric PH curves for the soft finger shape estimation is applied. This has enabled to address the estimation of the actuator inputs, which are used to set the desired shape of each soft finger for safe harvesting.

5.2 Gripper Design

The design of the soft gripper is inspired by human hand-picking during mushroom harvesting. Thus, a set of bio-inspired soft human fingers placed in parallel has been considered for the gripper design. The three soft fingers that often operate are the thumb, the index, and the middle finger. Each finger is composed of two phalanges. Their relative size and orientation allow a stable grasping motion.

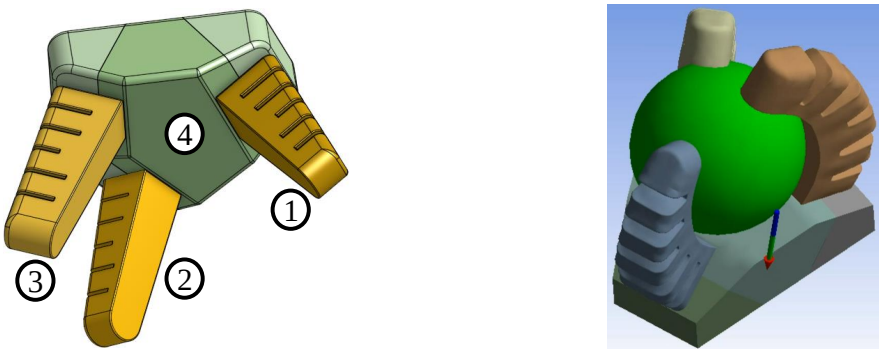

(a) Agro-Food Gripper parts

(b) Soft Finger Workspace

Figure 5.1: Agro-Food Gripper: Thumb (1), Middle-finger (2), Index (3), Palm (4).

5.2.1 Soft Actuator design

The configuration of a human hand during the harvesting process has been adopted. For that purpose, the thumb, index, and middle finger were considered regarding the size of an adult human hand. 70 mm has been considered for the thumb length while 75 mm and 85 mm have been used for the index and the middle finger respectively.

In order to ease the shape adaptability, the soft finger design has been based on a ribbed morphology. The ribbed morphology [Rus 2015] has the advantage of large bending. Each soft finger is made up of two phalanges actuated independently from each other. This has the advantage of allowing to track two different curvatures

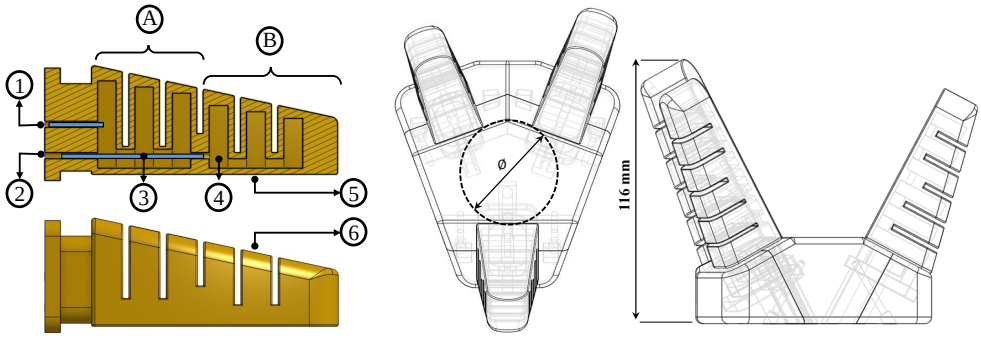

(a) Soft finger design (b) Gripper sizing

Figure 5.2: Soft finger architecture: 1^{st} phalange (A), 2^{nd} phalange (B), 1^{st} phalange Air inlet (1), 2^{nd} phalange Air inlet (2), Flexible air tube (3), Air chamber (4), unextensible layer (5), Flexible layer (6).

within the same shape (Fig. 5.2). In addition, in order to better capture non-constant curvature that might vary along with the shape of the mushrooms, the soft finger air chamber geometry which influences the most the bending are varying along the length of the soft actuator.

5.2.2 Material and Finite Elements Analysis

The finger has been designed with Dragon Skin 30 soft material. A general polynomial form (Eq. 5.1) for incompressible material has been adopted to characterize the material.

$$W = \sum_{i=1}^{3} C_i (I_1 - 3)^i, \tag{5.1}$$

W denotes the strain-energy density function, C_i and I_i represent the material constants. C_i were determined by fitting the model to uniaxial tensile test data using Ansys Software fitting process. They are used to calculate Young modulus based on the Yeoh hyperelastic material model:

$$2C_1 = \mu \tag{5.2}$$

and obviously,

$$E = 2\mu(1 + \nu). \tag{5.3}$$

The results of these tests were fitted using Ansys 2019 on the consistency of the Yeoh hyperelastic model for incompressible materials. The Tab. 5.1 describes the FEAs properties. After having modeled the material in Ansys 2019 R2, some simulations have been carried out in order to assess the real-world behavior of the bio-inspired gripper. The simulations have shown that the lift capabilities of the designed soft gripper might go up to 280 mg, which has proved to be enough for mushrooms harvesting while preserving their shape.

Table 5.1: FEAs parameters

FEAs materials constants	
C_1=12.02e^{-2} Mpa	C_2=2.2204e^{-14} Mpa
ν=0.45	C_3=1.8e^{-3} Mpa
E=0.7 Mpa	ρ=1080 kg.m^{-3}

5.2.3 Sensors and Embedded Electronics

The gripper designed is a proprioceptive soft gripper capable of shape adaptability. This feature aims to preserve the shape of the mushrooms during their harvesting.

1. **Sensing**

Each finger was equipped with a resistive bending sensor (Flexpoint Sensor System, Draper, UT, USA) placed conveniently at the bottom layer. The Flexpoint bending sensors are inextensible. According to the design, they have been placed at the neutral axis bending plane of the finger (Fig. 5.3). The advantage of this choice is that it allows capturing the effective bending of the finger part, which is in touch with the object during the grasping process. Hence, the real-time shape of the under-actuated finger can be measured and controlled for shape adaptation purposes during mushroom harvesting. In addition, Force Sensing Resistor (FSR) sensors were also used to evaluate gripping forces to avoid damaging the mushrooms during harvesting. Several tests and simulations were carried out to determine their optimal position in the in-extensible bottom layer (Fig. 5.3) of the soft actuators. The major advantage of the latter is to allow the shape control while maintaining an optimal contact value with the mushrooms without damaging them. The combined results of all the above, allow the soft gripper to achieve a form-enclosure grasping, suited for a safe mushrooms harvesting.

2. **Controller**

The control of the pressure to the FEAs is managed by a master system which perfoms a proportional regulation of the main pressure line by means of Festo proportional air regulators (FESTO VPPM-6L-L-1-G18-0L6H-V1P). The control architecture consists of a master control unit, running on a PC and developed in MATLAB/Simulink (Math-Works Inc., Natick, MA, USA), and a slave control unit (Dspace controller). While the slave unit accomplishes low-level control operations such as mastering the Proportional air regulators, reading the flex bend sensors signals, the master unit computes the reference of the main line pressure. Therefore, the computed value of the pressure is provided as reference to the pressure regulator of the main pressure line.

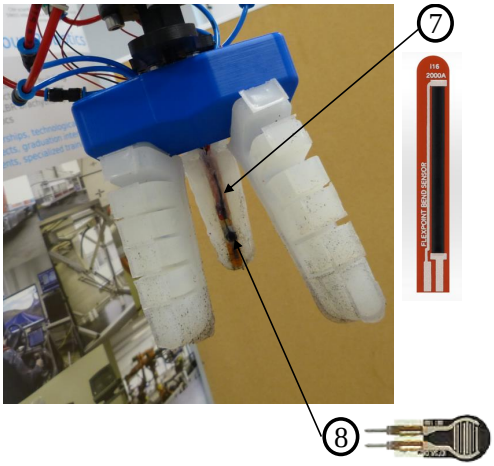

Figure 5.3: Integrated soft bionic gripper: FSR Interlinks electronics (7), Bend sensor, FlexPoint sensor system inc. (8)

5.2.4 Manufacturing

The soft bionic actuators have been manufactured by the molding process. Each of them is made up of two phalanges composed of a flexible layer and a rigid layer.

The manufacturing process has been structured in different steps: the first step has consisted in the mold fabrication before the casting phase. The finger mold has been designed using SolidWorks 2019 software and has been 3D-printed with ABS materials. It is composed of two parts: the upper part for the flexible layer and the lower part for the rigid layer. The flexible layer has been designed in such a way that, it allows two air inlets (see Fig. 5.2) for the actuation: one for the first phalange and the other for the second phalange.

After preparing the Dragon Skin 30 silicone material (Smooth-On, Inc), it was cast for the molding of the flexible actuator layer (see Fig. 5.4a). The demolding took place after about 16 hours of curing and the air tubes (blue and black) to supply air to the first and second phalanges were placed appropriately (see Fig. 5.4b). Then the lower layer was also poured into its mold and the already cured soft layer (with its air tubes) placed so that both layers polymerize (see Fig. 5.4c). This is to ensure continuity of the material to minimize delamination. Similarly, after approximately 16 hours of curing, the assembly was de-molded (see Fig. 5.4) and the flexible in-extensible sensors were bonded to its bottom layer (Fig. 5.3) using Sil-Poxy silicone adhesive (Smooth-On, Inc). This ensures that the bottom layer does not stretch during actuation, despite its hyper-elastic characteristics.

The soft finger palm was 3D printed in 3 parts to allow the soft fingers with their sensor wires and air tubes to be inserted without difficulty. Once the integrated soft finger has been placed, the 3 parts of the palm was screwed to make a stable assembly.

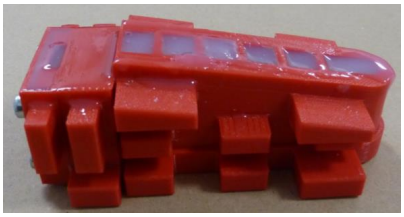

(a) Flexible layer molding

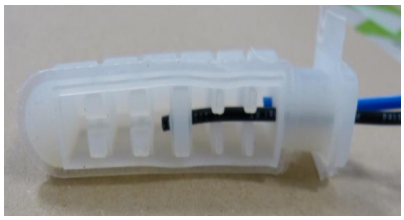

(b) Flexible layer with air tubes

(c) Bottom layer molding

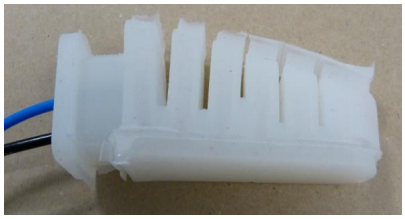

(d) Full soft actuator

Figure 5.4: Soft finger manufacturing process

5.3 Modeling

Our gripping strategy consists in extracting the shape of the object by image processing, capturing this shape by PH curves, and reproducing these curves as well as possible by driving the soft fingers. For this purpose, the modeling of the bio-inspired gripper is required. To implement real-time shape control, a relationship between the soft actuator shape and the actuator inputs has been established. The shape kinematic modeling has been discussed in chapter 3. In chapter 4, a modeling technique allowing the dynamics control inputs to be mapped to the shape of the soft actuator has been explored.

5.3.1 Actuation Modeling

Each of the soft actuators of the soft bio-inspired gripper has been designed to exhibit a planar bending motion in its corresponding workspace. Therefore, each phalange of the finger is actuated by only one dynamics control. A rectangular cross-section has been chosen for its simplicity during the manufacturing process.

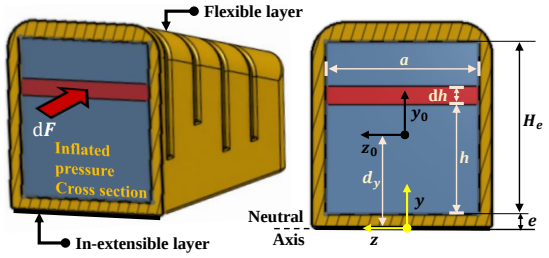

Figure 5.5: FEAs sizing concept

The details regarding the cross-section of the soft actuator are presented in Fig. 5.5. The infinitesimal normal force $\mathrm{d}F$ caused by the input pressure p_{in} can be computed as follows:

$$\mathrm{d}F = (ap_{in})\mathrm{d}h \tag{5.4}$$

If one control input p_{in} is considered for a given portion, the bending moment M_e (Fig. 4.2) can be described as proportional to p_{in} by a geometric constant Ψ_p:

$$M(s) = \int (h+e)\mathrm{d}F = \Psi_p p_{in} \tag{5.5}$$

where:

$$\Psi_p = aH_e(\frac{1}{2}H_e + e)p_{in}. \tag{5.6}$$

5.3.2 Shape dynamics modeling

The soft finger is made up of an in-extensible bottom layer. Thus, its length L remains constant during the actuation. Also, the air pressure is used as the actuation approach during the harvesting process. This induces an end moment M_e which causes the bending all along with the soft finger, as shown in Fig. 4.2.

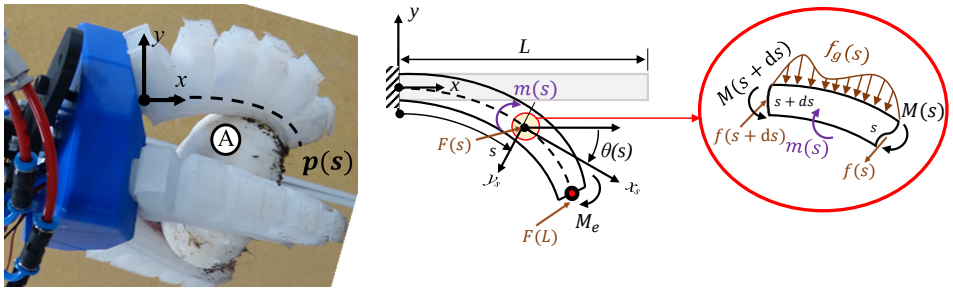

(a) Soft finger under external interactions A. Mushrooms

(b) Planar bending of a soft finger

Figure 5.6: Soft finger bending modeling during harvesting process

The external interactions F, issued from the contact with the mushroom, might influence the shape kinematics of the soft fingers. The self-weight, due to the distributed earth gravity is also taken into account. A single soft finger can be represented by a quintic PH curve with length L and is expressed in the form of the arc-length parametrization $p(s) : [0, L] \to \mathbb{R}^3$, see chapter 3. During the harvesting, a bending angle is observed. That is $\theta(s)$, the angle between the positive x-axis and the tangent to the neutral axis at point s (Fig. 5.6b).

Without loss of generalities, the planar dynamics of the structure can be described with :

$$\begin{cases} \mathrm{d}F(s) + f(s) = \rho\ddot{p}(s), \\ \mathrm{d}M(s) + p'(s) \times F(s) + m(s) = J\ddot{\theta}(s). \end{cases} \tag{5.7}$$

where all the equation terms have been defined in 4.2.3. The following is the behavior law of the each soft finger during the harvesting process:

$$\begin{cases} x'(s) = \cos\theta(s), \quad y'(s) = \sin\theta(s), \\ \theta''(s) = \dfrac{(f_{e_y} - \rho g(s-L))\sin\theta(s) - f_{e_x}\cos\theta(s)}{(EI)}. \end{cases} \tag{5.8}$$

and the boundary conditions read:

$$\begin{cases} p(s)|_{s=0} = 0, \\ \theta(s)|_{s=0} = 0, \quad \theta'(s)|_{s=L} = \dfrac{M_{e_x}}{(EI)_{eq_{x_s}}}, \\ F(s)|_{s=L} = F_e. \end{cases} \tag{5.9}$$

1. Soft finger forward dynamics

A Reduced-Order-Model (ROM) based on quintic PH curve is used to control each soft actuator. This allows mapping the finger shapes to the actuation inputs for a compliant grasping process.

The forward dynamics of each of the gripper soft actuator is to compute their control points p_k,$(k = 1 \cdots 5)$, with respect to the dynamic control inputs. This is to reconstruct the shape of the soft actuator accordingly. As it has been discussed in chapter 4, the boundaries conditions of the PH-based kinematics is consistent with:

$$\begin{aligned} p_c &= (0,0) \qquad & d_c &= (1,0) \\ p_f &= p_f(p_{in}), \qquad & d_f &= d_f(p_{in}). \end{aligned} \tag{5.10}$$

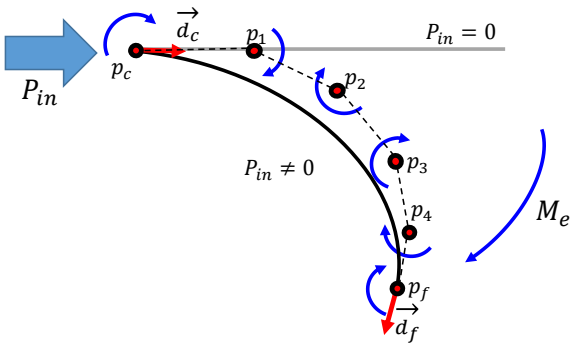

Figure 5.7: PH virtual control points

The control polygon $\Lambda_5(p) = \{p_0 \cdots p_5\}$,is termed relative to the input pressure $[p_{in}]$ (see Eq. 5.9) as follows:

$$\begin{aligned} p_1 &= p_0 + \frac{1}{5}\mathcal{C}_0\mathbf{i}\mathcal{C}_0^*, \quad p_2 = p_1 + \frac{1}{10}(\mathcal{C}_0\mathbf{i}\mathcal{C}_1^* + \mathcal{C}_1\mathbf{i}\mathcal{C}_0^*), \\ p_3 &= p_2 + \frac{1}{30}(\mathcal{C}_0\mathbf{i}\mathcal{C}_2^* + 4\mathcal{C}_1\mathbf{i}\mathcal{C}_1^* + \mathcal{C}_2\mathbf{i}\mathcal{C}_0^*), \\ p_4 &= p_3 + \frac{1}{10}(\mathcal{C}_1\mathbf{i}\mathcal{C}_2^* + \mathcal{A}_2\mathbf{i}\mathcal{C}_1^*), \quad p_5 = p_4 + \frac{1}{5}(\mathcal{C}_2\mathbf{i}\mathcal{C}_2^*), \end{aligned} \tag{5.11}$$

where $\mathcal{C}_m = \mathcal{A}_m(p_{in})$, $m = 0, 1, 2$, represent the quaternion pre-image, all related to end points pose interpolation (position and direction) and the prescribed length of the soft actuator. The shape of the soft structure is thus reconstructed with:

$$p(\xi, p_{in}) = \sum_{k=0}^{5} p_k(p_{in}) \binom{5}{k} (1-\xi)^{5-k} \xi^k \tag{5.12}$$

2. Soft finger inverse dynamics

EB modeling approach (see Eq. 4.9) is used to map the dynamic control inputs in the configuration space of each of the soft actuators as suggested in chapter 4. The desired shape $r(\xi)$ is identified with the knowledge of the desired control polygon $\Lambda_n(r) = \{r_0 ... r_n\}$ [Farouki 1994] issued from the shape of the mushroom hat to be grasped.

$$r(\xi) = \sum_{k=0}^{5} r_k \binom{5}{k} (1-\xi)^{5-k} \xi^k \tag{5.13}$$

The local curvature along the length of the soft structure holds with:

$$\kappa(\xi) = \frac{|r'(\xi) \times r(\xi)''|}{|r'(\xi)|^3}, \tag{5.14}$$

and the equivalent curvatures $\kappa_{1,2eq}$ of each phalange of the soft finger read:

$$\begin{aligned} \kappa_{1eq} &= \Big[\frac{1}{l_1} \int_0^{\zeta_1} \kappa(\xi) \mathrm{d}\xi\Big] \\ \kappa_{2eq} &= \Big[\frac{1}{l_2} \int_{\zeta_1}^{\zeta_2} \kappa(\xi) \mathrm{d}\xi\Big] \end{aligned} \tag{5.15}$$

Also, ζ_1 and $\zeta_2 (\zeta_2 = 1)$ denote respectively the normalized curvilinear coordinates on the length of the first and the second portion of the soft finger. The following equation allows mapping the dynamic control inputs in the configuration space of each soft finger.

$$\begin{aligned} P_{2in} &= \frac{E_2 I_2 {\Psi_{p_2}}^{-1}}{1 - I_2 \kappa_{2eq} {\Psi_{p_2}}^{-1} \kappa_{2eq}}, \\ P_{1in} &= \left[E_1 I_1 \kappa_{1eq} - \frac{E_2 I_2}{1 - I_2 \kappa_{2eq} {\Psi_{p_2}}^{-1} \kappa_{2eq}}\right] \frac{{\Psi_{p_1}}^{-1}}{1 - I_1 \kappa_{1eq} {\Psi_{p_1}}^{-1}} \end{aligned} \tag{5.16}$$

The parameters (E_1, I_1, Ψ_{p_1}) and (E_2, I_2, Ψ_{p_2}) are related to the first and the second portion of the soft finger respectively.

5.4 Soft gripper Control

The proposed control aims to allow a form enclosure gripping during the harvesting process while reducing the control dimension. The bio-inspired soft gripper

can be described by a parametric PH curve $p(\xi) : [0, 1] \to \mathbb{R}^3$, where ξ is a normalized curvilinear coordinate along with the soft finger. The mushrooms hat boundaries can be specified by the topological manifold $\mathscr{C}$ (Fig. 5.8). The control is applied to the control points (rather than to all points) of the curve so that the soft finger adapts to the shape of the mushroom's hat for safe grasping.

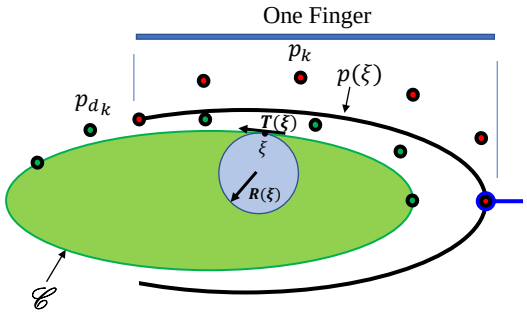

Figure 5.8: Grasping control illustration in 2D

With this approach, the target (the topological manifold $\mathscr{C}$ representing the mushroom's hat) is a set of points. In this application, the contours of the mushroom cap to be grasped while respecting their shape, are modeled by a repulsive and attractive potential field, simultaneously. The idea of the repulsive potential is to allow the soft fingers to conveniently approach the physical contour while avoiding the collision. Then, the attractive potential field is used to allow the soft actuators to grasp effectively while adapting to the shape at the gripping contact. The curvature of the soft finger is assumed to be controlled and the twisting motion is not considered.

$$\kappa(\xi) \leq \kappa_{\max}(\xi). \tag{5.17}$$

The assumption (5.17) describes the design constraints of the soft actuators, and the upper-bound $\kappa_{\max}$ specify the maximal curvature exhibited by the mushroom hats.

Define by $\Phi(p_k, p_{d_k}, \mathbb{O}_k) \geq 0$, the potential function depending on the position of $p_k \in \mathbb{R}^3$, the control points of the curve $p(\xi, t)$ representing the soft finger.

$p_{d_k} \in \mathbb{R}^3$ is one desired position to reach (attractor) according to the location on the soft finger. $\mathbb{O}_k \subset \mathbb{R}^3$ is a set of obstacles to be avoided which includes the object boundaries $\mathscr{C}$.

The proposed APF strategy is applied on the control points p_k of the PH curve $p(\xi, t)$, rather than all the curve points. The same algorithm used in chapter 3, is implemented except with some minor updates. The updates are made with regard to the target which is defined as a set $\{p_{d_k}\}$ rather than a single point.

It is made up two parts:

- $\Phi(p_k, p_{d_k}, \mathbb{O}_k) = 0$ is the attractive part located at one desired point where $p_k = p_{d_k}$

- $\Phi(p_k, p_{d_k}, \mathbb{O}_k) > 0$ is the repulsive part of the potential such that $\mathbb{O}_k : \{\forall p \in \Lambda_n(p_d) \backslash p_{d_k}, \lim_{p_k \to \mathbb{O}_k} \Phi(p_k, p_{d_k}, \mathbb{O}_k) = +\infty\}$.

The system behavior, namely the curvature κ as well as the proof of stability of the updated algorithm have been largely discussed in chapter 3.

5.5 Materials and Method

The experiments carried out in the frame of this research work were established with the help of some dedicated materials and very precise procedures.

5.5.1 Materials

The UR10, a 6-DoFs collaborative manipulator from Universal Robots Company, has been used to place the soft gripper at a required location. To this, the OnRobot Eyes vision system was used to identify the pose of the mushrooms. It consists of a stereo camera fixed to the Tool Center Point (TCP) of the manipulator, the control unit connected to the manipulator controller, and a PC through an Ethernet port. The system has build-in programs to provide the center point positions

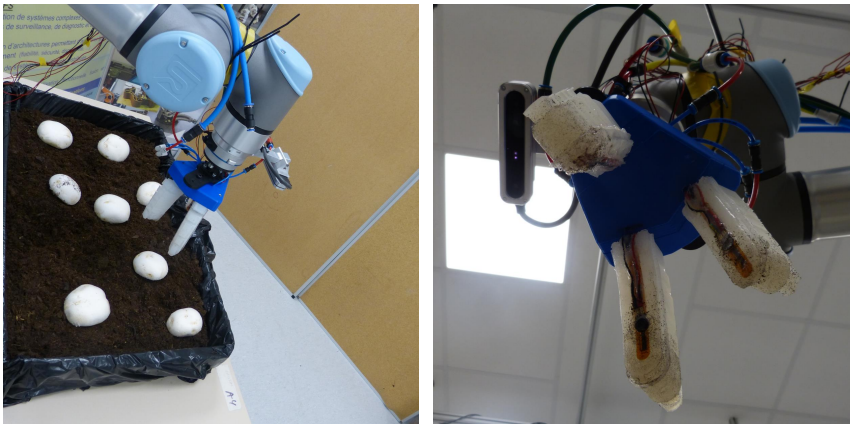

Figure 5.9: Harvesting scene

of registered workpieces with different shapes and colors in the manipulator base frame.

The Festo Proportional air regulators (FESTO VPPM-6L-L-1-G18-0L6H-V1P) have been employed for the air pressure control, while the Simulink Dspace has been used for the real-time acquisition. All the process has been performed using a PC Intel® CORE™ i5-8250U @1.60GHz 180GHz.

For more insight, the parameters used for the experiments are given in the table 5.2.

Table 5.2: Hardware characteristics

Hardware	Performances
Dspace controler	Frequency: 20 kHz
Air controller	Response time: 0.5 ms Repeatability: 0.5 % Resolution: 0.06 bar
Bending sensors	Repeatability : 0.3°
FSR	Repeatability: 0.2% Response time: $\leq$ 2 s
OnRobot Eyesvision system	Typical error: 0.6596 mm Accuracy: 2 mm Processing time: 0.5 s

5.5.2 Methods

Two main essential steps for the proposed approach have been considered: image processing and actuation control.

1. **Image processing**

The automatic detection of a mature mushroom is made by vision-based computer processing. This allows the contouring of the mushroom hat and the detection of the pose of its center point. Once the center point is obtained, the soft gripper can be guided by the UR10 to reach the required position of the detected mushroom. Based on the harvesting working field as shown in Fig. 5.9, the OnRobot Eyes detection program provides the contour and center of each detected mature mushroom. This latter is then used to compute the potential field (Fig. 5.12a) that will guide the soft gripper for the form enclosure grasping. Fig. 5.10 shows an example of detection results. The coordinate of each center point in the frame of the manipulator base will be provided to the control unit of the manipulator so that it can guide the soft gripper to the positions of mature mushrooms one after another. Once the mushroom's hats contour has been extracted, a reference shape is identified using PH control polygon (See Fig. 5.7). This latter allows specifying the required curvatures for each phalange of the soft fingers as discussed in Eq. 5.15.

2. **Actuation control**

With the extracted mushrooms contour, the equivalent curvature can be computed according to Eq. 5.15 after having identified the desired control polygon $\{p_{d_k}\}$ as shown in Fig. 5.8. The dynamic inputs are set by Eq. 5.16. The input air

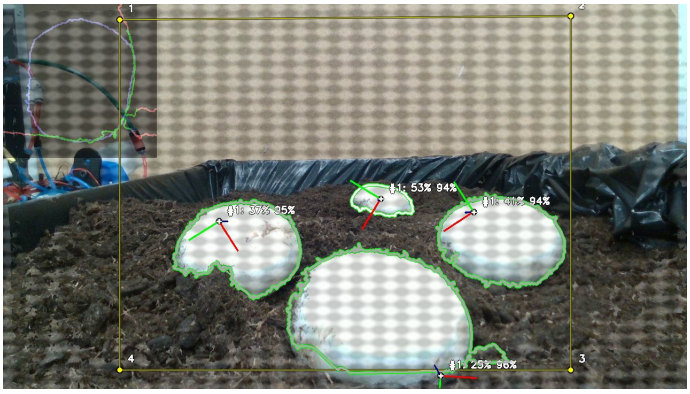

Figure 5.10: Mushroom detection

pressure is converted to an analog signal and is provided to the proportional air regulator using the Simulink Dspace controller. Once the soft finger has been actuated, the force sensors allow evaluating the contact as well as the sliding motion at the contact. An adaptative force value is also provided and the air is supplied until the reference value is reached. This adaptative value relies on the absence of the sliding at the contact with the mushroom's hats. If sliding occurs, then the gripping forces become unstable while decreasing. The control system tries to overcome the sliding by supplying pressure until a stable behavior of the measured forces is reached.

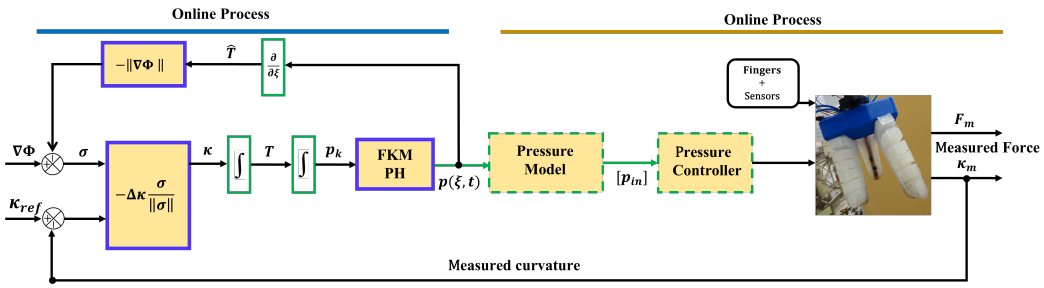

Figure 5.11: Finger control scheme

5.6 Results and discussions

The validation process consists of two main steps: in the first step, a simulation analysis (Section 5.6.1) is performed. In the second step, an online analysis is discussed (Section 5.6.2) with the real-world experiments.

5.6.1 Numerical results

The considered APF formulation is given as follows:

$$\Phi(p_k, p_{d_k}; \mathbb{O}) = \| p_{d_k} - p_k \| \sum_{j \neq k}^{5} \frac{1}{\| p_{d_j} - p_k \|}, \quad p_{d_j} \in \mathbb{O} \tag{5.18}$$

Fig. 5.12 is an illustration of the proposed soft gripper modeling concept using the APF (5.18) formulation. In the latter, the soft gripper approaches a target food (green caption) while the others (red caption), have been included in the $\mathbb{O}$ obstacle set (Fig. 5.12a).

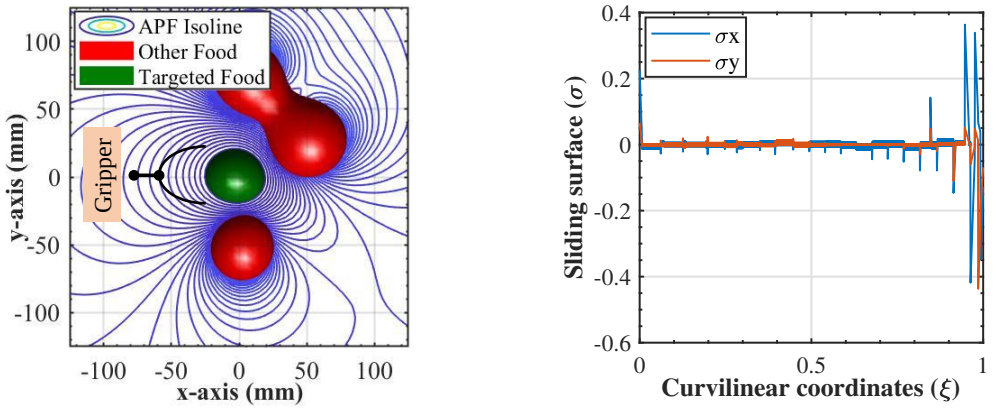

(a) APF modeling

(b) Sliding surface

Figure 5.12: Grasping modeling approach

The minimum potential energy of the soft fingers, represented by curves, is taken into account by the PH formulation. The SMC (Fig. 5.12) is applied to the control points. This enables to guarantee the shape kinematics requirements for the real physical system while approaching the target considering the minimum potential. The control polygon is then defined accordingly on the consistency of the potential energy minimization requirements.

5.6.2 Experimental validation

The experiments have been for the harvesting of various shapes of mushrooms from several poses. The curvature given by the image processing computation is set as the reference value and is tracked by the soft finger. The quantitative analysis of a grasping case is discussed in Fig. 5.14 and Fig. 5.15a.

In Fig. 5.14a, the reference value of the curvature, which has been computed by the imaging system, is tracked by the soft fingers. To assess the quality of the curvature tracking control during the grasping, the real-time values given by the bending sensors have been plotted. The analyses of the results show that, after reaching the steady state, the tracking error relative to the reference curvature remains at the neighbourhood of zero (Fig. 5.15b).

However, the viscous properties of the material, which induce a certain relaxation with time can explain the efforts variations during the grasping after 5*sec*. This is

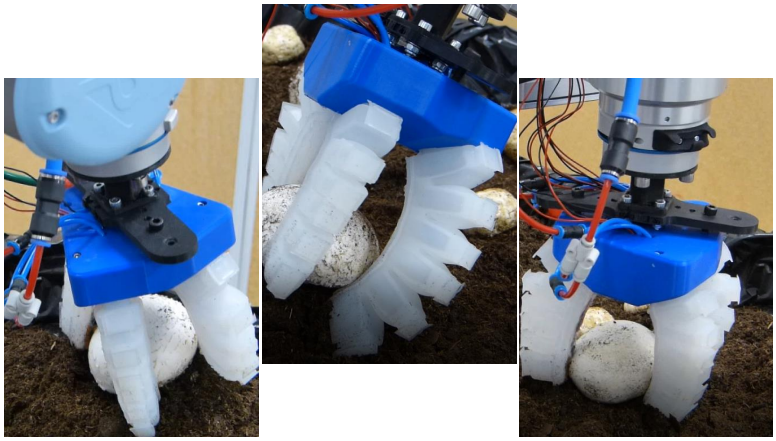

Figure 5.13: Mushroom harvesting illustration

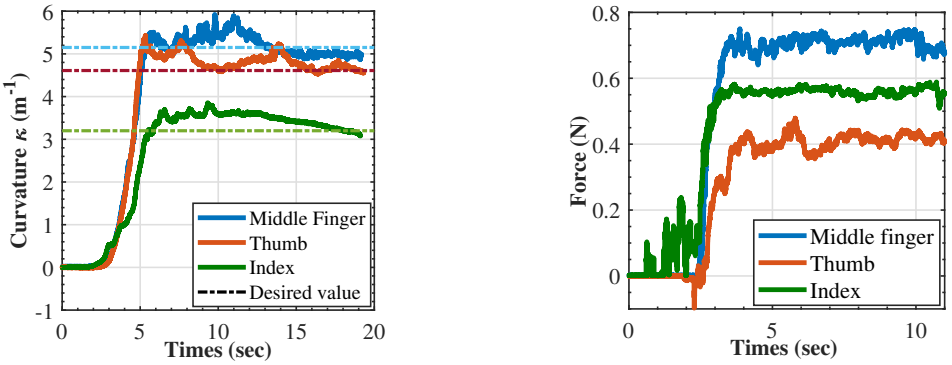

(a) Mushroom curvature tracking

(b) Measured grasping force

Figure 5.14: Grasping measurements

following the behavior of the forces measured by the sensors in Fig. 5.14b, where the values at the steady-state seem to decrease. The time-dependent viscous properties lead to an internal energy loss after structure relaxation. This can be compensated by adaptive control of the air pressure inputs.

External disturbances have been applied on the soft finger and discussed in Fig. 5.16. This was to assess the robustness of the grasping task. In this case, the physical contact disturbances are applied on the mushrooms (Fig. 5.16a) and lead to an increase of the air pressure inputs. The sliding phenomena that occur at the contact might explain this behavior. This observation is described in Fig. 5.16b where the contact forces are higher compared to Fig. 5.14b. This proves that the system is trying to overcome the kinematics disturbances using a permanent air pressure control to maintain the compliant contact with the mushroom. However, the unstable behavior of the forces measured at each of the fingers would probably have been caused by slippage that induces a significant loss of the normal force read by the sensors.

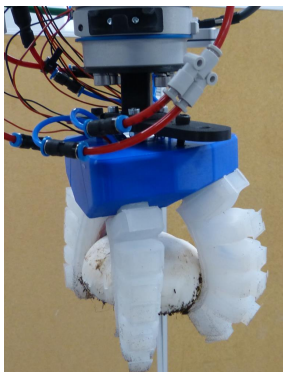

(a) Mushroom grasping case

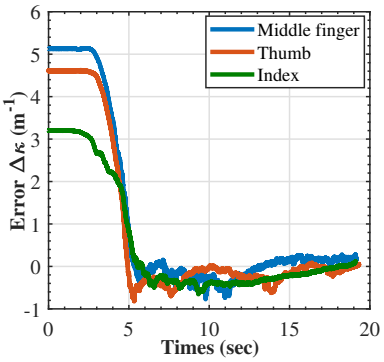

(b) Curvature error

Figure 5.15: Mushroom soft grasping illustration

(a) Grasping subject to external disturbances

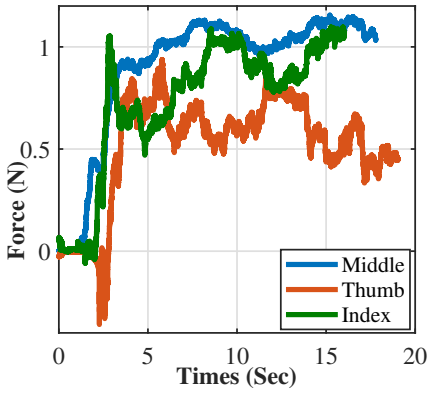

(b) Grasping force regulation

Figure 5.16: Grasping performances under external disturbances

Some limitations were reported during the experiments and certainly led to some of the errors observed in the present investigation. First, the camera is subject to occlusion during the grasping process and therefore cannot update information about the shape of the food being grasped. This may sometimes not be appropriate for soft foods such as mushrooms that may deform under external interactions. A shape model-based observer could solve this problem by updating the shape model in real-time. As already mentioned in Chapter 3, most of the APF-based trajectory planning suffers from a lack of convergence guarantee for special obstacle arrangements, e.g., a concave arrangement. Thus, the APF formulation used for control must be carefully considered. Finally, for an efficient form enclosure grasping, it is necessary to find an optimal distribution of actuation inputs along the length of the soft fingers to solve the problem related to the difference in arc length between the shape to be tracked and the soft fingers. It can be noted that some errors exist between the values obtained by the computation of the image processing and the

values read by the sensors. Several causes can justify these errors. Indeed, the difference in the arc length between the desired shape and soft finger might potentially explain the curvature tracking error. However, it can be observed that the accuracy is increasing with the size of the mushrooms hats to be grasped. This is consistent with the fact that, for an accurate shape conformation, the arc length of mushroom boundaries should be considered for the distribution of actuation inputs along the length of the soft fingers. Also, some errors might be induced from the material characterization. First, the elastic young modulus E of the material has been obtained from the fitting process, knowing the general fitting process error. Second, the interaction with the mushrooms has probably influenced the soft finger shape during grasping the process, and therefore the related curvature. All these latter, in addition to some neglected behaviors (shear force, inflated air dynamics, non-linear inertia moment, etc.) might have potentially contributed to errors observed.

5.7 Conclusion

In this chapter, an integrated design of a soft gripper for mushroom harvesting has been investigated. The proposed gripper is a bio-inspired concept, which respects the most commonly used hand grasping strategy (thumb, middle finger, and index finger). A kinematic shape controller based on APF motion planning and that relies on sliding mode, was proposed to address the problem related to the form enclosure grasping, which is more secure than the force enclosure grasping. A ROM that uses PH-based modeling techniques was considered. This allowed low-order kinematic modeling of the shape of the continuum soft fingers. Then, the EB theory was applied to estimate the dynamic inputs leading to the desired PH shape. The proposed soft gripper was found to be effective in harvesting the mushrooms and kept them safe due to the embedded sensing feedback of the contact force. The adaptive tracking of the targets and its adaptive grasping are both issues to be investigated in future works in the framework of mushroom harvesting. For the soft finger control, finding an optimal distribution of actuation inputs along the length of the soft fingers in order to solve the problem related to the difference in arc length between the shape to be tracked and the soft fingers is also a future consideration.

Chapter 6

Conclusion and prospective work

Contents

6.1 Summary of the contributions

In the present Ph.D. work, an integrated approach for the shape dynamic control of Mobile Soft-Continuum Manipulators (MSCM) has been investigated. The issue raised in the research work is related to the control of a very high order kinematic chain, due to the very large number of degrees of freedom (DoFs) exhibited by the Mobile Soft-Continuum Manipulators (MSCM). To reach this objective, first, a Pythagorean Hodograph curve has been used to reduce the order of the Mobile Soft-Continuum Manipulators (MSCM) kinematic while keeping the spatial configuration of its shape. Then, to manage the Mobile Soft-Continuum Manipulators (MSCM) trajectory planning in unstructured environments, a Artificial Potential Field (APF)-based algorithm is applied in the space configuration, repulsive in case of obstacles and attractive in case of target encapsulation. To maintain the shape of the Mobile Soft-Continuum Manipulators (MSCM) stable, a Sliding Mode Control (SMC) in the space configuration is designed and applied to the finite control points of its representative Pythagorean Hodograph (PH) curve. Finally, the shape of the Mobile Soft-Continuum Manipulators (MSCM) is dynamically controlled through physical inputs estimated from Euler-Bernoulli (EB). The integrated approach has been experimented on a class of soft grippers for agricultural harvesting and on a class Mobile Soft-Continuum Manipulators (MSCM) robots for autonomous navigation with obstacles avoidance. In this last chapter, a summary of the research results is highlighted and prospective works are listed.

6.2 General Conclusions

In light of all the above, the scientific literature related to technologies and the control of soft robots was first developed, from which the main advantages of these technologies in terms of better adaptability to the constraints imposed by external environments have been highlighted. It has been deduced from this review of the literature that the Reduced-Order-Model (ROM) of a Mobile Soft-Continuum Manipulators (MSCM) makes it possible to reconstruct its kinematic and dynamic behaviors while guaranteeing the tracking precision and the implementation in real-time. Several promising research studies have discussed Reduced-Order-Model (ROM)-based models. However, the relation between the Reduced-Order-Model (ROM) and the physical inputs of the soft robot is not established. This relation is necessary for the dynamic control of its shape. For this reason, the main results of this research work are focused on:

- Model Order Reduction of an Mobile Soft-Continuum Manipulators (MSCM) model by means of a parametric Pythagorean hodograph (Pythagorean Hodograph (PH)) curve, constrained by the curve length,
- Motion planning of an Mobile Soft-Continuum Manipulators (MSCM) through a potential field Artificial Potential Field (APF),
- Non-linear kinematic control of the shape of an Mobile Soft-Continuum Manipulators (MSCM), based on Sliding Mode Control (SMC) and applied to the control points of the Pythagorean Hodograph (PH) curve through a potential field,
- Controllable physical inputs (estimated from the curvature of the Pythagorean Hodograph (PH) curve) according to the type of soft robot, based on the Euler Bernoulli theory,
- Validation of the integrated approach for the dynamic control of an Mobile Soft-Continuum Manipulators (MSCM), applied to a soft bio-inspired gripper for handling tasks and also on mobile and bio-inspired elephant trunk for obstacle avoidance.

The Reduced-Order-Model (ROM) kinematic modeling of the Mobile Soft-Continuum Manipulators (MSCM) has been realized by using Pythagorean Hodograph (PH) curves. To respect the work-space boundaries, a new formulation is proposed, taking into consideration the actual length of the Mobile Soft-Continuum Manipulators (MSCM) as an input parameter. The inverse Reduced-Order-Model (ROM) kinematic modeling has been discussed and has enabled us to faithfully describe the shape kinematics of the Mobile Soft-Continuum Manipulators (MSCM), by computing a finite set of Bézier control points. Hence, the quintic Pythagorean Hodograph (PH) curve, composed of five Bézier control points, with prescribed

length has been considered for the shape kinematics modeling of the Mobile Soft-Continuum Manipulators (MSCM). However, the related Bézier control polygon doesn't allow independent motions of its control points while preserving Pythagorean Hodograph (PH) properties. This was found to be unsuitable in the case where some adjustments of the posture are required from the control points. To tackle this issue, a rectified control polygon that relies on Gauss-Lobatto quadrature has been explored. However, the first non-trivial case has been proved to occur for a septic Pythagorean Hodograph (PH) curve. Parallel to this, the rectifying control polygon cannot define itself the shape kinematics. Thus, the degree elevation process has been used and applied to the quintic Pythagorean Hodograph (PH) curve describing the Mobile Soft-Continuum Manipulators (MSCM). This has allowed mapping the Gauss-Lobatto control polygon to the Bézier control polygon and vice-versa. A local motion of the Bézier control polygon has then been made feasible without any loss of generality regarding its Pythagorean Hodograph (PH) properties. Henceforth, the Forward Kinematics Modeling (FKM) of the Mobile Soft-Continuum Manipulators (MSCM) could be achieved accordingly. Experimental analysis on two classes of Mobile Soft-Continuum Manipulators (MSCM) (Robotino-XT and soft finger) have been discussed and compared with other kinematics modeling approaches often used in the literature. A balance has been highlighted particularly regarding the energy optimization, the time cost, until five times smaller compared to other Reduced-Order-Model (ROM) models, and the tracking accuracy smaller than 5% with the robot arc length, that such an approach can offer. However, some limitations have been claimed regarding length constraints which suppose a perfect knowledge of the behavior of the robot material in particular about its extension, in terms of parameter uncertainties (e.g. Hooke's parameter, etc.). This can be sometimes hard to assess especially in the case of hyper-elastic materials.

Furthermore, a motion planning-based control technique applied to Pythagorean Hodograph (PH) parametric curves, has been investigated to address the kinematics shape control. The Artificial Potential Field (APF) approach has been chosen for its feature, related to the fast-time convergence over other existing motion planning approaches. This motion planning has been applied to the control points rather than all the curves. The non-linear control Sliding Mode Control (SMC) is then applied in the space configuration and has allowed keeping the curve in its optimal bending energy configuration. The idea of the curve shape control algorithm is to ensure that the tangent vector to the curve points, remains in the direction of the decreasing potential which is opposite to the gradient of the potential. The normalized curvilinear coordinate along the Mobile Soft-Continuum Manipulators (MSCM) is defined as the independent variable for the Sliding Mode Control (SMC). The latter has appeared to be one of the novelties of the proposed research works comparing to existing Sliding Mode Control (SMC) approaches where the time is defined rather as the independent variable. The stability and the convergence of the proposed control law have been rigorously proved by the standard technique using the quadratic Lyapunov function. The robustness of the control approach under dynamic space-time disturbances has been evaluated through two types of

Mobile Soft-Continuum Manipulators (MSCM): Robotino-XT (mobile bio-inspired elephant trunk) and a three-fingers bio-inspired soft gripper. Although its real-time applications for kinematics shape control, some Artificial Potential Field (APF)-based obstacle avoidance formulation can suffer from a lack of convergence guarantee for special arrangements of the obstacles, such as a concave arrangement.

With the end to meet physically the shape requirements issued from the motion planning, the dynamic modeling and control using Euler-Bernoulli (EB) have also been addressed to compute the physical control inputs of the Mobile Soft-Continuum Manipulators (MSCM) to map a prescribed shape configuration. Therefore, the forward dynamic modeling has been obtained, making the relationship between the curvature of the Pythagorean Hodograph (PH) curve and the physical inputs of Mobile Soft-Continuum Manipulators (MSCM) such as the pressure effort. This has enabled to control the Mobile Soft-Continuum Manipulators (MSCM) shape from an optimal and finite number of physical actuation inputs. However, inverting the dynamics appeared to be strongly required to drive the physical actuation to map a predefined posture. To this end, the Pythagorean Hodograph (PH)-based inverse dynamic approach has been analyzed and has yielded the physical control inputs to be specified according to the spatial configuration of the Bézier control polygon.

Experiments have been carried out on the same types of Mobile Soft-Continuum Manipulators (MSCM) under external disturbances. The obtained results have shown that the estimated physical control inputs can drive the kinematics of the Mobile Soft-Continuum Manipulators (MSCM) shape to be consistent with the prescribed control polygon. It is based on the estimation of the soft actuation status from their representative parametric curve Pythagorean Hodograph (PH). Comparison with other dynamic models of soft manipulators based on polynomial curves has been realized. The time cost and the accuracy obtained have demonstrated the interest of estimating the physical control inputs of the Mobile Soft-Continuum Manipulators (MSCM) from the Pythagorean Hodograph (PH) control points' position.

The integrated approach for shape dynamic control has been tested on a new design of a bio-inspired soft gripper, composed of three fingers. The latter has been used for mushrooms harvesting. The main issue solved is related to form-enclosure grasping, which requires shape adaptation with regard to the soft finger during the grasping process. The shape control strategy has proved to be efficient for real-time mushroom grasping in an unstructured environment.

6.3 Prospective Works

6.3.1 AI techniques for intrinsic parameter estimation

In the framework of the present research work, the second moment of inertia I has been supposed to be known and was taken as a constant. Also, it has been assumed that the soft robot material exhibits a perfect elastic behavior, and the

related Young modulus E has thus been taken constant as well as its length during the actuation process. This has lead to approach the dynamics of the soft structure with Euler-Bernoulli (EB) modeling techniques which do not take into consideration the stretch and the compression developed under actuation. However, it appears that one of the major errors observed comparing to real-world experiments and the Ansys multiphysics modeling is related to the influence of the physical control inputs (actuation) on the macro-structure of the soft manipulator. First, this includes the effects induced by the shear and tangent efforts on the geometry, and even on the stiffness of the soft structure. These effects occurred during the actuation and lead to a change of the cross area section. Second, the compressed fluid pressure depending on the fluid nature (air, gas, water, oil, etc.) might influence accordingly the bending stiffness. Parallel to this, for a non-regular geometry along the Mobile Soft-Continuum Manipulators (MSCM), the second moment of inertia I might be very complex to model. A qualitative solution based on artificial intelligence (AI) techniques can be investigated to estimate the bending stiffness EI to lower modeling error for the real-time control. For that, during the design test of the soft actuator, a set of parametric data from ANSYS, Finite Element Methods (FEM) and experiments can be acquired and trained to reproduce the shear forces and tangent efforts to come to more realistic dynamics. Thus, the idea is to allow estimating the longitudinal stretch to update the length with the Pythagorean Hodograph (PH) formulation while using the updated length constraints. Several benefits can be outlined using this approach.

6.3.2 Actuators placement Vs control points dynamics

One of the main issues concerning the control of the shape of the soft actuators is the geometric configuration of the actuator over the length of the soft continuum manipulators. Indeed, the kinematic behavior of the Fluidic Elastomeric Actuators (FEAs) to meet a prescribed shape depends strongly on the design and placement of the soft actuator. Typically, for Fluidic Elastomeric Actuators (FEAs), a number of them are designed on the consistency of the intrinsic actuation. However, the geometry of the shape to be tracked is not always equivalent to that of the soft actuator. This might result in some inaccuracy of convergence regarding the real-time shape control. For that, two types of shape control should be considered; one parallel to the actuator length to map the prescribed length of the tracked shape; the second to control the local curvature and act vertically to the length at the control points for shape control as a puppet motion control. The first aspect may induce the control of the stretch of the soft actuator, and the second the control of the local bending. For prospective work, it can be investigated an optimal design of soft actuators that can allow to physically control the virtual control points to address external interactions. The idea is to be able to drive the soft manipulator shape like the puppets' shape control leading to a wide range of complex shape tracking. Many advantages can be highlighted considering this approach notably smooth tracking and real-time local control of the soft manipulators.

Acronyms

AFEs Actionneurs Fluidiques en Élastomère. ii

AM Assumed Modes. 18

APF Artificial Potential Field. 3, 5, 6, 8, 21, 23–25, 27, 44, 49–51, 68, 76, 79, 80, 82–87

B-Spline Bézier Splines. 24

CBHA Compact Bionic Handling Assistant. 5, 42, 43, 46, 47, 51, 52, 59, 65

CC Constante Curvature. 6, 17, 20

DDL degrés de liberté. ii

DoFs degrees of freedom. i, 2–4, 6, 10, 11, 16, 17, 20, 36, 84, 111

EB Euler-Bernoulli. i, ii, 52, 54, 56–58, 62–66, 68, 84, 87, 88, 111

FEAs Fluidic Elastomeric Actuators. i, 3, 4, 6, 14, 15, 52–57, 64, 69, 70, 88, 111

FEM Finite Element Methods. 6, 17, 20, 24, 88

FKM Forward Kinematics Modeling. 27, 32, 33, 86

GNRON Goals Non Reachable with Obstacle Nearby. 23, 24

IKM Inverse Kinematics Modeling. 27, 32

MMSC Manipulateurs Mobiles Souples et Continuum. ii

MOR Modeling-Order-Reduction. 20, 24, 25

MSCM Mobile Soft-Continuum Manipulators. ix, 2–8, 21, 23–29, 31–37, 39, 41–44, 46, 47, 50, 84–88

NURBS Non-Uniformal Rational B-Splines. 18, 24

ODEs Ordinary Differential Equations. 19

PC Parametrization of the Curvature. 18, 20

PCC Piecewiese Constant Curvature. 16, 17, 20, 25

PDEs Partial Differential Equations. 17

PDMS Polydimethylsiloxane. 14

PH Pythagorean Hodograph. i, 3, 4, 6–8, 19, 24–30, 32–34, 36–41, 43, 46, 48, 50–52, 56, 57, 61–66, 68, 72–74, 76, 78, 80, 83–88, 111

POD Proper Orthogonal Decomposition. 20

PRM Probabilistic Road Map. 21, 23

PS Parametrization of the Shape. 18–20

PVW Principle of Virtual Works. 19

ROM Reduced-Order-Model. i, 2–4, 6, 7, 17–20, 24, 25, 74, 83, 85, 86, 111

RRG Rapid Random Graph. 21

RRT Rapid Random Tree. 21

SF Shape Functions. 19

SMC Sliding Mode Control. 3, 6, 8, 51, 84–86

Appendix A

Pythagorean Hodograph Fundamentals

A.1 Definition

A spatial polynomial curve $p(s) = (x(s), y(s), z(s))$ is called a pythagorean hodograph (PH) curve if and only if its derivative $p'(s) = (x'(s), y'(s), z'(s))$ satifies the pythagorean condition

$$x'(s)^2 + y'(s)^2 + z'(s)^2 = \sigma(s)^2 \tag{A.1}$$

for some polynomial $\sigma(s)$.

A.2 Quaternion form of a PH curves

By using a correspondence between $\mathbb{R}^3$ and the set of pure quaternions $\mathbb{H}$, a spatial curve $p(s) = (x(s), y(s), z(s))$ can be expressed as follows:

$$p(s) = x(s)\mathbf{i} + y(s)\mathbf{j} + z(s)\mathbf{k} \tag{A.2}$$

in the space of pure quaternions. $\mathbf{i}, \mathbf{j}, \mathbf{k}$ represent the 3 quaternions basis elements of the set of quaternions. In [Choi 2002], it has been established that the hodograph of a PH curve $p(s)$ can be obtained by the following :

$$p'(s) = \mathcal{A}(s)\mathbf{i}\mathcal{A}(s)^* \tag{A.3}$$

where $\mathcal{A}(s)$ and $\mathcal{A}(s)^*$ are respectively the quaternion polynomial and its conjugate of the form :

$$\begin{aligned} \mathcal{A}(s) &= u(s) + v(s)\mathbf{i} + r(s)\mathbf{j} + q(s)\mathbf{k} \\ \mathcal{A}^*(s) &= u(s) - v(s)\mathbf{i} - r(s)\mathbf{j} - q(s)\mathbf{k}. \end{aligned} \tag{A.4}$$

Note that $\mathcal{A}(s)\mathbf{i}\mathcal{A}(s)^*$ is always a pure quaternion. The parametric speed polynomial is specified by:

$$\sigma(s) = \|p'(t)\| = \|\mathcal{A}(s)\mathbf{i}\mathcal{A}(s)^*\| = u(s)^2 + v(s)^2 + r(s)^2 + q(s)^2 \tag{A.5}$$

A.3 Solution to a pure quaternion $\mathcal{A}\mathbf{i}\mathcal{A}^* = \mathbf{c}$

For two quaternions $\mathcal{A}$ and $\mathcal{B}$, a binary operation $\bigstar$ has been defined as follows [Šír 2007] :

$$\mathcal{A}\bigstar\mathcal{B} = \frac{1}{2}\left(\mathcal{A}\mathbf{i}\mathcal{B}^* + \mathcal{B}\mathbf{i}\mathcal{A}^*\right) \tag{A.6}$$

$\mathcal{A}\bigstar\mathcal{B}$ is always a pure quaternion, which is the vector part of $\mathcal{A}\mathbf{i}\mathcal{B}^*$. Henceforth, the n-th power of the quaternion $\mathcal{A}$ is denoted $\mathcal{A}^{n\bigstar}$. However, when using PH for modeling, the main issue often requires the solution to the quaternion equation:

$$\mathcal{A}^{2\bigstar} = \mathcal{A}\mathbf{i}\mathcal{A}^* = \mathbf{c} \tag{A.7}$$

where $\mathbf{c}$ is a pure quaternion. Let $v = \mathbf{c}/|\mathbf{c}| = (\lambda, \mu, \nu)$ be a unit vector in the direction of $\mathbf{c}$, the solution of the previous equation of the form of one parameter family [Farouki 2002]:

$$\mathcal{A}(\phi) = \sqrt{\frac{1}{2}(1+\lambda)|\mathbf{c}|}\left(\mathbf{i} + \frac{\mu}{1+\lambda}\mathbf{j} + \frac{\nu}{1+\lambda}\mathbf{k}\right)\mathcal{Q}(\phi) \tag{A.8}$$

where $\mathcal{Q}(\phi) = \cos\phi + \sin\phi\mathbf{i}$ and ϕ a parameter. $\mathbf{c}$ must be a non negative multiple of $\mathbf{i}$.

It is also defined as [Farouki 2015] [Šír 2007]:

$$\mathcal{A}(\phi) = \sqrt{|\mathbf{c}|}\frac{\frac{\mathbf{c}}{|\mathbf{c}|} + \mathbf{i}}{|\frac{\mathbf{c}}{|\mathbf{c}|} + \mathbf{i}|}\mathcal{Q}(\phi) \tag{A.9}$$

Among the one parameter family of solutions, $\mathcal{A}(0)$ is a particular solution. A new notation ($\bigstar$-*square root*) for this particular solution has been derived in [Kim 2019b].

Definition A.3.1. For a pure quaternion $\mathbf{c}$ that is not a negative multiple of $\mathbf{i}$, the $\bigstar$-*square root* is defined by:

$$\sqrt[\bigstar]{\mathbf{c}} = \sqrt{|\mathbf{c}|}\frac{\frac{\mathbf{c}}{|\mathbf{c}|} + \mathbf{i}}{|\frac{\mathbf{c}}{|\mathbf{c}|} + \mathbf{i}|} \tag{A.10}$$

A.4 Degree elevation of spatial PH curves

The degree elevation procedure have been described for Bézier curves [Farouki].

$$p(s) = \sum_{k=0}^{n} p_k \binom{5}{k} (1-s)^{5-k} s^k = \sum_{k=0}^{n+1} p_k' \binom{5}{k} (1-s)^{5-k} s^k \tag{A.11}$$

where the control points $p_k^{'}$ for the degree-elevated representation are given by:

$$\begin{cases} p_0^{'} = p_0, \\ p_{n+1}^{'} = p_n \\ p_k^{'} = \dfrac{k}{n+1} p_{k+1} + \big(1 - \dfrac{k}{n+1}\big) p_k, \text{ for } k = 1, \cdots, n \end{cases} \tag{A.12}$$

Therefore, it is possible to elevate the degree of any PH curve without compromising the Pythagorean nature of its hodograph, since degree elevation amounts merely to a redundant representation.

Bibliography

[Abramowitz 1964] Milton Abramowitz and Irene A Stegun. Handbook of mathematical functions with formulas, graphs, and mathematical tables, volume 55. US Government printing office, 1964. (Cited on pages 33 and 34.)

[Ahmed 2016] J Ahmed, M Nasir, K Flashman, J Khan and A Parvaiz. *Totally robotic rectal resection: an experience of the first 100 consecutive cases*. International journal of colorectal disease, vol. 31, no. 4, pages 869–876, 2016. (Cited on page 14.)

[Amanov 2021] E Amanov, T D Nguyen and J Burgner-Kahrs. *Tendon-driven Continuum Robots with Extensible Sections - A Model-based Evaluation of Path Following Motions*. International Journal of Robotics Research, vol. 40, no. 1, pages 7–23, 2021. (Cited on pages ix and 12.)

[Ataka 2017] Ahmad Ataka, Ali Shiva, Ali Shafti, Helge Wurdemann and Kaspar Althoefer. *Reactive motion planning for mobile continuum arm in dynamic industrial environment*. In Advances in Cooperative Robotics, pages 178–185. World Scientific, 2017. (Cited on page 23.)

[Bailly 2011] Yan Bailly, Yacine Amirat and Georges Fried. *Modeling and control of a continuum style microrobot for endovascular surgery*. IEEE Transactions on Robotics, vol. 27, no. 5, pages 1024–1030, 2011. (Cited on page 12.)

[Benner 2005] Peter Benner, Volker Mehrmann and Danny C Sorensen. Dimension reduction of large-scale systems, volume 45. Springer, 2005. (Cited on page 20.)

[Bieze 2018a] Thor Morales Bieze, Frederick Largilliere, Alexandre Kruszewski, Zhongkai Zhang, Rochdi Merzouki and Christian Duriez. *FEM-based kinematics and closed-loop control of soft, continuum manipulators*. 2018. (Cited on page 17.)

[Bieze 2018b] Thor Morales Bieze, Frederick Largilliere, Alexandre Kruszewski, Zhongkai Zhang, Rochdi Merzouki and Christian Duriez. *Finite element method-based kinematics and closed-loop control of soft, continuum manipulators*. Soft robotics, vol. 5, no. 3, pages 348–364, 2018. (Cited on pages 6 and 17.)

[Borenstein 1989] Johann Borenstein and Yoram Koren. *Real-time obstacle avoidance for fast mobile robots*. IEEE Transactions on systems, Man, and Cybernetics, vol. 19, no. 5, pages 1179–1187, 1989. (Cited on page 23.)

[Boyer 2015] Frédéric Boyer and Mathieu Porez. *Multibody system dynamics for bio-inspired locomotion: from geometric structures to computational aspects*.

Bioinspiration & biomimetics, vol. 10, no. 2, page 025007, 2015. (Cited on page 17.)

[Boyer 2020] Frédéric Boyer, Vincent Lebastard, Fabien Candelier and Federico Renda. *Dynamics of Continuum and Soft Robots: A Strain Parameterization Based Approach*. IEEE Transactions on Robotics, 2020. (Cited on page 19.)

[Brown 2021] Jasper Brown and Salah Sukkarieh. *Design and evaluation of a modular robotic plum harvesting system utilizing soft components*. Journal of Field Robotics, vol. 38, no. 2, pages 289–306, 2021. (Cited on page 15.)

[Bruno 2010] Siciliano Bruno, Sciavicco Lorenzo, Villani Luigi and Oriolo Giuseppe. *Robotics: modelling, planning and control*, 2010. (Cited on pages 1 and 15.)

[Bryson 2014] Caroline E Bryson and D Caleb Rucker. *Toward parallel continuum manipulators*. In 2014 IEEE International Conference on Robotics and Automation (ICRA), pages 778–785. IEEE, 2014. (Cited on page 11.)

[Burgner-Kahrs 2015] Jessica Burgner-Kahrs, D Caleb Rucker and Howie Choset. *Continuum robots for medical applications: A survey*. IEEE Transactions on Robotics, vol. 31, no. 6, pages 1261–1280, 2015. (Cited on page 13.)

[Camarillo 2008a] D. B. Camarillo, C. F. Milne, C. R. Carlson, M. R. Zinn and J. K. Salisbury. *Mechanics Modeling of Tendon-Driven Continuum Manipulators*. IEEE Transactions on Robotics, vol. 24, no. 6, pages 1262–1273, Dec 2008. (Cited on page 11.)

[Camarillo 2008b] David B Camarillo, Christopher F Milne, Christopher R Carlson, Michael R Zinn and J Kenneth Salisbury. *Mechanics modeling of tendon-driven continuum manipulators*. IEEE transactions on robotics, vol. 24, no. 6, pages 1262–1273, 2008. (Cited on page 12.)

[Case 2015] Jennifer C Case, Edward L White and Rebecca K Kramer. *Soft material characterization for robotic applications*. Soft Robotics, vol. 2, no. 2, pages 80–87, 2015. (Cited on page 1.)

[Chirikjian 1992] Gregory Scott Chirikjian. *Theory and applications of hyper-redundant robotic manipulators*. PhD thesis, California Institute of Technology, 1992. (Cited on page 18.)

[Chirikjian 1994] Gregory S Chirikjian and Joel W Burdick. *A modal approach to hyper-redundant manipulator kinematics*. IEEE Transactions on Robotics and Automation, vol. 10, no. 3, pages 343–354, 1994. (Cited on pages 18 and 22.)

[Chitta 2012] Sachin Chitta, Ioan Sucan and Steve Cousins. *Moveit![ros topics]*. IEEE Robotics & Automation Magazine, vol. 19, no. 1, pages 18–19, 2012. (Cited on page 21.)

[Choi 2002] Hyeong In Choi, Doo Seok Lee and Hwan Pyo Moon. *Clifford algebra, spin representation, and rational parameterization of curves and surfaces.* Advances in Computational Mathematics, vol. 17, no. 1-2, pages 5–48, 2002. (Cited on pages 28 and 91.)

[Cismasiu 2010] Corneliu Cismasiu. Shape memory alloys. BoD–Books on Demand, 2010. (Cited on pages ix and 12.)

[Clements 2019] Warren Clements, Madeleine Scicchitano, Jim Koukounaras, Tim Joseph and Gerard S Goh. *Use of the Magellan robotic system for conventional transarterial chemoembolization (cTACE): a 6-patient case series showing safety and technical success.* Journal of Clinical Interventional Radiology ISVIR, vol. 3, no. 02, pages 142–146, 2019. (Cited on pages ix and 13.)

[Connolly 1990] C.I. Connolly, J.B. Burns and R. Weiss. *Path planning using Laplace's equation.* In Proceedings., IEEE International Conference on Robotics and Automation, pages 2102–2106 vol.3, 1990. (Cited on page 23.)

[Dario 2000] Paolo Dario, Maria Chiarra Carrozza, Maurilio Marcacci, Simona D'Attanasio, Bernardo Magnami, Oliver Tonet and Giuseppe Megali. *A novel mechatronic tool for computer-assisted arthroscopy.* IEEE transactions on information technology in biomedicine, vol. 4, no. 1, pages 15–29, 2000. (Cited on page 12.)

[de Moura 2019] Diogo Turiani Hourneaux de Moura, Hiroyuki Aihara, Pichamol Jirapinyo, Galileu Farias, Kelly E Hathorn, Ahmad Bazarbashi, Amit Sachdev and Christopher C Thompson. *Robot-assisted endoscopic submucosal dissection versus conventional ESD for colorectal lesions: outcomes of a randomized pilot study in endoscopists without prior ESD experience (with video).* Gastrointestinal endoscopy, vol. 90, no. 2, pages 290–298, 2019. (Cited on pages ix and 13.)

[Della Santina 2018] Cosimo Della Santina, Dominic Lakatos, Antonio Bicchi and Alin Albu-Schaeffer. *Using nonlinear normal modes for execution of efficient cyclic motions in soft robots.* arXiv preprint arXiv:1806.08389, 2018. (Cited on page 19.)

[Della Santina 2019] Cosimo Della Santina and Daniela Rus. *Control oriented modeling of soft robots: the polynomial curvature case.* IEEE Robotics and Automation Letters, vol. 5, no. 2, pages 290–298, 2019. (Cited on pages 17 and 20.)

[Della Santina 2020a] Cosimo Della Santina. *The Soft Inverted Pendulum with Affine Curvature.* In 2020 59th IEEE Conference on Decision and Control (CDC), pages 4135–4142. IEEE, 2020. (Cited on pages 20 and 22.)

[Della Santina 2020b] Cosimo Della Santina, Antonio Bicchi and Daniela Rus. *On an improved state parametrization for soft robots with piecewise constant curvature and its use in model based control.* IEEE Robotics and Automation Letters, vol. 5, no. 2, pages 1001–1008, 2020. (Cited on pages 2, 20 and 22.)

[Della Santina 2020c] Cosimo Della Santina, Robert K Katzschmann, Antonio Bicchi and Daniela Rus. *Model-based dynamic feedback control of a planar soft robot: Trajectory tracking and interaction with the environment.* The International Journal of Robotics Research, vol. 39, no. 4, pages 490–513, 2020. (Cited on pages 2, 20 and 22.)

[Drakunov 1992] Sergey V Drakunov and Vadim I Utkin. *Sliding mode control in dynamic systems.* International Journal of Control, vol. 55, no. 4, pages 1029–1037, 1992. (Cited on page 42.)

[Duriez 2013] Christian Duriez. *Control of elastic soft robots based on real-time finite element method.* In 2013 IEEE international conference on robotics and automation, pages 3982–3987. IEEE, 2013. (Cited on page 17.)

[Elgeneidy 2018] Khaled Elgeneidy, Niels Lohse and Michael Jackson. *Bending angle prediction and control of soft pneumatic actuators with embedded flex sensors–a data-driven approach.* Mechatronics, vol. 50, pages 234–247, 2018. (Cited on page 16.)

[Escande 2015] Coralie Escande, Taha Chettibi, Rochdi Merzouki, Vincent Coelen and Pushparaj Mani Pathak. *Kinematic calibration of a multisection bionic manipulator.* IEEE/ASME transactions on mechatronics, vol. 20, no. 2, pages 663–674, 2015. (Cited on pages 6 and 17.)

[Falkenhahn 2015] Valentin Falkenhahn, Tobias Mahl, Alexander Hildebrandt, Rüdiger Neumann and Oliver Sawodny. *Dynamic modeling of bellows-actuated continuum robots using the Euler–Lagrange formalism.* IEEE Transactions on Robotics, vol. 31, no. 6, pages 1483–1496, 2015. (Cited on page 17.)

[Falkenhahn 2016] Valentin Falkenhahn, Alexander Hildebrandt, Ruediger Neumann and Oliver Sawodny. *Dynamic control of the bionic handling assistant.* IEEE/ASME Transactions on Mechatronics, vol. 22, no. 1, pages 6–17, 2016. (Cited on pages ix, 16 and 17.)

[Farouki] RT Farouki. *Pythagorean Hodograph Curves: Algebra and Geometry Inseparable. 2008.* (Cited on pages 26 and 92.)

[Farouki 1990] Rida T Farouki and Takis Sakkalis. *Pythagorean hodographs.* IBM Journal of Research and Development, vol. 34, no. 5, pages 736–752, 1990. (Cited on page 28.)

[Farouki 1994] Rida T. Farouki and Takis Sakkalis. *Pythagorean-hodograph space curves.* Advances in Computational Mathematics, vol. 2, no. 1, pages 41–66, Jan 1994. (Cited on pages 57 and 75.)

[Farouki 2002] Rida T Farouki, Mohammad al Kandari and Takis Sakkalis. *Hermite interpolation by rotation-invariant spatial Pythagorean-hodograph curves.* Advances in Computational Mathematics, vol. 17, no. 4, pages 369–383, 2002. (Cited on pages 31, 38 and 92.)

[Farouki 2015] Rida T Farouki, Carlotta Giannelli and Alessandra Sestini. *Identification and âreverse engineeringâ of Pythagorean-hodograph curves.* Computer Aided Geometric Design, vol. 34, pages 21–36, 2015. (Cited on pages 33 and 92.)

[Farouki 2019] Rida T Farouki. *Existence of Pythagorean-hodograph quintic interpolants to spatial G1 Hermite data with prescribed arc lengths.* Journal of Symbolic Computation, vol. 95, pages 202–216, 2019. (Cited on page 31.)

[Ficuciello 2018] Fanny Ficuciello, Alessandro Migliozzi, Eulalie Coevoet, Antoine Petit and Christian Duriez. *FEM-based deformation control for dexterous manipulation of 3D soft objects.* In 2018 IEEE/RSJ International Conference on Intelligent Robots and Systems (IROS), pages 4007–4013. IEEE, 2018. (Cited on page 21.)

[Galley 2019] Alexandre Galley, George K Knopf and Mohamed Kashkoush. *Pneumatic hyperelastic actuators for grasping curved organic objects.* In Actuators, volume 8, page 76. Multidisciplinary Digital Publishing Institute, 2019. (Cited on page 14.)

[Galloway 2016] Kevin C Galloway, Kaitlyn P Becker, Brennan Phillips, Jordan Kirby, Stephen Licht, Dan Tchernov, Robert J Wood and David F Gruber. *Soft robotic grippers for biological sampling on deep reefs.* Soft robotics, vol. 3, no. 1, pages 23–33, 2016. (Cited on pages ix, 2 and 15.)

[Gayle 2005] Russell Gayle, Paul Segars, Ming C Lin and Dinesh Manocha. *Path planning for deformable robots in complex environments.* In Robotics: Science and Systems, volume 2005, pages 225–232, 2005. (Cited on page 23.)

[Ge 2000] S.S. Ge and Y.J. Cui. *New potential functions for mobile robot path planning.* IEEE Transactions on Robotics and Automation, vol. 16, no. 5, pages 615–620, 2000. (Cited on page 24.)

[Godage 2011] Isuru S Godage, David T Branson, Emanuele Guglielmino, Gustavo A Medrano-Cerda and Darwin G Caldwell. *Shape function-based kinematics and dynamics for variable length continuum robotic arms.* In 2011 IEEE International Conference on Robotics and Automation, pages 452–457. IEEE, 2011. (Cited on page 19.)

[Godage 2016] Isuru S Godage, Gustavo A Medrano-Cerda, David T Branson, Emanuele Guglielmino and Darwin G Caldwell. *Dynamics for variable length multisection continuum arms.* The International Journal of Robotics Research, vol. 35, no. 6, pages 695–722, 2016. (Cited on page 22.)

[Gong 2016] Wenhui Gong, Junfeng Cai, Zhe Wang, Anqing Chen, Xiaofeng Ye, Haiqing Li and Qiang Zhao. *Robot-assisted coronary artery bypass grafting improves short-term outcomes compared with minimally invasive direct coronary artery bypass grafting.* Journal of thoracic disease, vol. 8, no. 3, page 459, 2016. (Cited on page 13.)

[Gosline 2012] Andrew H Gosline, Nikolay V Vasilyev, Evan J Butler, Chris Folk, Adam Cohen, Rich Chen, Nora Lang, Pedro J Del Nido and Pierre E Dupont. *Percutaneous intracardiac beating-heart surgery using metal MEMS tissue approximation tools.* The International journal of robotics research, vol. 31, no. 9, pages 1081–1093, 2012. (Cited on pages ix and 14.)

[Goury 2018] Olivier Goury and Christian Duriez. *Fast, generic, and reliable control and simulation of soft robots using model order reduction.* IEEE Transactions on Robotics, vol. 34, no. 6, pages 1565–1576, 2018. (Cited on pages 20 and 22.)

[Grazioso 2019] Stanislao Grazioso, Giuseppe Di Gironimo and Bruno Siciliano. *A geometrically exact model for soft continuum robots: The finite element deformation space formulation.* Soft robotics, vol. 6, no. 6, pages 790–811, 2019. (Cited on pages 17 and 22.)

[Gunderman 2021] Anthony L Gunderman, Jeremy Collins, Andrea Myer, Renee Threlfall and Yue Chen. *Tendon-Driven Soft Robotic Gripper for Berry Harvesting.* arXiv preprint arXiv:2103.04270, 2021. (Cited on pages ix, 2, 14 and 15.)

[Hannan 2003] Michael W Hannan and Ian D Walker. *Kinematics and the implementation of an elephant's trunk manipulator and other continuum style robots.* Journal of Robotic Systems, vol. 20, no. 2, pages 45–63, 2003. (Cited on pages ix and 16.)

[Hendrick 2015] Richard J Hendrick, Christopher R Mitchell, S Duke Herrell and Robert J Webster III. *Hand-held transendoscopic robotic manipulators: A transurethral laser prostate surgery case study.* The International journal of robotics research, vol. 34, no. 13, pages 1559–1572, 2015. (Cited on pages ix, 13 and 14.)

[Hilario 2011] L. Hilario, N. Montés, M.C. Mora and A. Falcó. *Real-time bezier trajectory deformation for potential fields planning methods.* In 2011 IEEE/RSJ International Conference on Intelligent Robots and Systems, pages 1567–1572, 2011. (Cited on page 23.)

[Hindman 2019] Amy Hindman. *Robotic bronchoscopy*. Oncology Issues, vol. 34, no. 2, pages 16–20, 2019. (Cited on pages ix and 13.)

[Hirose 1993] Shigeo Hirose. *Biologically inspired robots*. Snake-Like Locomotors and Manipulators, 1993. (Cited on page 10.)

[Hughes 2016] Josie Hughes, Utku Culha, Fabio Giardina, Fabian Guenther, Andre Rosendo and Fumiya Iida. *Soft manipulators and grippers: a review*. Frontiers in Robotics and AI, vol. 3, page 69, 2016. (Cited on pages 2 and 10.)

[Ikuta 2006] Koji Ikuta, Hironobu Ichikawa, Katsuya Suzuki and Daisuke Yajima. *Multi-degree of freedom hydraulic pressure driven safety active catheter*. In Proceedings 2006 IEEE International Conference on Robotics and Automation, 2006. ICRA 2006., pages 4161–4166. IEEE, 2006. (Cited on page 12.)

[Ikuta 2011] Koji Ikuta, Yoshikatsu Matsuda, Daisuke Yajima and Yusuke Ota. *Pressure pulse drive: A control method for the precise bending of hydraulic active catheters*. IEEE/ASME Transactions on Mechatronics, vol. 17, no. 5, pages 876–883, 2011. (Cited on page 12.)

[Immega 1995] Guy Immega and Keith Antonelli. *The KSI tentacle manipulator*. In Robotics and Automation, 1995. Proceedings., 1995 IEEE International Conference on, volume 3, pages 3149–3154. IEEE, 1995. (Cited on page 12.)

[Ivanescu 1995] Mircea Ivanescu and Viorel Stoian. *A variable structure controller for a tentacle manipulator*. In Proceedings of 1995 IEEE international conference on robotics and automation, volume 3, pages 3155–3160. IEEE, 1995. (Cited on page 12.)

[Karaman 2010] Sertac Karaman and Emilio Frazzoli. *Optimal kinodynamic motion planning using incremental sampling-based methods*. In 49th IEEE conference on decision and control (CDC), pages 7681–7687. IEEE, 2010. (Cited on page 21.)

[Katzschmann 2019] Robert K Katzschmann, Cosimo Della Santina, Yasunori Toshimitsu, Antonio Bicchi and Daniela Rus. *Dynamic motion control of multi-segment soft robots using piecewise constant curvature matched with an augmented rigid body model*. In 2019 2nd IEEE International Conference on Soft Robotics (RoboSoft), pages 454–461. IEEE, 2019. (Cited on page 17.)

[Kavraki 1996] Lydia E Kavraki, Petr Svestka, J-C Latombe and Mark H Overmars. *Probabilistic roadmaps for path planning in high-dimensional configuration spaces*. IEEE transactions on Robotics and Automation, vol. 12, no. 4, pages 566–580, 1996. (Cited on page 21.)

[Khatib 1986] Oussama Khatib. *Real-time obstacle avoidance for manipulators and mobile robots*. In Autonomous Robot Vehicles, pages 396–404. Springer, 1986. (Cited on page 23.)

[Kim 1992] Jin-Oh Kim and Pradeep Khosla. *Real-time obstacle avoidance using harmonic potential functions.* 1992. (Cited on page 23.)

[Kim 2017] Soo Hyun Kim and Hwan Pyo Moon. *Rectifying control polygon for planar Pythagorean hodograph curves.* Computer Aided Geometric Design, vol. 54, pages 1–14, 2017. (Cited on page 36.)

[Kim 2019a] Soo Hyun Kim and Hwan Pyo Moon. *Deformation of spatial septic Pythagorean hodograph curves using Gauss–Legendre polygon.* Computer Aided Geometric Design, vol. 73, pages 16–34, 2019. (Cited on page 38.)

[Kim 2019b] Soo Hyun Kim and Hwan Pyo Moon. *Deformation of spatial septic Pythagorean hodograph curves using Gauss–Legendre polygon.* Computer Aided Geometric Design, vol. 73, pages 16–34, 2019. (Cited on page 92.)

[Koehler 2019] Margaret Koehler, Allison M Okamura and Christian Duriez. *Stiffness control of deformable robots using finite element modeling.* IEEE Robotics and Automation Letters, vol. 4, no. 2, pages 469–476, 2019. (Cited on page 21.)

[Kuntz 2017] A. Kuntz, A. W. Mahoney, N. E. Peckman, P. L. Anderson, F. Maldonado, R. J. Webster and R. Alterovitz. *Motion planning for continuum reconfigurable incisionless surgical parallel robots.* In 2017 IEEE/RSJ International Conference on Intelligent Robots and Systems (IROS), pages 6463–6469, 2017. (Cited on page 21.)

[Kuntz 2019] A. Kuntz, M. Fu and R. Alterovitz. *Planning High-Quality Motions for Concentric Tube Robots in Point Clouds via Parallel Sampling and optimization.* In 2019 IEEE/RSJ International Conference on Intelligent Robots and Systems (IROS), pages 2205–2212, 2019. (Cited on page 23.)

[Kuntz 2020] Alan Kuntz, Armaan Sethi, Robert J Webster and Ron Alterovitz. *Learning the Complete Shape of Concentric Tube Robots.* IEEE Transactions on Medical Robotics and Bionics, vol. 2, no. 2, pages 140–147, 2020. (Cited on pages ix and 16.)

[Kutzer 2011] Michael DM Kutzer, Sean M Segreti, Christopher Y Brown, Mehran Armand, Russell H Taylor and Simon C Mears. *Design of a new cable-driven manipulator with a large open lumen: Preliminary applications in the minimally-invasive removal of osteolysis.* In 2011 IEEE International Conference on Robotics and Automation, pages 2913–2920. IEEE, 2011. (Cited on pages 11 and 12.)

[Kwok 2012] Ka-Wai Kwok, Kuen Hung Tsoi, Valentina Vitiello, James Clark, Gary CT Chow, Wayne Luk and Guang-Zhong Yang. *Dimensionality reduction in controlling articulated snake robot for endoscopy under dynamic active constraints.* IEEE Transactions on robotics, vol. 29, no. 1, pages 15–31, 2012. (Cited on page 12.)

[Kythe 2005] Prem K Kythe and Michael R Schäferkotter. *Computational methods for integration*, 2005. (Cited on page 34.)

[Lakhal 2015] Othman Lakhal, Achille Melingui and Rochdi Merzouki. *Hybrid approach for modeling and solving of kinematics of a compact bionic handling assistant manipulator.* IEEE/ASME Transactions on Mechatronics, vol. 21, no. 3, pages 1326–1335, 2015. (Cited on pages 46 and 51.)

[Lakhal 2016] Othman Lakhal, Achille Melingui and Rochdi Merzouki. *Hybrid approach for modeling and solving of kinematics of a compact bionic handling assistant manipulator.* IEEE/ASME Transactions on Mechatronics, vol. 21, no. 3, pages 1326–1335, 2016. (Cited on page 6.)

[Lamiraux 2001a] Florent Lamiraux and Lydia E Kavraki. *Planning paths for elastic objects under manipulation constraints.* The International Journal of Robotics Research, vol. 20, no. 3, pages 188–208, 2001. (Cited on page 21.)

[Lamiraux 2001b] Florent Lamiraux and Lydia E Kavraki. *Planning paths for elastic objects under manipulation constraints.* The International Journal of Robotics Research, vol. 20, no. 3, pages 188–208, 2001. (Cited on page 21.)

[LaValle 1998] Steven M LaValle*et al.* *Rapidly-exploring random trees: A new tool for path planning.* 1998. (Cited on page 21.)

[Lyons 2009] L. A. Lyons, R. J. Webster and R. Alterovitz. *Motion planning for active cannulas.* In IEEE/RSJ International Conference on Intelligent Robots and Systems, pages 801–806, 2009. (Cited on page 17.)

[Maeder-York 2014] Paxton Maeder-York, Tyler Clites, Emily Boggs, Ryan Neff, Panagiotis Polygerinos, Dónal Holland, Leia Stirling, Kevin Galloway, Catherine Wee and Conor Walsh. *Biologically inspired soft robot for thumb rehabilitation.* Journal of Medical Devices, vol. 8, no. 2, 2014. (Cited on page 14.)

[Marco 2007] Ana Marco, José-Javier Martı*et al.* *A fast and accurate algorithm for solving Bernstein–Vandermonde linear systems.* Linear algebra and its applications, vol. 422, no. 2-3, pages 616–628, 2007. (Cited on page 38.)

[Martinez 2013] Ramses V. Martinez, Jamie L. Branch, Carina R. Fish, Lihua Jin, Robert F. Shepherd, Rui M. D. Nunes, Zhigang Suo and George M. Whitesides. *Robotic Tentacles with Three-Dimensional Mobility Based on Flexible Elastomers.* Advanced Materials, vol. 25, no. 2, pages 205–212, 2013. (Cited on pages ix and 12.)

[Mattei 2014] Tobias A Mattei, Abraham Hafiz Rodriguez, Deepak Sambhara and Ehud Mendel. *Current state-of-the-art and future perspectives of robotic technology in neurosurgery.* Neurosurgical review, vol. 37, no. 3, pages 357–366, 2014. (Cited on page 13.)

[Mbakop 2020] Steeve Mbakop, Gilles Tagne, Othman Lakhal, Rochdi Merzouki and Sergey V Drakunov. *Path Planning and Control of Mobile Soft Manipulators with Obstacle Avoidance.* In 2020 3rd IEEE International Conference on Soft Robotics (RoboSoft), pages 64–69. IEEE, 2020. (Cited on pages 6 and 27.)

[Mbakop 2021a] Steeve Mbakop, Gilles Tagne, Sergey Drakunov and Rochdi Merzouki. *Parametric PH Curves-Model Based Kinematic Control of the Shape of Mobile Soft-Manipulators in Unstructured Environment.* IEEE Transactions on Industrial Electronics, 2021. (Cited on pages 6 and 27.)

[Mbakop 2021b] Steeve Mbakop, Gilles Tagne, Marc-Henri Frouin, Achille Melingui and Rochdi Merzouki. *Inverse Dynamics Model-Based Shape Control of Soft Continuum Finger Robot Using Parametric Curve.* IEEE Robotics and Automation Letters, vol. 6, no. 4, pages 8053–8060, 2021. (Cited on pages 6 and 58.)

[Mbakop 2021c] Steeve Mbakop, Gilles Tagne, Marc-Henri Frouin and Rochdi Merzouki. *Interoperable Models for Dynamics and Shape Tracking of Soft Fingers.* In 2021 IEEE 4th International Conference on Soft Robotics (RoboSoft), pages 199–206. IEEE, 2021. (Cited on pages 6 and 68.)

[Mbakop 2022] Steeve Mbakop, Gilles Tagne, Xinrui Yang, Mouad Kahouadji, Michel Pollart and Rochdi Merzouki. *Integrated Design of a Bio-Inspired Soft Agri-Food Gripper for Mushroom Harvesting.* IEEE/ASME Transactions on Mechatronics (In review), 2022. (Cited on page 6.)

[Melingui 2015] Achille Melingui, Othman Lakhal, Boubaker Daachi, Jean Bosco Mbede and Rochdi Merzouki. *Adaptive neural network control of a compact bionic handling arm.* IEEE/ASME Transactions on Mechatronics, vol. 20, no. 6, pages 2862–2875, 2015. (Cited on pages 6 and 16.)

[Mihael Brojan 2007] Mihael Brojan, Tomaz Videnic and Franc Kosel. *Non-prismatic Non-linearly Elastic Cantilever Beams Subjected to an End Moment.* Journal of Reinforced Plastics and Composites, vol. 26, no. 11, pages 1071–1082, 2007. (Cited on page 54.)

[Moll 2006] Mark Moll and Lydia E Kavraki. *Path planning for deformable linear objects.* IEEE Transactions on Robotics, vol. 22, no. 4, pages 625–636, 2006. (Cited on page 23.)

[Montiel 2015] Oscar Montiel, Ulises Orozco-Rosas and Roberto Sepúlveda. *Path planning for mobile robots using bacterial potential field for avoiding static and dynamic obstacles.* Expert Systems with Applications, vol. 42, no. 12, pages 5177–5191, 2015. (Cited on page 23.)

[Moses 2013] Matthew S Moses, Michael DM Kutzer, Hans Ma and Mehran Armand. *A continuum manipulator made of interlocking fibers.* In 2013 IEEE

International Conference on Robotics and Automation, pages 4008–4015. IEEE, 2013. (Cited on page 11.)

[Neudorfer 2018] Clemens Neudorfer, Stefan Hunsche, Martin Hellmich, Faycal El Majdoub and Mohammad Maarouf. *Comparative study of robot-assisted versus conventional frame-based deep brain stimulation stereotactic neurosurgery.* Stereotactic and functional neurosurgery, vol. 96, no. 5, pages 327–334, 2018. (Cited on page 13.)

[Orekhov 2020] Andrew L Orekhov and Nabil Simaan. *Solving cosserat rod models via collocation and the magnus expansion.* In 2020 IEEE/RSJ International Conference on Intelligent Robots and Systems (IROS), pages 8653–8660. IEEE, 2020. (Cited on page 19.)

[Panzer 2010] Heiko Panzer, Jan Mohring, Rudy Eid and Boris Lohmann. *Parametric model order reduction by matrix interpolation.* 2010. (Cited on page 20.)

[Park 2014] Yong-Lae Park, Bor-rong Chen, Néstor O Pérez-Arancibia, Diana Young, Leia Stirling, Robert J Wood, Eugene C Goldfield and Radhika Nagpal. *Design and control of a bio-inspired soft wearable robotic device for ankle–foot rehabilitation.* Bioinspiration & biomimetics, vol. 9, no. 1, page 016007, 2014. (Cited on page 14.)

[Patle 2019] BK Patle, Anish Pandey, DRK Parhi, A Jagadeesh*et al. A review: On path planning strategies for navigation of mobile robot.* Defence Technology, vol. 15, no. 4, pages 582–606, 2019. (Cited on page 2.)

[Petruska 2015] Andrew J Petruska and Bradley J Nelson. *Minimum bounds on the number of electromagnets required for remote magnetic manipulation.* IEEE Transactions on Robotics, vol. 31, no. 3, pages 714–722, 2015. (Cited on page 13.)

[Petruska 2016] Andrew J Petruska, Fabio Ruetz, Ayoung Hong, Luca Regli, Oguzkan Sürücü, Ajmal Zemmar and Bradley J Nelson. *Magnetic needle guidance for neurosurgery: Initial design and proof of concept.* In 2016 IEEE International Conference on Robotics and Automation (ICRA), pages 4392–4397. IEEE, 2016. (Cited on page 13.)

[Polygerinos 2015] Panagiotis Polygerinos, Zheng Wang, Kevin C Galloway, Robert J Wood and Conor J Walsh. *Soft robotic glove for combined assistance and at-home rehabilitation.* Robotics and Autonomous Systems, vol. 73, pages 135–143, 2015. (Cited on pages ix, 14 and 15.)

[Polygerinos 2017] Panagiotis Polygerinos, Nikolaus Correll, Stephen A Morin, Bobak Mosadegh, Cagdas D Onal, Kirstin Petersen, Matteo Cianchetti,

Michael T Tolley and Robert F Shepherd. *Soft robotics: Review of fluid-driven intrinsically soft devices; manufacturing, sensing, control, and applications in human-robot interaction.* Advanced Engineering Materials, vol. 19, no. 12, page 1700016, 2017. (Cited on page 10.)

[Quarteroni 2010] Alfio Quarteroni, Riccardo Sacco and Fausto Saleri. Numerical mathematics, volume 37. Springer Science & Business Media, 2010. (Cited on pages 33 and 34.)

[Reed 2001] JN Reed, SJ Miles, J Butler, M Baldwin and R Noble. *AEâAutomation and emerging technologies: Automatic mushroom harvester development.* Journal of Agricultural Engineering Research, vol. 78, no. 1, pages 15–23, 2001. (Cited on page 14.)

[Renda 2012] Federico Renda, Matteo Cianchetti, Michele Giorelli, Andrea Arienti and Cecilia Laschi. *A 3D steady-state model of a tendon-driven continuum soft manipulator inspired by the octopus arm.* Bioinspiration & biomimetics, vol. 7, no. 2, page 025006, 2012. (Cited on page 17.)

[Renda 2014] Federico Renda, Michele Giorelli, Marcello Calisti, Matteo Cianchetti and Cecilia Laschi. *Dynamic model of a multibending soft robot arm driven by cables.* IEEE Transactions on Robotics, vol. 30, no. 5, pages 1109–1122, 2014. (Cited on page 17.)

[Renda 2015] Federico Renda, Francesco Giorgio-Serchi, Frédéric Boyer and Cecilia Laschi. *Modelling cephalopod-inspired pulsed-jet locomotion for underwater soft robots.* Bioinspiration & biomimetics, vol. 10, no. 5, page 055005, 2015. (Cited on page 17.)

[Renda 2018a] Federico Renda, Frédéric Boyer, Jorge Dias and Lakmal Seneviratne. *Discrete cosserat approach for multisection soft manipulator dynamics.* IEEE Transactions on Robotics, vol. 34, no. 6, pages 1518–1533, 2018. (Cited on page 17.)

[Renda 2018b] Federico Renda, Francesco Giorgio-Serchi, Frederic Boyer, Cecilia Laschi, Jorge Dias and Lakmal Seneviratne. *A unified multi-soft-body dynamic model for underwater soft robots.* The International Journal of Robotics Research, vol. 37, no. 6, pages 648–666, 2018. (Cited on page 17.)

[Rimon 1992] E. Rimon and D.E. Koditschek. *Exact robot navigation using artificial potential functions.* IEEE Transactions on Robotics and Automation, vol. 8, no. 5, pages 501–518, 1992. (Cited on page 23.)

[Robinson 1999] Graham Robinson and J Bruce C Davies. *Continuum robots-a state of the art.* In Robotics and Automation, 1999. Proceedings. 1999 IEEE International Conference on, volume 4, pages 2849–2854. IEEE, 1999. (Cited on page 10.)

[Robotics] Advanced Robotics and Mechanism Applications Laboratory. Vanderbilt University [Online 2021, Nov 15] Available: http://arma.vuse.vanderbilt.edu/. (Cited on pages ix and 12.)

[Rong 2021] Jiacheng Rong, Pengbo Wang, Qian Yang and Feng Huang. *A Field-Tested Harvesting Robot for Oyster Mushroom in Greenhouse*. Agronomy, vol. 11, no. 6, page 1210, 2021. (Cited on page 15.)

[Rosemurgy 2019] Alexander Rosemurgy, Sharona Ross, Timothy Bourdeau, Danielle Craigg, Janelle Spence, Joshua Alvior and Iswanto Sucandy. *Robotic pancreaticoduodenectomy is the future: here and now*. Journal of the American College of Surgeons, vol. 228, no. 4, pages 613–624, 2019. (Cited on page 14.)

[Roussel 2014a] Olivier Roussel and Michel Taïx. *Deformable Linear Object manipulation planning with contacts*. 2014. (Cited on page 21.)

[Roussel 2014b] Olivier Roussel, Michel Taïx and Timothy Bretl. *Motion planning for a deformable linear object*. 2014. (Cited on page 21.)

[Rucker 2010] D Caleb Rucker, Bryan A Jones and Robert J Webster III. *A geometrically exact model for externally loaded concentric-tube continuum robots*. IEEE transactions on robotics, vol. 26, no. 5, pages 769–780, 2010. (Cited on pages ix and 16.)

[Rucker 2011] D Caleb Rucker and Robert J Webster III. *Statics and dynamics of continuum robots with general tendon routing and external loading*. IEEE Transactions on Robotics, vol. 27, no. 6, pages 1033–1044, 2011. (Cited on page 17.)

[Runge 2017] G Runge, M Wiese, L Günther and A Raatz. *A framework for the kinematic modeling of soft material robots combining finite element analysis and piecewise constant curvature kinematics*. In 2017 3rd International Conference on Control, Automation and Robotics (ICCAR), pages 7–14. IEEE, 2017. (Cited on page 17.)

[Rus 2015] Daniela Rus and Michael T Tolley. *Design, fabrication and control of soft robots*. Nature, vol. 521, no. 7553, pages 467–475, 2015. (Cited on pages 1, 10 and 68.)

[Sadati 2017] SM Hadi Sadati, S Elnaz Naghibi, Ian D Walker, Kaspar Althoefer and Thrishantha Nanayakkara. *Control space reduction and real-time accurate modeling of continuum manipulators using ritz and ritz–galerkin methods*. IEEE Robotics and Automation Letters, vol. 3, no. 1, pages 328–335, 2017. (Cited on pages 18, 19 and 22.)

[Sadati 2019] SM Hadi Sadati, S Elnaz Naghibi, Ali Shiva, Brendan Michael, Ludovic Renson, Matthew Howard, Caleb D Rucker, Kaspar Althoefer, Thrishantha Nanayakkara, Steffen Zschaler*et al. TMTDyn: A matlab package for modeling and control of hybrid rigid–continuum robots based on discretized lumped systems and reduced-order models.* The International Journal of Robotics Research, page 0278364919881685, 2019. (Cited on pages 22, 48 and 49.)

[Sayahkarajy 2018] Mostafa Sayahkarajy. *Mode shape analysis, modal linearization, and control of an elastic two-link manipulator based on the normal modes.* Applied Mathematical Modelling, vol. 59, pages 546–570, 2018. (Cited on page 18.)

[Sfeir 2011] Joe Sfeir, Maarouf Saad and Hamadou Saliah-Hassane. *An improved artificial potential field approach to real-time mobile robot path planning in an unknown environment.* In 2011 IEEE international symposium on robotic and sensors environments (ROSE), pages 208–213. IEEE, 2011. (Cited on page 24.)

[Shi 2009] Pu Shi and Yiwen Zhao. *An efficient path planning algorithm for mobile robot using improved potential field.* In 2009 IEEE International Conference on Robotics and Biomimetics (ROBIO), pages 1704–1708. IEEE, 2009. (Cited on page 24.)

[Siciliano 2016] Bruno Siciliano and Oussama Khatib. Springer handbook of robotics. Springer, 2016. (Cited on page 1.)

[Simaan 2009] Nabil Simaan, Kai Xu, Wei Wei, Ankur Kapoor, Peter Kazanzides, Russell Taylor and Paul Flint. *Design and integration of a telerobotic system for minimally invasive surgery of the throat.* The International journal of robotics research, vol. 28, no. 9, pages 1134–1153, 2009. (Cited on page 11.)

[Sinatra 2019] Nina R Sinatra, Clark B Teeple, Daniel M Vogt, Kevin Kit Parker, David F Gruber and Robert J Wood. *Ultragentle manipulation of delicate structures using a soft robotic gripper.* Science Robotics, vol. 4, no. 33, 2019. (Cited on pages ix, 14 and 15.)

[Singh 2017] Inderjeet Singh, Othman Lakhal, Yacine Amara, Vincent Coelen, Pushparaj Mani Pathak and Rochdi Merzouki. *Performances evaluation of inverse kinematic models of a compact bionic handling assistant.* In Robotics and Biomimetics (ROBIO), 2017 IEEE International Conference on, pages 264–269. IEEE, 2017. (Cited on page 24.)

[Singh 2018a] Inderjeet Singh. *Curve Based Approach for Shape Reconstruction of Continuum Manipulators.* PhD thesis, Universite de Lille, 2018. (Cited on page 24.)

[Singh 2018b] Inderjeet Singh, Yacine Amara, Achille Melingui, Pushparaj Mani Pathak and Rochdi Merzouki. *Modeling of Continuum Manipulators Using Pythagorean Hodograph Curves.* Soft robotics, 2018. (Cited on pages 2, 6, 18, 19, 22, 27, 46, 48, 49, 58 and 65.)

[Singh 2018c] Inderjeet Singh, Yacine Amara, Manarshhjot Singh and Rochdi Merzouki. *Towards Accurate Shape Reconstruction of Compact Bionic Handling Arm.* In 2018 IEEE/ASME International Conference on Advanced Intelligent Mechatronics (AIM), pages 742–747. IEEE, 2018. (Cited on page 24.)

[Šír 2007] Zbyněk Šír and Bert Jüttler. *C^2 Hermite interpolation by Pythagorean hodograph space curves.* Mathematics of Computation, vol. 76, no. 259, pages 1373–1391, 2007. (Cited on page 92.)

[Thieffry 2018a] Maxime Thieffry, Alexandre Kruszewski, Christian Duriez and Thierry-Marie Guerra. *Control design for soft robots based on reduced-order model.* IEEE Robotics and Automation Letters, vol. 4, no. 1, pages 25–32, 2018. (Cited on pages 20 and 22.)

[Thieffry 2018b] Maxime Thieffry, Alexandre Kruszewski, Thierry-Marie Guerra and Christian Duriez. *Reduced order control of soft robots with guaranteed stability.* In 2018 European Control Conference (ECC), pages 635–640. IEEE, 2018. (Cited on pages 2, 20 and 22.)

[Till 2015] John Till, Caroline E Bryson, Scotty Chung, Andrew Orekhov and D Caleb Rucker. *Efficient computation of multiple coupled Cosserat rod models for real-time simulation and control of parallel continuum manipulators.* In 2015 IEEE International Conference on Robotics and Automation (ICRA), pages 5067–5074. IEEE, 2015. (Cited on page 11.)

[Torres 2015] L. G. Torres, A. Kuntz, H. B. Gilbert, P. J. Swaney, R. J. Hendrick, R. J. Webster and R. Alterovitz. *A motion planning approach to automatic obstacle avoidance during concentric tube robot teleoperation.* In 2015 IEEE International Conference on Robotics and Automation (ICRA), pages 2361–2367, 2015. (Cited on page 21.)

[Trivedi 2007] D. Trivedi, A. Lotfi and C. D. Rahn. *Geometrically exact dynamic models for soft robotic manipulators.* In 2007 IEEE/RSJ International Conference on Intelligent Robots and Systems, pages 1497–1502, Oct 2007. (Cited on page 17.)

[Trivedi 2008a] Deepak Trivedi, Amir Lotfi and Christopher D Rahn. *Geometrically exact models for soft robotic manipulators.* IEEE Transactions on Robotics, vol. 24, no. 4, pages 773–780, 2008. (Cited on page 54.)

[Trivedi 2008b] Deepak Trivedi, Christopher D Rahn, William M Kier and Ian D Walker. *Soft robotics: Biological inspiration, state of the art, and future*

research. Applied bionics and biomechanics, vol. 5, no. 3, pages 99–117, 2008. (Cited on pages 2 and 10.)

[Webster, III 2009] R. J. Webster, III, J. M. Romano and N. J. Cowan. *Mechanics of Precurved-Tube Continuum Robots*. IEEE Transactions on Robotics, vol. 25, no. 1, pages 67–78, Feb 2009. (Cited on page 17.)

[Webster III 2010] Robert J Webster III and Bryan A Jones. *Design and kinematic modeling of constant curvature continuum robots: A review*. The International Journal of Robotics Research, vol. 29, no. 13, pages 1661–1683, 2010. (Cited on page 17.)

[Weeger 2017] Oliver Weeger, Sai-Kit Yeung and Martin L Dunn. *Isogeometric collocation methods for Cosserat rods and rod structures*. Computer Methods in Applied Mechanics and Engineering, vol. 316, pages 100–122, 2017. (Cited on page 19.)

[Wielgosz 2005] C Wielgosz*et al.* *Bending and buckling of inflatable beams: some new theoretical results*. Thin-walled structures, vol. 43, no. 8, pages 1166–1187, 2005. (Cited on page 54.)

[Wiese 2019] Mats Wiese, Kenneth Rüstmann and Annika Raatzl. *Kinematic Modeling of a Soft Pneumatic Actuator Using Cubic Hermite Splines*. In 2019 IEEE/RSJ International Conference on Intelligent Robots and Systems (IROS), pages 7176–7182. IEEE, 2019. (Cited on page 19.)

[Wu 2016] Long Wu and Paolo Tiso. *Nonlinear model order reduction for flexible multibody dynamics: a modal derivatives approach*. Multibody System Dynamics, vol. 36, no. 4, pages 405–425, 2016. (Cited on page 18.)

[Xiong 2018] Ya Xiong, Pal Johan From and Volkan Isler. *Design and evaluation of a novel cable-driven gripper with perception capabilities for strawberry picking robots*. In 2018 IEEE International Conference on Robotics and Automation (ICRA), pages 7384–7391. IEEE, 2018. (Cited on pages 2 and 14.)

[Yoon 2013] Hyun-Soo Yoon, Hyo-Jeong Cha, Jaeheon Chung and Byung-Ju Yi. *Compact design of a dual master-slave system for maxillary sinus surgery*. In 2013 IEEE/RSJ International Conference on Intelligent Robots and Systems, pages 5027–5032. IEEE, 2013. (Cited on pages ix and 14.)

[Zhang 2016] Zhongkai Zhang, Jeremie Dequidt, Alexandre Kruszewski, Frederick Largilliere and Christian Duriez. *Kinematic modeling and observer based control of soft robot using real-time finite element method*. In 2016 IEEE/RSJ International Conference on Intelligent Robots and Systems (IROS), pages 5509–5514. IEEE, 2016. (Cited on page 17.)

[Zheng 2020] Gang Zheng, Yuan Zhou and Mingda Ju. *Robust control of a silicone soft robot using neural networks.* ISA transactions, vol. 100, pages 38–45, 2020. (Cited on page 16.)

[Zhong 2019] Guoliang Zhong, Yangdong Hou and Weiqiang Dou. *A soft pneumatic dexterous gripper with convertible grasping modes.* International Journal of Mechanical Sciences, vol. 153, pages 445–456, 2019. (Cited on page 16.)

[Zhou 2021] Liang Zhou, Lili Ren, You Chen, Shichao Niu, Zhiwu Han and Luquan Ren. *Bio-Inspired Soft Grippers Based on Impactive Gripping.* Advanced Science, vol. 8, no. 9, page 2002017, 2021. (Cited on page 3.)

Towards Dynamic Shape Control of Mobile Soft Continuum Manipulators: Parametric curve-based approach

Abstract

Nowadays, soft continuum robots are increasingly used in everyday life (logistics, agriculture, medical therapy, baking, human collaboration, etc.) due to the multiple advantages they offer over rigid robots. They are often made up of soft and hyper-elastic materials that give them resilience, flexibility and conformation, making them good candidates to meet some real-life needs (form enclosure grasping, obstacle-free navigation, etc.). However, the control of their shape remains a major challenge for the scientific community due to their very large number of degrees of freedom (DoFs). Unfortunately, it is not physically possible to control all the DoFs to drive their 3D motion. To address that issue, the present research work focuses on a Reduced-Order-Model (ROM) based shape control using Pythagorean Hodograph (PH) parametric curves. The proposed approach allows to describe the high-order kinematics of soft continuum manipulators with a set of finite points called control points. Hence, the control dimension of the latter can be reduced to that of this set of finite control points. Moreover, to address shape adaptability issues during external interactions (gripping task, collision-free trajectory, spatio-temporal disturbances, etc.), the motions of the control points (shape kinematics) have been described with respect to real dynamic physical inputs considering the Euler-Bernoulli (EB) theory consistent with the large deflections. To validate the proposed approaches, several experimental tests have been performed on several classes of Soft Continuum Robots in various scenarios: Fluidic Elastomeric Actuators (FEAs) for the control of gripping tasks and a Robotino-XT for the control of motion planning with obstacles avoidance.

Keywords: Soft continuum manipulators, Pythagorean Hodograph curves, Shape kinematics, Shape dynamics, Control.